Activity-driven Formation and Stabilization of Functional Spine Synapses

Dissertation

zur Erlangung des Grades eines
Doktors der Naturwissenschaften

an der Fakultät für Biologie
der Ludwig-Maximilians-Universität
München,

vorgelegt von
Cvetalina N. Coneva

München, 15. Juli 2015

Erstgutachter:	Prof. Dr. Tobias Bonhoeffer
Zweitgutachter:	Prof. Dr. Christian Leibold
Tag der mündlichen Prüfung:	10. Oktober 2015

To my Grandmother Stanka

Eidesstattliche Erklärung

Ich versichere hiermit an Eides statt, dass die vorgelegte Dissertation von mir selbständig und ohne unerlaubte Hilfe angefertigt ist.

München, 15. Juli 2015 Cvetalina N. Coneva

Erklärung

Hiermit erkläre ich,

dass die Dissertation **nicht** ganz oder in wesentlichen Teilen einer anderen Prüfungskommission vorgelegt worden ist.

dass ich mich anderweitig einer Doktorprüfung ohne Erfolg **nicht** unterzogen habe.

München, 15. Juli 2015 Cvetalina N. Coneva

Contents

List of Figures

Abbreviations

3D	three dimensional
4-AP	4-aminopyridine
AAV	adeno-associated virus
ACSF	artificial cerebrospinal fluid
AMPA	aminomethylphosphonic acid
AP	action potential
AP5	(2*R*)-amino-5-phosphonovaleric acid
CA1	Cornu ammonis 1
CA2	Cornu ammonis 2
CA3	Cornu ammonis 3
CaMKII	Ca^{2+}/calmodulin-dependent protein kinase II
cAMP	cyclic adenosine monophosphate
ChR2	channelrhodopsin 2
CREB	cAMP response element-binding protein
DAQ	data acquisition
DG	dentate gyrus
DIV	days *in vitro*
DMSO	dimethyl sulfoxide
EC	entorhinal cortex
EGTA	ethylene glycol tetraacetic acid
EM	electron microscopy
EPSCs	excitatory postsynaptic currents
eYFP	enhanced yellow fluorescent protein
F&R	forskolin and rolipram
fEPSPs	field excitatory postsynaptic potentials
FOV	field of view
GBSS	Gey's balanced salt solution
GECI	genetically encoded calcium indicator
HBSS	Hank's balanced salt solution
HEPES	4-(2-hydroxyethyl)-1-piperazineethanesulfonic acid

ID	identification
LTP	long-term potentiation
MEM	modified eagle medium
mGluRs	metobotropic glutamate receptors
MRPcv	multipleROIpredator
NBQX	2,3-Dioxo-6-nitro-1,2,3,4-tetrahydrobenzo[*f*]quinoxaline sulfonamide
NMDA	N-methyl-D-aspartic acid
NO	nitric oxide
n.s.	not significant
OD	optic density
PKA	protein kinase A
PKC	protein kinase C
PMT	photomultiplier tube
PSD	postsynaptic density
PTP	post-tetanic potentiation
ROI	region of interest
SCE	single cell electroporation
sCRACM	subcellular channelrhodopsin-2-assisted circuit mapping
SEM	standard error of mean
STD	standard deviation
STDP	spike-timing-dependent plasticity
STP	short-term plasticity
Syn	synapsin
TBS	theta-burst stimulation
TTX	tetrodotoxin
VGCC	voltage-gated calcium channel

1. Summary

Physical changes in neuronal connections, dictated by the neuronal network activity, are believed to be essential for learning and memory. Long-term potentiation (LTP) of synaptic transmission has emerged as a model to study activity-driven plasticity. The majority of excitatory contacts between neurons, called synapses, are found on spines, small dendritic protrusions. LTP is known to trigger the formation and stabilization of new dendritic spines *in vitro*. Similarly, experience-dependent plasticity *in vivo* is associated with changes in the number and stability of spines. However, to date, the contribution of excitatory synaptogenesis to the enhanced synaptic transmission after LTP remains elusive. Do new spines form functional synapses with the inputs stimulated during LTP induction and thereby follow Hebbian co-activation rules, or do they connect with random partners? Furthermore, at which time-point are *de novo* spines functionally integrated into the network?

I developed an optical approach to stably and exclusively stimulate the axons of a defined channelrhodopsin-2 (ChR2)-transduced subset of CA3 cell in mature hippocampal slice culture over extended periods of time (up to 24h). I continuously monitored synaptic activation and synaptic structure of CA1 cells dendrites using two-photon imaging. To control the dendritic location where LTP and associated spinogenesis were allowed to take place, I globally blocked Na^+-dependent action potential firing and directly evoke neurotransmitter release by local light-evoked depolarization of ChR2-expressing presynaptic boutons (in TTX, 4-AP). I induced optical LTP specifically at this location by combining optogenetic activation with chemical pairing (in low $[Mg^{2+}]_o$, high $[Ca^{2+}]_o$, forskolin, and rolipram). Taking advantage of the NMDA-receptor mediated calcium influx during synaptic activation I assessed the formation of functional synapses using the genetically encoded calcium indicator GCaMP6s.

I find that optical LTP led to the generation of new spines, decreased the stability of preexisting spines and increased the stability of new spines. Under optical LTP conditions, a fraction of new spines responded to optical presynaptic stimulation within hours after formation. However, the occurrence of the first synaptic calcium response in *de novo* spines varied considerably, ranging from 8.5 min to 25 h. Most new spines became responsive within 4 h (1.2 ± 0.9 h, mean ± S.D., n = 16 out of 20), whereas the remainder showed their first response only on the second experimental day (18.2 ± 3.7 h). Importantly, new spines generated under optical LTP were more likely to build functional synapses with light-activated,

ChR2-expressing axons than spontaneously formed spines (new responsive spines under optical LTP: 64 ± 4 %; control 1: 0%; control 2: 13 ± 4 %; control 3: 11 ± 4 %). Furthermore, new spines that were responsive to optical presynaptic stimulation were less prone to be eliminated after overnight incubation than new spines that failed to respond (% overnight spine survival; 81 ± 3 % new responsive spines; 58 ± 4 % of new unresponsive spines).

In summary, the results from my thesis demonstrate that synapses can form rapidly in an input-specific manner.

2. Introduction

The complexity and inner workings of the brain have fascinated people ever since it was proposed that the brain is the place where not only mental processes occur but also personality and emotions are shaped. According to the records the very first person who declared the brain to be the place where the mind was located was Alcmaeon of Croton (5th century BC) [1]. He believed:

> "[…] the seat of sensation is in the brain. This contains the governing faculty. All the senses are connected in some way in the brain; consequently they are incapable of action if the brain is disturbed […] the power of the brain to synthetize sensations makes it also the seat of thought: the storing up of perceptions gives memory and belief and when these are stabilized you get knowledge "

The most straightforward and efficient way to study the brain, or any complex process or machinery for that matter, is to break it down into its individual building blocks and try to understand how those parts fit and work together. So, with the ability to look into the inner structures of the brain the era of modern neuroscience began. The beautiful drawings of Santiago Ramón y Cajal who used the silver staining technique developed by Camillo Golgi, provided one of the first visual evidence that networks of neurons were not cytoplasmically connected, as believed at the time, but that they communicated with each other at special contact points. These contact points were termed synapses (Greek sunapsis, point of contact) by Sherrington [2]. One of the first to suggest that the contact points between neurons were the places where changes occur during learning of a behavior were the Canadian psychologist Donald Hebb and the polish neurophysiologist Jerzy Konorski in the 1940s. They postulated that there has to be a coincident rule where the synapse linking two cells is strengthened when the cells are co-active at the same time [3, 4]. This postulate, widely known as 'Cells that fire together wire together', has been at the foundation of modern neuroscience ever since. The very first experimental evidence for strengthening of such a synapse came along in the early 1970s when Bliss and Lømo described long-term potentiation (LTP) [5]. Since then, LTP has attracted a lot of attention and has been widely used to study the mechanisms underlying learning and memory at the cellular and molecular level.

While many studies have investigated the structural changes at preexisting synapses, the function of newly formed synapses after plasticity has still remained speculative.

In my thesis, I set out to investigate the role of newly formed synapses after plasticity induction. To this end, I used organotypic hippocampal slices and followed the formation and functionalization of new synapses after LTP by using two-photon live cell structural and functional imaging.

2.1 The hippocampus

The hippocampal formation is found bilaterally in the medial temporal lobe of the brain at the floor of the inferior horn of the lateral ventricle. The term hippocampus which was derived from the Greek word for sea horse was first coined during the 16th century by the anatomist Arantius (1587) who found the striking resemblance of the shape of the hippocampus to that of the sea creature [6]. The pyramidal and granular cells of the hippocampus originate from the ventricular germinal layer and migrate to their final target regions [7]. Interestingly, while the pyramidal cell layer of the hippocampus forms quite early in development (during the first half of pregnancy) [8], the generation of the granule cells of the dentate gyrus takes much longer. It continues into the postnatal period and at a reduced rate into the adulthood, making the dentate gyrus one of the unique regions in the brain where adult neurogenesis can take place [9].

The hippocampal circuitry is well-established and depicted in Figure 2-1.

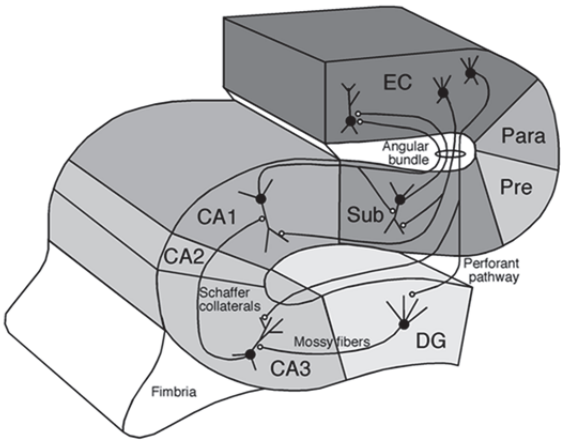

Figure 2-1: The hippocampal formation
Depicted are the components and internal connections of the hippocampal formation.
DG: dentate gyrus; CA: Cornu Ammonis; Sub: subiculum; Pre: Presubiculum; Para: parasubiculum; EC: entorhinal cortex. Figure taken from [6]

The hippocampal formation is comprised of the dentate gyrus, cornu ammonis area, which includes the CA3, CA2, and CA1 regions, the subiculum and the entorhinal cortex. The intrinsic

laminar hippocampal connectivity is quite well-known. Neurons from layer II of the EC project to the DG and the CA3 field of the hippocampus. The projections from the EC to the dentate gyrus represent the major hippocampal input path also known as the perforant path. This path is unidirectional since the dentate gyrus does not project back to the EC and the information is routed through the hippocampus before it can reach again the EC. The granule cells of the DG extend their axons, known as mossy fiber projections, to the proximal part of the apical dendrites of CA3 cells. Those then project their axons via the Schaffer collaterals to the apical dendrites of CA1 cells which project unidirectional to the subiculum. The information loop is closed by neurons from CA1 hippocampal region and the subiculum projecting back to the EC but now in its deeper layers. Despite the fact that the hippocampal formation is quite often viewed as an autonomous network on its own, it also has a broad range of afferent and efferent connections. The hippocampus receives input via the EC from the visual or auditory unimodal as well as polymodal cortical areas [10], from the amygdala, the septal area, and the contralateral hippocampus. Its outputs travel through the subiculum to the EC and via the fimbria and fornix mainly to the mammillary bodies and the septal area. Some fibers also project to the anterior thalamic nucleus, bed nucleus of the stria terminalis and ventromedial hypothalamic nucleus. The hippocampal formation is connected directly via the nonfornical fibers to the entorhinal area, the posterior cingulate, retrosplenial cortices and the amygdala [11, 12].

The function of the hippocampus has long been debated. Until the 1930s the hippocampal formation was considered to be part of the olfactory system. Another hypothesis was proposed by James W. Papez (1937) that the hippocampus was part of a circuitry involved in emotion. In his famous circuit (Papez circuit) he described the hippocampus as the place where all sensory information was collected and where an emotional ‘state’ was developed and transferred to the mammillary bodies [6]. This debate could finally be brought to an end after the undefeatable observations made on brain damaged patients by William Scoville and Brenda Milner in 1957 [13]. Their most famous patient, H.M., suffered from a severe anterograde and partial retrograde amnesia after a large part of his hippocampal formation and surrounding cortical regions were surgically removed to relieve his severe epileptic seizures. This observation placed the hippocampal formation as a major player in the learning and memory processes. Microelectrode recordings from single neurons in the hippocampus of

awake, intact animals revealed that the hippocampus can act as a cognitive map and helps animals form spatial memory and navigate in their environment [14].

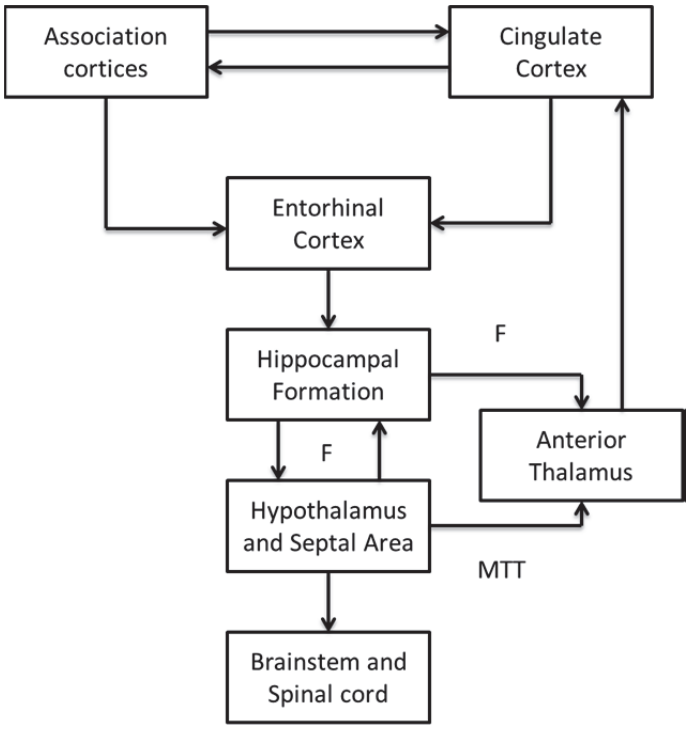

Figure 2-2: Connections of the hippocampal formation
The schema depicts the major afferent and efferent connections from and to the hippocampal formation. F: Fornix, MTT: Mammillothalamic tract.
Modified from [11].

Local field potential recordings from the hippocampus showed that there are two main types of oscillations i.e. synchronized neuronal activity – theta and gamma. Theta rhythm has relatively slow frequency (4 – 10 Hz) and has been detected in all mammals including humans [15, 16]. Those oscillations are associated with different behaviors (e.g voluntary movement and active exploration in rat) and are also present during REM sleep [15]. The second type of synchronized neuronal activity recorded from the hippocampus is the gamma oscillations, which range in frequency from ~ 25 - 140 Hz and are, therefore, beyond the range of conscious perception. They are not as stable as the theta oscillations, appear in bursts and are believed to synchronize activity in particular cell assemblies that are required for processing of certain information [17].

A major progress in the hippocampal research was made with the development of the hippocampal slice preparation [18-20]. With this preparation, hippocampal circuitry is preserved and neurons can be kept viable and studied for more than 10 hours (in acute slices) or for weeks (in organotypic slices). Furthermore, since hippocampal slices also support the induction and maintenance of LTP, they have emerged as a widely-used model for disentangling its underlying molecular and cellular mechanisms.

2.2 Long-term potentiation – a synaptic model of memory

The very first LTP experiment was performed by Bliss and Lømo [5]. They showed that a single burst of high frequency stimulation at the perforant path of the hippocampus of anaesthetized rabbits resulted in an immediate and long-lasting increase of the synaptic transmission at the postsynaptic connections in the dentate gyrus (Figure 2-3). Since then, LTP has become one of the most explored models for activity-dependent synaptic plasticity in the mammalian brain.

2.2.1 Basic properties of LTP

The three basic properties of LTP are: 1. input specificity, 2. cooperativity and, 3. associativity. Input specificity describes the property that only the contacts that receive the LTP-inducing stimulus are potentiated, while contacts that are farther than 70 µm from the potentiation site and receive control stimulation are not [21, 22]. Cooperativity means that a certain amount of presynaptic activity is required to trigger LTP [23]. Therefore, weak stimulation results in post tetanic potentiation (PTP) or short-term potentiation (STP) and only when enough fibers are activated and cooperate, LTP can be induced [24]. The last property – associativity, describes the property that even a weak stimulus can trigger LTP if it is synchronized with a strong stimulus that takes place in a separate but convergent pathway [25]. Those three LTP properties explain why a synapse can be potentiated if it is active at the same time when the dendrite it is found on is depolarized enough [24]. Therefore, also low frequency stimulation can trigger LTP as long as it occurs during a postsynaptic depolarization [26] and limiting the depolarization at a cell can block the induction of LTP [27].

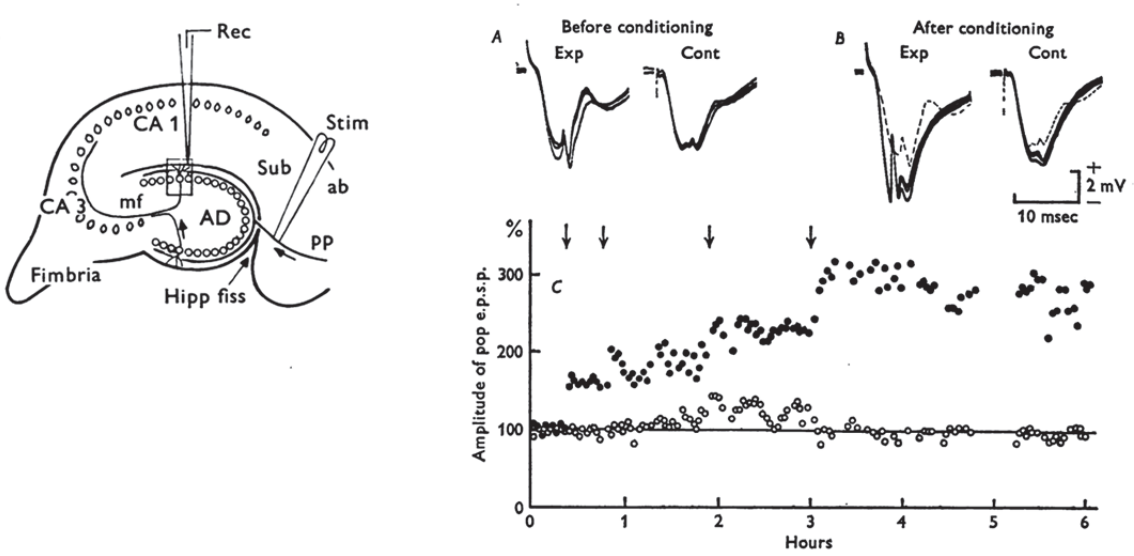

Figure 2-3: The original LTP experiment performed by Bliss and Lømo
On the left side: A diagram showing where the stimulating (Stim) and recording (Rec) electrodes were positioned. On the right side: Superimposed responses from both experimental and control pathway A) before stimulation and B) after the last high frequency stimulation train. The graph showing the amplitude of the population EPSP for the experimental pathway (filled circles) and the control pathway (open circles). Source [5].

2.2.2 LTP triggering mechanism

The most common form of LTP induction depends on the activation of postsynaptic N-methyl-D-aspartate receptors (NMDARs). However, not all synapses require the activation of those receptors to be potentiated. One of the most extensively examined NMDAR-independent form of LTP takes place at the mossy fiber synapses in the hippocampus, formed between the axons of the granule cells of the DG and the dendrites of CA3 cells [28]. Other synapses with such properties are found in the cerebellum (between the parallel fibers and the Purkinje cells) and in the corticothalamic projections [29, 30].

LTP at the majority of the CNS synapses, however, do depend on NMDAR activation. NMDARs are perfectly suited to support the coincidence detection properties of LTP because their activation can only take place if neurotransmitter binding coincides with membrane depolarization. At resting membrane potential the conductance of NMDARs is blocked by Mg^{2+} ions which are removed after depolarization-driven conformational shift. Therefore, during repetitive tetanic stimulation or direct postsynaptic depolarization the Mg^{2+} block is removed

from NMDARs allowing conductance of sodium, potassium and calcium ions. In this way postsynaptic, intracellular calcium concentration can rise, which is known to play a major role in the induction of LTP at the majority of CNS synapses. The local increase of calcium concentration fits with the input specificity of LTP, while associativity might occur because strong activation of some synapses might lead to a depolarization of a neighboring dendritic branch [31]. The most straightforward evidence in favor of the essential role of NMDARs and calcium for LTP induction comes from loss-of-function experiments. Block of NMDARs or buffering of postsynaptic calcium elevation by calcium chelators inhibits LTP induction [31, 32]. Interestingly, while certain changes in calcium concentration and dynamics can trigger LTP, others that do not reach the threshold for LTP induction, can result in STP or in long-term depression (LTD), a process associated with a long-lasting decrease in synaptic transmission [31]. Although NMDARs are the primary source for calcium influx, activation of voltage-gated calcium channels (VGCCs) can also substantially raise the intracellular calcium concentration. Furthermore, calcium-triggered calcium release from intracellular stores adds to the complexity and diversity of calcium dynamics and amplitude. Apart from the classical LTP that mainly depends on NMDARs activation, there are reports of different forms of LTP which also require the activation of metabotropic glutamate receptors (mGluRs). Induction of large amplitude or long-lasting late phase LTP by a strong or repeated stimulation protocols has been shown to involve the activation of mGluRs [33, 34].

There are numerous signaling pathways that translate the increased calcium concentration into enhancement of synaptic strength. However, one of the major contributors is the calcium/calmodulin-dependent protein kinase II (CaMKII). The activation of CaMKII can both mimic and occlude LTP [35]. Autophosphorylation makes CaMKII activity independent of calcium - calmodulin and, thus, biochemical cascades can be triggered long after calcium concentration has returned to baseline levels [36]. Furthermore, autophosphorylation is essential for LTP induction because single point mutation that prevents phosphorylation at the respective residue,Thr286, blocks LTP [37].

Another kinase reported to play a role in synaptic strengthening is cyclic adenosine 3', 5'-monophosphate (cAMP) – dependent protein kinase A (PKA). PKA enhances the effect of CaMKII activation by reducing the activity of protein phosphatase, known to dephosphorylate CaMKII and other target proteins [31]. An increase of intracellular cAMP and activation of the

PKA pathway are triggered by a brief treatment with Forskolin and Rolipram (F&R) which is used in this study [38].

It has long been debated over the locus of LTP induction and expression. It is now accepted that in the majority of CNS synapses both the pre- and postsynaptic side contribute. To involve the presynaptic side in synaptic strengthening a retrograde messenger needs to report the postsynaptic event presynaptically. Molecules considered as possible retrograde messengers are nitric oxide (NO), carbon monoxide and arachidonic acid [31]. NO is so far judged as the most likely retrograde messenger because inhibition of NO signaling impairs the induction of LTP [39, 40].

2.2.3 LTP expression mechanism

The expression mechanisms of LTP are diverse and complex. The simplest model for LTP expression suggests both postsynaptic changes including modifications of AMPARs function and number, and presynaptic changes such as an increase of neurotransmitter release probability. It is known that the activation of CaMKII and PKA following LTP induction results in the phosphorylation of AMPARs which enhances the channel conductance [41]. Furthermore, AMPARs are delivered to spines after induction of LTP, allowing the transformation of synapses from silent (possessing mainly NMDARs) to not silent (possessing both NMDARs and AMPARs). This was shown by both electrophysiological and optical tagging of AMPARs. Overexpression of the AMPARs subunits GluR1 result in the assembly of homodimeric AMPARs which show a different rectifying property compared to the wild type heterodimeric receptors. This unique electrophysiological signature revealed that increased CaMKII activity caused the delivery of the overexpressed AMPAR subunits to the surface [42]. Furthermore, another study showed that fluorescently tagged AMPARs were rapidly delivered into dendritic spines after tetanic synaptic stimulation [43]. The accommodation of AMPARs at the membrane is coordinated by the phosphorylation of multiple cytoskeleton components by CaMKII (Figure 2-4).

Presynaptically, synaptopHlourins were used to optically monitor activity-driven changes in synaptic function. SynaptopHlourin is a pH-sensitive variant of GFP that is fused to the lumenal domain of a vesicular protein, VAMP2. The fluorophore is only fluorescent when exposed to the pH-neutral environment after vesicular exocytosis. In this way, it was demonstrated that

the presynaptic function was enhanced following theta-burst or 200 Hz stimulation and this was sensitive to blocking L-VGCCs and not NMDARs [44].

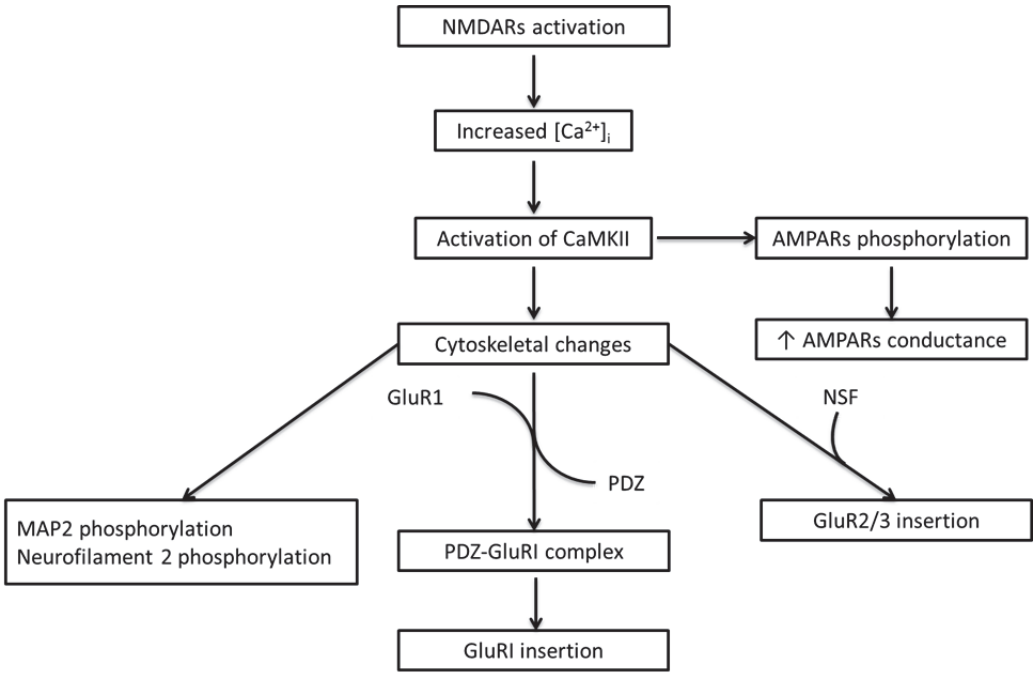

Figure 2-4: Signaling cascade initiated after NMDARs activation
The transient increase of internal calcium concentration leads to the activation of CaMKII which phosphorylates multiple targets. There is an increased AMPARs conductance as a result of direct channel phosphorylation by CaMKII and increased AMPARs recycling triggered by CaMKII induced changes in cytoskeletal proteins. Source [45].

While early LTP (E-LTP) depends mainly on posttranslational modifications, late phases of LTP (L-LTP) require translation and transcription to take place. The rapid effect of translational inhibitors on LTP suggests that the initial stages of L-LTP require protein synthesis from preexisting mRNA in the dendrites close to the potentiated synapses [6]. This has been persuasively demonstrated by the fact that isolated from the soma dendrites can support L-LTP induction and maintenance for as long as 5 hours via translation of preexisting mRNAs [46]. Moreover, ribosomes and other machinery required for protein synthesis are found at the dendrite close to many synapses [47]. Unlike translation, blocking transcription affects LTP with a further delay of several hours [48]. This delay is explained by the period of time required for the signal to travel from the stimulated synapses to the nucleus where gene transcription can be trigger. LTP induction is reported to upregulate the transcription of

multiple genes like immediate early genes (IEG) (*c-fos*, *zif268* and *arc/arg3*) [49]. Transcription factors essential for the activity-triggered gene transcription are those that bind to cAMP response elements (CREs) in the regulatory regions of target genes. Apart from IEG, there are multiple target genes for cAMP response elements-binding proteins (CREB), including those coding for neurotransmitters and peptides, growth factors and their receptors, structure-related proteins, proteins involved in cellular metabolism and others [6].

After their production, mRNA and proteins are transported back to the potentiated synapses where they are needed for stabilizing LTP. The hypothesis, how nuclear products 'know' for which synapses they are needed, was proposed by Frey and Morris (1997) [50] and is currently known as the 'synaptic tagging' hypothesis. According to this hypothesis, after potentiation synapses leave a protein-synthesis independent marker or a tag that is recognized by mRNAs or protein products coming from the soma. Although the true nature of the tag is still unknown, experimental evidence in support of this idea has been demonstrated. It was shown that giving a tetanic stimulation in one pathway could still generate L-LTP even in the presence of protein synthesis inhibitor if a second pathway was tetanized within a time window of several hours before or after the first tetanus [50]. Furthermore, it was demonstrated that E-LTP triggered by a stimulation that was too weak to induce L-LTP could be converted to L-LTP by a preceding or subsequent tetanus stimulation given to a second pathway. This is due to the fact that while the weak stimulus generated the tags, the strong stimulus could trigger the protein synthesis and the products would be caught at the tagged synapses [50].

2.2.4 Physiological significance of LTP – LTP and learning

LTP is a well-accepted model for investigating learning and memory. However, is LTP occurring in the brain of the living animals when they learn?

Indeed, it was shown by multi-electrode recordings in the hippocampus of living rats that, as they learnt a single-trial inhibitory avoidance task, there was an enhancement of the field potentials in some areas of the CA1 region. Most importantly, learning-induced enhancement of field potentials occluded the occurrence of subsequent LTP triggered by tetanic stimulation [51]. In another study, with the help of *in vivo* whole-cell recordings from somatosensory cortex layer 2/3 cells, the authors reported an enhancement of postsynaptic potential after giving a rhythmic 8 Hz whisker stimulation [52]. Furthermore, LTP and learning share many common mechanisms. For example, both LTP and place learning (a hippocampus-dependent

behavior task in spatial learning) are impaired after block of NMDARs activation [53]. Not only for LTP (see above), but also for learning changes in recycling of AMPARs play an important role. Sensory alteration in the barrel cortex by whisker trimming drove AMPARs insertion into synapses between layer 4 and layer 2/3 neurons of the barrel cortex [54]. Furthermore, it was reported that fear conditioning learning also required AMPARs trafficking because interfering with AMPARs insertion into a small population of neurons in the lateral amygdala prevented the acquisition of a fear memory [55]. Preventing the targeting of CaMKII RNA to dendrites inhibited not only L-LTP but also spatial memory, associative fear conditioning and object recognition memory [56], indicating the essential role of this kinase locally at the dendrites for plasticity induction. Another shared mechanism between LTP and learning is the activation of the cAMP/PKA signaling pathway. Mutant animals that lacked the enzyme adenylyl cyclase, and thus displayed reduced levels of cAMP, exhibited spatial memory deficits in the hidden platform version of the water maze task [57]. Furthermore, mutant mice expressing a dominant-negative form of the regulatory subunit of PKA displayed a normal initial learning of the hidden platform version of the water maze but showed deficits in the memory retrieval tests, suggesting that the activation of PKA during training sets cascades into motion that were important for memory storage [58].

2.3 Structural plasticity of dendritic spines

Currently, it is accepted that activity-driven functional changes in the neuronal network have an underlying structural correlate. This includes, on one hand, changes at preexisting synapses, and on the other hand, plasticity-driven formation of new functional contacts and elimination of old ones. The combination of those two types of structural changes provides the neuronal network with the flexibility to physically alter its connectivity in order to continuously accommodate, update and retrieve new information.

2.3.1 Structural changes at preexisting contacts

Synaptic plasticity has been shown to affect the shape and mobility of dendritic spines [59]. Furthermore, plasticity induction triggered by repetitive glutamate uncaging resulted in a rapid and selective enlargement of the stimulated spines [60]. This enlargement is associated both with an increase of synaptic strength and with synapse stabilization. The increase of synaptic

strength at preexisting synapses is to a large extent attributed to the change of the number and properties of receptors expressed on the spines [61]. Moreover, LTP-inducing stimulus at single spines promotes their survival [62]. Therefore, it is believed that the strengthening and stabilization of a subpopulation of spines are possible structural correlates of memory storage. The molecular mechanisms behind spine stabilization are overlapping with those contributing to synaptic plasticity (Figure 2-5). It has been shown that spine stabilization requires phosphorylation of multiple targets via CaMKII and protein kinase C (PKC) [63, 64], protein synthesis [65], and actin-regulatory proteins that control the spine actin cytoskeleton [66].

2.3.2 Remodeling of connectivity - spine and synapse turnover

There is an ongoing synapse turnover (synapse formation and elimination) in the brain throughout development and into adulthood [67]. Although the synapse turnover decreases with age, it never stops, thus providing the organism with the possibility of a continuous adaptation to its environment. In fact, multiple studies, both *in vitro* and *in vivo*, have shown that triggering plasticity leads to an enhanced spine turnover rate. Pioneering *in vitro* studies reported that induction of LTP resulted in the generation of new spines [68-70]. More recent work confirmed this finding and complemented it with the observation that LTP also promoted the destabilization of preexisting spines [71].

To investigate spine dynamics *in vivo* chronic two-photon imaging has been used in multiple studies which demonstrated that spine remodeling occurs after experience-dependent plasticity. It has been shown that adaptation to enriched environmental and alterations in sensory experiences (such as closure of one eye, i.e. monocular deprivation) required synapses assembly and disassembly and could lead to an increase in the spine density [65, 72]. Furthermore, learning of a motor task was shown to trigger rapidly, within hours, the formation of new spines. Moreover, the subsequent training stabilized the newly formed spines and their numbers correlated with how well the animal had learnt the motor task [73]. Another long-term spine imaging study revealed that a small fraction of new spines formed after motor learning or novel sensory experience was preserved for many months throughout adulthood, providing the putative long-lasting structural correlate of memory [74].

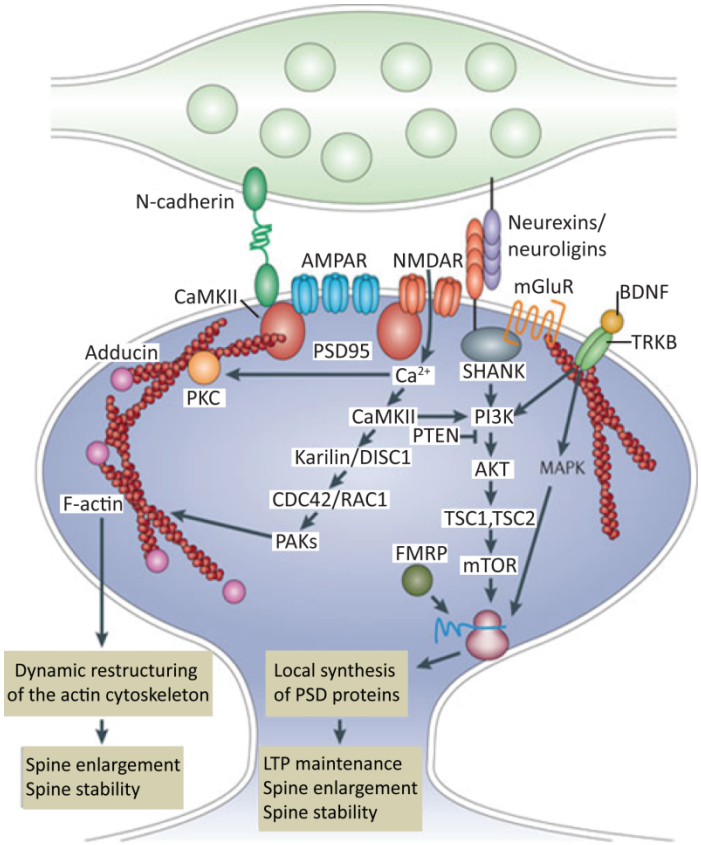

Figure 2-5: Activity-mediated stabilization of dendritic spines
Plasticity induction at synapses is associated with spine head enlargement, increased spine efficacy and synapse stabilization. Involved in these processes is the activation of protein kinases (PKC: protein kinase C and CaMKII: calcium/calmodulin kinase II), local protein synthesis (for example of BDNF: brain-derived neurotrophic factor, TRKB: tyrosine kinase B, MAPK: mitogen-activated protein kinase, PI3K: phosphoinositol 3-kinase, PTEN: phosphatase and tensin homologue, and others), proteins involved in the actin cytoskeleton (DISC1: disturbed in schizophrenia 1, adducing, CDC42: cell division control protein 42, RAC1: Ras-related C3 botulinum toxin substrate1). In addition, adhesion molecules (neuroligins, N-cadherins), proteins of the postsynaptic density (PSD95: postsynaptic density protein of 95 kDa, SHANKs: SH3 and multiple ankyrin repeat domains proteins), and AMPARs and NMDARs are implicated in LTP maintenance, spine enlargement and stabilization. [75]

Investigating spine changes in layer 5 pyramidal neurons in the mouse frontal association cortex during fear learning and fear extinction has demonstrated opposing changes at the spine level. While fear conditioning increased the rate of spine elimination, fear extinction resulted in spine formation. Interestingly, spine elimination and formation after fear conditioning and fear extinction, respectively, occurred at the same dendritic branch [76]. In another report it was demonstrated that plasticity induction triggered spine formation in the

vicinity of activated spines [71]. This observation was also supported by an *in vivo* study in which repetitive learning of a motor task resulted in a clustered spines formation and showed that clustered spines were more likely to persist than non-clustered ones [77].

Formation and elimination of synaptic contacts between neurons, i.e. synaptic rewiring, strongly increases the information storage capacity of the neuronal network [78]. The ability of the brain to recover from trauma, to store life-long memories while constantly acquiring new information must indeed require a vast storage capacity. The fact that the brain is a sparse neuronal network, meaning that the absolute number of neuronal connections represents only a small fraction of all possible connections between every given pair of neurons [79] makes the rewiring of connectivity a very powerful way of saving vast amounts of information. However, the ability of a postsynaptic cell to choose between multiple possible presynaptic partners presents the problem of how it efficiently 'identifies' the correct partners to connect to. This is an essential question that still remains elusive but the answer most likely involves a process of evaluation and comparison of geometrically reachable presynaptic partners which display the adequate patterns of activity. Taken together, rewiring of the connections between neurons after synaptic plasticity and learning offers a plausible mechanism of how the processes of learning and memory can occur (Figure 2-6).

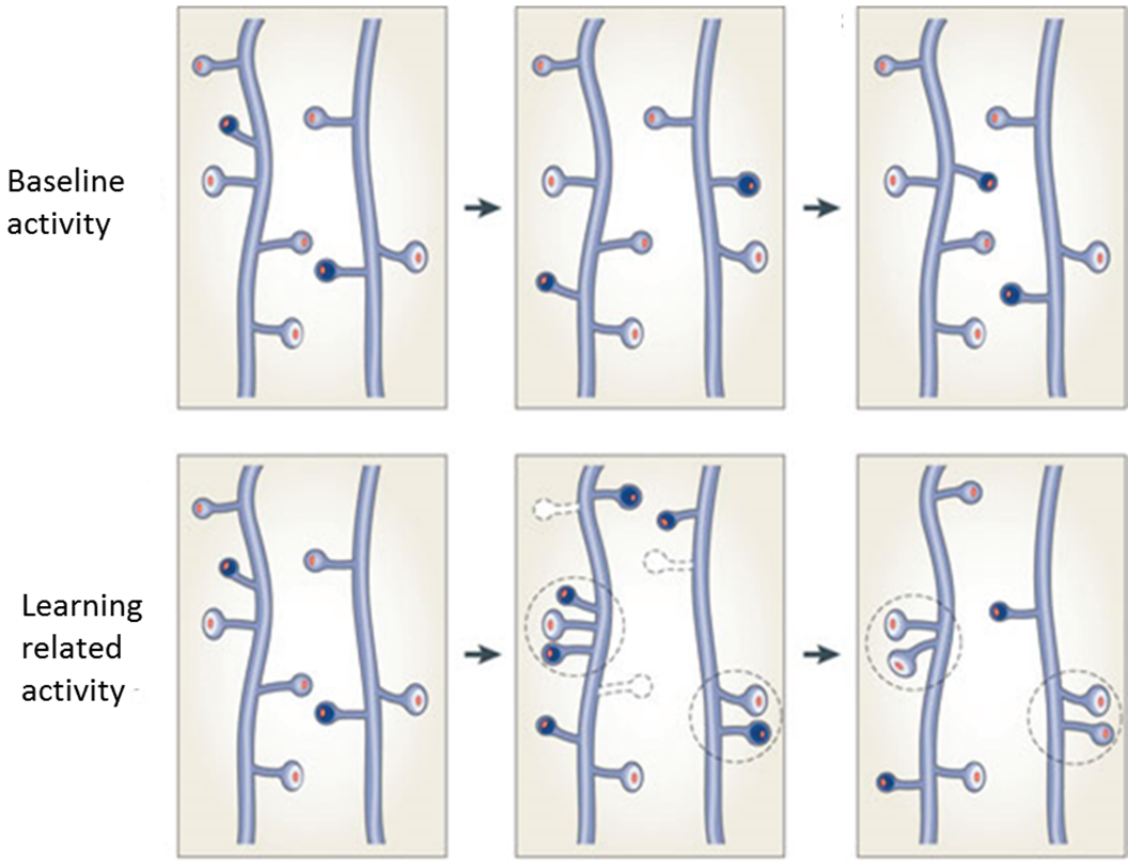

Figure 2-6: A model for structural rewiring of the neuronal network after learning
Schema showing spine turnover under baseline activity conditions where only a small number of transient spines (dark head spines) are affected and the majority of stable and persistent spines are left unchanged. Under conditions of learning-related triggered activity, spine turnover is enhanced, leading to the formation of more new spines (dark spines) and the elimination of preexisting spines (dashed-line spines). Despite the changes in connectivity, the spine density might stay unchanged. The new spines tend to occur in clusters (encircled areas) and exhibit a higher probability of getting stabilized [75].

2.4 Objective of the study

Long-term live cell imaging allows following spine changes both after LTP in brain slices and after learning in the living brain. This offers an unprecedented view of the inner workings of the brain and has revealed that both changes in synaptic strength at preexisting spines and formation of new spines take place after LTP and learning. It is believed that an increase of synaptic strength is essential for LTP induction and early LTP (E-LTP). However, it is still unclear

what the role of the new spines is? Based on current data, it is speculated that new spines, triggered by synaptic plasticity, might be the structural building blocks required for modifying the connectivity of the neuronal network so that it can continuously offer long-term storage of new information. However, the experimental proof for this is still missing. If new spines, indeed, support the later stages of the synaptic enhancement triggered by LTP induction, then they must form functional synapses with the axons that were activated during the LTP induction.

Therefore, I set out to test whether new spines formed after LTP build functional contacts with a subpopulation of axons that is co-active during the induction of plasticity (Figure 2-7). Furthermore, I want to address the still controversial question: how long does it take for a new spine to form a functional synapse?

To this end, I used organotypic hippocampal slices and controlled the locus of synaptic transmission with optogenetics and pharmacology. Thus, by using light stimulation I activated exclusively ChR2-expressing axons during LTP induction. I performed two-photon time-lapse imaging to detect the formation of new spines after LTP and spine calcium imaging after light stimulation to assess their functionality.

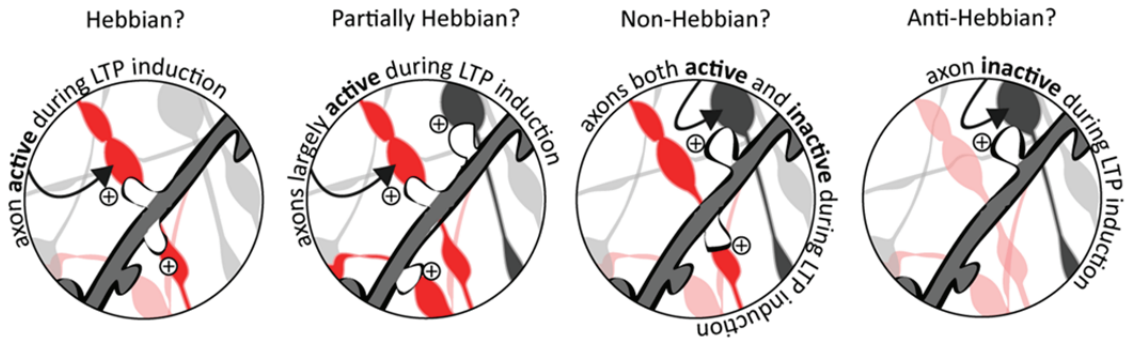

Figure 2-7: A schematic representation of the question behind the project
Do new spines (indicated with a plus) form synapses in a Hebbian manner i.e. only with active presynaptic partner (red boutons and axon), in a partially Hebbian manner i.e. more often with active than with inactive partners (black boutons and axons), in a non-Hebbian manner i.e. without any detectable preference for active or inactive presynaptic partners or in an anti-Hebbian manner i.e. only with inactive presynaptic partners?

3. Material & Methods

3.1 Material

3.1.1 Viruses

Virus	Titer (GC/ml)	Supplier
AAV2/1.Syn.ChR2(HR).eYFP	9.0 X 10^{11}	Penn Vector Core
AAV1.CAG.hChR2(H134R)mCherry.WPRE.SV40	6.7 X 10^{12}	Penn Vector Core

3.1.2 DNA constructs

DNA plasmid	Promoter	Resistance
pAAV- hSyn1-mTurquoise2-RSG-P2A-GC6s[1]	synapsin	Ampicillin

3.1.3 Chemicals

Chemical	Supplier
NaCl	VWR
KCl	Carl Roth GmbH
$CaCl_2$*$2H_2O$	Merck
$MgCl_2$	Sigma/Merck
NaH_2PO_4	Merck
$NaHCO_3$	Merck
$C_{14}H_{18}O_4$ (Trolox)	Sigma-Aldrich
D(+)-Glucose * H_2O	Carl Roth GmbH

[1] Complete sequence in Appendix A

K-Gluconate	Sigma Aldrich
4-(2-hydroxyethyl)-1-piperazineethanesulfonic acid (HEPES)	Sigma-Aldrich
ethylene glycol tetraacetic acid (EGTA)	Sigma-Aldrich
Magnesium adenosine triphosphate (MgATP)	Sigma-Aldrich
Sucrose	Merck
$MgSO_4$ * 7 H_2O	VWR/Merck
Minimum Essential medium (MEM)	Invitrogen/Gibco
Hank's Balanced Salt Solution (HBSS)	Invitrogen/Gibco
Horse Serum	Invitrogen/Gibco
KH_2PO_4	VWR/Merck
$MgCl_2$ * 6 H_2O	Merck
Kynurenic acid	Sigma
4-Aminopyridine (4-AP)	Sigma-Aldrich
Tetrodotoxin (TTX)	Biotrend/Tocris
D-Serine	Tocris
DL-2-Amino-5-phosphonovaleric acid (AP5 sodium salt)	Biotrend/Tocris
2,3-dihydroxy-6-nitro-7-sulfamoyl-benzo[f]quinoxaline-2,3-dione (NBQX disodium salt)	Biotrend/Tocris
Forskolin	Biotrend/Tocris
Rolipram	Biotrend/Tocris
Dimethyl sulfoxide (DMSO)	Sigma-Aldrich
Alexa 594	Life Technologies

3.1.4 Media and solutions

Media/Solution	Composition	Concentration (mM)
Artificial cerebrospinal fluid (ACSF)		
	NaCl	127.13
	KCl	2.50
	$CaCl_2*2H_2O$	3.70
	$MgCl_2$	0.15
	NaH_2PO_4	1.25
	$NaHCO_3$	16
	$C_{14}H_{18}O_4$ (Trolox)	1
	D(+)-Glucose * H_2O	20
	TTX	$1 X 10^{-3}$
	4-AP	$1 X 10^{-1}$
	Serine	$1 X 10^{-2}$
+ Forskolin and Rolipram		
	Forskolin	$5 X 10^{-2}$
	Rolipram	$1 X 10^{-4}$
K-Gluconate internal solution		
	K-Gluconate	140
	KCl	10
	NaCl	5
	HEPES	10

	EGTA	1×10^{-1}
	MgATP	2
Slice culture medium		
	95.5 MEM 1x	
	50 ml HBSS 1x	
	HEPES	12.5
	Glucose	45.83
Gey's balanced Salt Solution (GBSS)		
	$CaCl_2 * 2 H_2O$	1.5
	KCl	4.96
	KH_2PO_4	0.22
	$MgCl_2 * 6 H_2O$	1.03
	$MgSO_4 * 7 H_2O$	0.28
	NaCl	136.89
	$NaHCO_3$	2.70
	Na_2HPO_4	0.87
	D(+)-Glucose * H_2O	5.55
Slice preparation solution		
	98 ml GBSS	
	Kynurenic acid	1
	50 ml Horse Serum	
	Glucose	45.83

Cortex buffer		
	NaCl	125
	KCl	5
	D(+)-Glucose * H_2O	10
	HEPES	10
	$CaCl_2$*$2H_2O$	2
	$MgSO_4$*$7H_2O$	2
Electroporation solution		
	DNA (100ng/µl)	
	Cortex buffer	
	Alexa 594	0.05

3.1.5 Equipment

Material	**Supplier**
Slice preparation	
Dissection instruments	Fine Science Tools (FST)
Millicell cell culture inserts	Millipore
McIlwain tissue chopper	Mickle Lab Engineering,
Razor blade	Fine Science Tools (FST)
Dissection microscope	Nikon
Syringe filter Millex GP	Millipore
Syringe 50 ml BD Plastipak	VWR

6-well plates	TPP
Incubator	Thermo Scientific
Virus infections	
Borosilicate glass capillary (thick wall, 1.5 OD; 0.86 ID)	Harvard Apparatus
Horizontal puller P-97	Sutter Instruments Co.
Forceps (N°5)	Fine Science Tools (FST)
Pneumatic Pico Pump PV 820	World Precision Instruments (WPI)
Microscope	Olympus BX51W1
Micromanipulator	Luigs and Neumann
4x objective	Olympus Plan N 4x/0.10
Water bath	Julabe
Single cell electroporation	
Ultrafree –MC and –CL Centrifugal Filter	Millipore
Centrifuge 5415 R	Eppendorf
Vertical puller Model PC-10	Narishige
40x objective	Zeiss 40x/0.8 W
Axoporator 800A	Molecular Devices , Inc.
Two-photon microscope	
Vibration isolation optical table	Thorlabs
Mai Tai laser system	Spectra-Physics
Pockel cell	Polytec
MPM BCU conditioner unit	Thorlabs

MPM200 multiphoton system	Thorlabs
Dichroic mirror FF01-720/SP	Semrock
Primary dichroic mirror TLAB -0033	Semrock
Emission filter	Semrock
ND filter Optical density: 6.0	Thorlabs
LED (470 nm)	CoolLED
Shutter	Uniblitz
Shutter controller	Uniblitz
PMTs	Hamamatsu
PMT amplifiers	Thorlabs
Objective 40x	Olympus LUMPlanFI/IR 40x/0.8 W
Objective 5x	Zeiss Achrostigmat 5x/0.12
BNC-2090A DAQ	National Instruments (NI)
Electrophysiology	
Perfusion pump	Gilson
Nalgene 4mm syringe filters	Thermo Scientific
1 ml syringe Omnifix-F	B.Braun
MultiClamp 700 B Amplifier	Axon Instruments
Micromanipulators	Luigs and Neumann
Glass capillaries (thin-walled Gl. 1.50 D)	World Precision Instruments (WPI)
Software	
MATLAB	MathWorks

ImageJ	National Institutes of Health (NIH)
Scan image, Ephus	Janelia Farm
Mai Tai software	Spectra-Physics

3.2 Methods

3.2.1 Organotypic hippocampal slices

Hippocampal organotypic slices were prepared from Wistar rats of age P 5 - P 6 postnatal day according to the well-known and widely used protocol summarized by Stoppini et al. [19]. Hippocampal slices were placed on sterile, transparent membranes and could be kept in the incubator for several weeks. Before slice preparation all dissection instruments were disinfected with 80 % ethanol and dried using Bunsen burner. A razor blade was cleaned with cotton stick soaked with ether, disinfected with 100 % ethanol and fixed at the McIlwain tissue chopper under the laminal hood. Slice preparation medium was prepared and placed on ice under laminal flow hood where the entire preparation procedure was carried out. Rats were decapitated. Skin on the head was cut along the midline and removed to the side to expose the skull. The complete brain was then detached from the skull and placed in cold preparation medium. The hippocampi on both sides were isolated under dissection microscope. The dissected hippocampi were transferred to the McIlwain tissue chopper and 400 µm transverse sections were rapidly chopped. The freshly cut sections were immediately floated with cold preparation medium and separated from each other. The best sections were selected and transferred to fresh preparation medium. After 45 minutes incubation at 4°C the individual slices were carefully placed on a membrane of a cell culture insert in pre-warmed 6-well plates containing 1 ml culture medium per well. Two slices were positioned on each insert and the liquid around them was carefully removed with a pipette. Finally, the 6-well plates were placed in incubator at 35°C with 5%CO_2 enriched atmosphere where they remained until used for experiments. Half of the culture medium in each well was exchanged with fresh one roughly every 3-4 day.

3.2.2 Virus injections

In order to introduce ChR2 in a large population of CA3 cells in the hippocampal slices, AAV viral infection was used. A small virus aliquot (3 µl) (AAV1.CAG.hChR2 (H134R)-mCherry.WPRE.SV40 or AAV2/1.Syn.Chr2(HR).eYFP) was thawed on ice. Roughly 10 ml of cortex buffer was pre-warmed to 37°C in a water bath. A borosilicate glass capillary (1.5mm OD, 0.86 ID) was pulled on a horizontal puller (used parameters: Heat = Ramp + 20 = 760, Pull = 170, Velocity =120, Time = 120) to produce very long and thin hair-like ends. Then using sterile forceps roughly 1 cm of the tips of the glass capillary was broken to result in an opening of 10 µm. Inserts with slices (age of 1 – 3 DIV) were transported from the incubator to the virus injection/electroporation setup in 30 mm plates with pre-warmed medium. The chamber where the insert was placed was cleaned thoroughly with 70 % ethanol and filled with pre-warmed cortex buffer. Slices were kept at the interphase between cortex buffer and air during the injections. Under visual guidance (4x objective) a glass capillary backfilled with virus and connected to Pneumatic Pico Pump PV 820 was positioned above the CA3 hippocampal region. Before entering the tissue a test pressure pulse was given in order to assure that the pipette was not clocked and that a drop with a diameter of roughly 80 - 100 µm was produced. Injection settings were 20 psi 100 ms but they were varied slightly in order to produce roughly the same drop diameter for every injection. Finally, the pipette tip was carefully positioned into the tissue and three to four pressure pulses were given per location in the CA3 region. Usually 3 - 4 locations per slice were injected in order to cover the whole CA3 region (from dentate gyrus to CA2 region). After the virus injection, slices were returned to the incubator to allow the expression of ChR2. On average 2 weeks of ChR2 expression was allowed before the slices could be used for experiments (Figure 4-1).

3.2.3 Single cell electroporation

To express a structural (mTurquoise2) and a functional (calcium indicator GCaMP6s) marker in individual CA1 neurons, single cell electroporation (SCE) was used. The SCE protocol was adapted from Judkewitz et.al. [80]. Expression of these constructs allowed both to structurally visualize spines and to assess whether they possess a functional synapse with ChR2-expressing axons (Figure 4-1). Before every experiment slices were prescreened for fluorescence signal and only those that showed spine calcium responses to light stimulation were used further. The electroporation solution was sterile filtered with Ultrafree MC Centrifugal Filter (0.22 µm

pore size) and placed on ice. A borosilicate glass capillary (1.5 mm OD, 0.86 ID) was pulled with a vertical puller (temperature as follows: T1 = 72.6 arb .units, T2 = 48.0 arb. units) in order to obtain electrode tip resistance of 10 - 15 MΩ and the back of the electrode was fire polished. The chamber, where inserts with slices were placed, was cleaned thoroughly with 80 % ethanol and filled with pre-warmed cortex buffer solution. Slices (14 - 17 DIV) were kept at room temperature in submerged conditions during SCE. The tip of the electrode was backfilled with electroporation solution. Positive pressure was applied so that fluorescent electroporation solution could be seen to exit the pipette tip when an excitation light source (HBP lamp) was briefly switched on. Using a low magnification objective (4X) the glass electrode was positioned in the CA1 hippocampal region. Then, with a higher magnification objective (40X) and with acoustic output for monitoring the electrode tip resistance, the pipette tip was positioned next to a cell body and when resistance went up to 20 - 30 MΩ the positive pressure was released so that the pipette tip attached loosely to the cell membrane. Then a train of pulses of -12 V, 0.5 ms duration at 50 Hz for 1 second was given with the help of Axoporator 800A. One second after the end of the pulse train, pipette tip was gently retracted away from the cell and a positive pressure was reestablished before the next cell was targeted. Usually 3 - 4 CA1 cells were electroporated per slice. Finally, slices were returned to the incubator to allow expression of the injected DNA for another 3 - 5 days.

3.2.4 Electrophysiology

Whole-cell voltage-clamp recordings

Whole-cell recordings were made from CA1 pyramidal hippocampal neurons in slices expressing ChR2 in the presynaptic CA3 neurons. Slices were fixed at the floor of the recording chamber and submerged in carbonated ACSF (95%O_2, 5%CO_2) which was recycled via a perfusions system and a pump at a speed of roughly 0.5 ml/min. The time needed for a solution to reach recording chamber was measured before the experiments were performed and rechecked every time the pump or tubing were exchanged. Recording pipettes (resistance 3 - 5 MΩ) were prepared from glass capillaries (thin-walled) using a vertical puller (temperature t1 = 72 arb. Units, t2 = 48 arb. Units), fire polished and backfilled with filtered internal solution. After applying positive pressure (30 - 50 mbar) and injecting a negative rectangular voltage test pulse (5 mV) the recording electrode was carefully descended towards

the slice. After the pipette offset was corrected, the electrode tip was positioned next to a cell so that the positive pressure results in a dimple on the cell membrane. By removing the positive pressure (and sometimes applying slight negative pressure) at the pipette tip an instantaneous gigaseal conformation was obtained. A pulse of gentle suction was given to rupture the cell membrane and to go in a whole-cell configuration. Access resistance of roughly 10 - 20 MΩ was achieved. Postsynaptic currents triggered by light activation (470 nm) of ChR2-expressing axons were measured until access resistance increased by more than 20 % of the initial value when the recording was stopped.

Field recordings

Field excitatory postsynaptic potentials (fEPSPs) after light stimulation were recorded from the cell body layer of CA1 hippocampal neurons in slices injected with ChR2 (15 - 19 days post infection). Recording electrodes were prepared from thin-walled glass capillaries using a vertical puller (temperature setting: t1= 72 arb. units, t2 = 48.3 arb. units), fire polished and backfilled with filtered ACSF solution. Positive pressure was applied as the recording electrode was descended in the slice. In structural and functional imaging experiments the recording pipette was positioned in the immediate vicinity to the imaged CA1 cell. Positive pressure was reduced to a minimum, pipette offset was cancelled and fEPSPs triggered by light stimulation of ChR2-expressing axons were measured in current clamp mode at a gain of 100 and passed through 2 kHz Bessel filter and 1 Hz AC filter. Light stimulation intensity was set to evoke fEPSPs of half-maximum amplitude which ranged between 0.2 mV to 1.7 mV in the different experiments. However, in experiments where in addition to the electrophysiological recording structural and functional imaging was performed, light stimulation intensity was adjusted so that it resulted in spine calcium responses but not in global calcium spikes. Nevertheless, global calcium events during baseline recordings could not always be avoided. Light stimulation test pulse frequency was given once every 2 minutes unless stated otherwise.

LTP induction

LTP induction via pairing depolarization and light stimulation

Experiments were performed in the presence of TTX (1 µM) and 4-AP (100 µM) so that only ChR2-expressing axons could be externally activated with light while the remaining axons were

silenced. To test whether LTP can be induced under this condition I used a pairing protocol. In whole-cell voltage-clamp recording after a brief baseline collection (5 minutes), the cell was clamped at depolarizing potential (0 mV) and stimulated with 200 light pulses of 1 ms length at 2 Hz.

LTP induction by Forskolin and Rolipram (F&R) perfusion and light stimulation

To trigger input-specific LTP in a noninvasive manner I adapted a protocol from Otmakhov et al [81] and modified it to fit the experimental design. Throughout the experiment slices were perfused with ACSF containing low Mg (0.15 mM), serine (10µM), TTX (1 µM) and 4-AP (100 µM) at 32°C. Light test pulse stimulation was given once every 2 minutes to measure light evoked fEPSPs. After a minimum of 10 baseline measurement points, forskolin (50µM) and rolipram (0.1µM) were washed in for 15 minutes while test light pulse was continued at the test pulse frequency. If baseline fEPSPs responses were not stable experiment was stopped and a new slice was tested.

3.2.5 Two-photon laser-scanning microscopy

Imaging was performed on a Thorlabs multiphoton system MPM200 which was custom modified to fit the experimental design. Overview of the experimental setup is shown in Figure 3-1 A.

A Mai Tai laser system was used for two-photon excitation. It comprised of a solid state 532 nm laser that was used as a pump source for a mode locked Ti:Sa pulsed laser. This laser system can deliver output in the infrared region (from 700 nm to 1020 nm) at a femtosecond frequency. The laser beam was passed through a pockel cell (electro – optical modulator) in order to tune the laser intensity as desired before it entered the MPM-BCU beam conditioner unit (Figure 3-1B). In the beam conditioner unit the laser beam was directed by two mirrors through the beam expander. Next, another three mirrors delivered the beam to the periscope input where it followed the MPM200 Optical path (Figure 3-2). The attenuator was not used as its function was taken over by the electro-optical attenuator in front of the beam conditioner unit. The beam expander was adjusted to overfill the back aperture of the objective. After the beam conditioner unit, the beam entered the periscope that provided change of its elevation as it reached the scanning system. XY scanning at a speed of 30 frames per second at 512*512

A

1. Ti:Sapphire laser
2. Electro-optical modulator
3. MPM-BCU beam conditioner unit
4. MPM200 Multiphoton system
5. PSY24 motorized stage
6. Thorlabs ultra series optical table

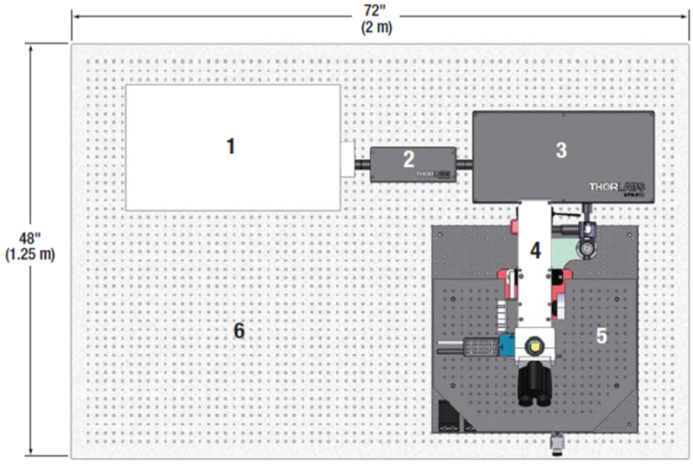

B

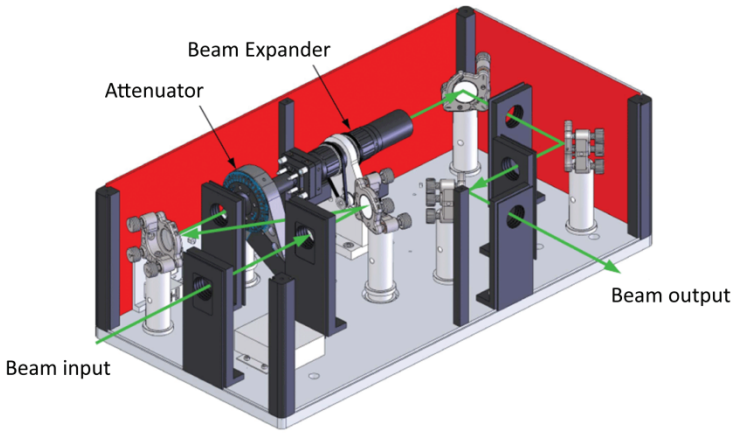

Figure 3-1: Setup diagram & beam conditioner unit
A) Imaging setup comprised of a laser (1), electro-optical modulator (2), beam conditioner unit (3) that feeds the laser beam into microscope (4). All components were positioned on a vibration isolation optical table (6). Illustration modified from Thorlabs. B) The beam conditioner unit consisted of 5 mirrors, attenuator and expander. It was used to optimize and align the laser beam before it entered the microscope. Illustration Thorlabs

pixels was achieved by galvo-resonant scanner pair. The scanning beam was passed through scan and tube lens. The primary dichroic mirror (TLAB-0033) transmitted the stimulation light to the sample and reflects the emission fluorescence to the detector module comprised of photomultiplier tubes (PMTs). A near infrared blocking filter prevented any scattered excitation light to enter the sensitive PMTs and emission filter (BrightLine HC 510/84) allowed detecting signal from Turquoise and GCaMP6s (GC6s). Two PMTs modules were mounted behind the objective (for epi detection) and two behind the condenser (for trans detection) so

that as many emitted photons as possible could be collected. Blue light stimulation for optogenetics required the integration of a secondary beam path. A 470 nm light emitting diode (CoolLED pE excitation system) was coupled to the system after the galvanometric scanner at a microscope body (Nikon) positioned above the laser beam path. The LED light was mirrored downward toward the objective. To allow blue light to access the specimen the prism mirror was substituted with a dichroic (FF01-720/SP) which transmitted blue light and reflected laser excitation light. Shutter protection was integrated in front of the PMTs to block any LED light from entering them. Due to space restriction only one of the two epi PMTs and one of the two trans PMTs were protected with shutters. The other PMTs were not used and optical density filters (optical density 6.0) were placed in front of them. Detected signal from each PMTs was amplified and combined for the epi and trans PMTs.

Data acquisition software ScanImage and Ephus (HHMI/Janelia Farm) were used for image acquisition, electrophysiological recordings and optogenetic stimulation. All output channels (e.g. shutter triggering, LED stimulation, pockel cell etc.) and input channels (e.g. frame acquisition time, electrophysiology recordings, imaging etc.) reached through NI DAQ boards (BNC-2090A) the external device or the data acquisition PC, respectively. As a master acquisition trigger the shutter in front of the 2P laser was used. Usually 2785 ms after the first frame was acquired the shutters in front of the PMTs were closed, a single light pulse of 5 ms length was delivered and the shutters were reopened 20 ms after closing so that the remaining of the in total 200-300 frames could be recorded.

3.2.6 Image acquisition

Structural and functional imaging required different stimulation wavelength from the same laser so they could only be performed in an alternating fashion. All images were acquired with 40x objective (Olympus LUMplanFI/IR 40x/0.80W). A dendritic stretch was imaged at 840 nm for Turquoise signal and at 980nm for GCaMP6s signal. Structural data comprised of 3D image stacks where individual z-planes were acquired at a distance of 0.5 µm from each other. The field of view typically spanned 77 µm x 77 µm in x/y (1024 x 1024 pixels). Image acquisition took place at a frame acquisition speed of 15 Hz. For functional (calcium) imaging an individual z–plane was imaged with a typical field of view of 32 µm x 32 µm (256 x 256 pixels) at a frame acquisition speed of 60 Hz. The light stimulation typically consisted of one 5 ms pulse with

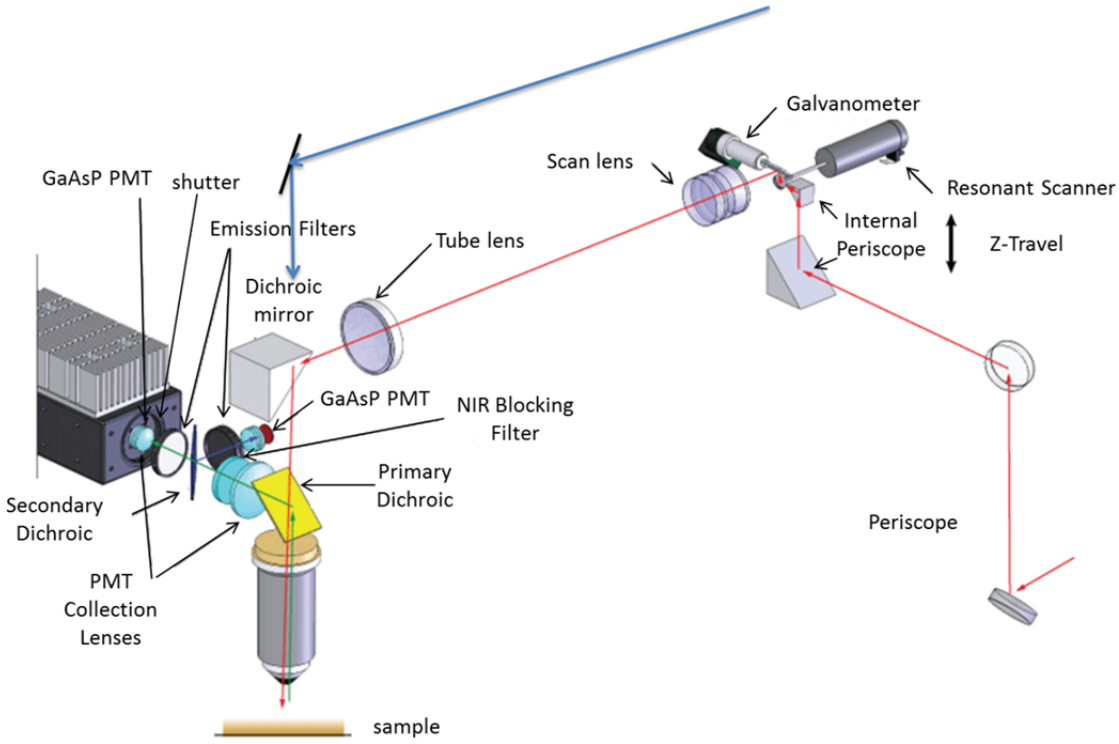

Figure 3-2: Light path of the laser (red) and the LED (blue) beam
The light path of the MPM200 system was optically separated from the wide field/LED path. The laser beam was passed through a periscope, scanning system, reflected by a dichroic (FF01-720/SP) and transmitted by the primary dichroic (TLAB-0033) to the sample. The LED beam travelled above the laser beam. It is reflected downwards, transmitted by the dichroic and the primary dichroic to the sample. Emission fluorescence from the sample was reflected by the primary dichroic, cleaned from remnant IR light and entered through the emission filters the PMTs. The shutter in front of the PMTs was synchronized to the LED pulses. It was closed shortly before a LED pulse was given and opened shortly after the end of the pulse in order to prevent any LED light to enter the PMTs. Illustration modified from Thorlabs.

power below 2 mW (experimental day 1) and below 3.5 mW (experimental day 2) as measured after the objective. Light stimulation was delivered through a closed field aperture (diameter roughly 70 µm). For every experiment, light stimulation intensity was adjusted to trigger spine calcium responses and kept constant throughout experimental day 1. During calcium imaging acquisition usually 100 baseline frames were collected, followed by closing of the shutter to protect the PMTs as the light stimulation was delivered (1 - 2 frames). After reopening of the shutter the remaining of the in total 200 - 300 frames were collected. Due to time jitter between the opening of the 2P shutter and the actual image acquisition, the number of baseline frames could vary between individual calcium imaging trials. Therefore, frame

acquisition time and stimulation time were recorded in order to extract the exact number of baseline and post stimulus frames on trial to trial basis.

3.2.7 Experimental timeline

All experiments were performed in ACSF with low Mg^{2+} (0.15 mM) concentration and in the presence of 4-AP (100 µM), TTX (1 µM) and serine (10 µM). The apical dendrites of Turquoise2AGC6s-expressing CA1 cell were screened for spine calcium responses at different LED stimulation intensities in order to identify an area where ChR2-positive axons were present. If there were no spine responses after light stimulation, the slices were discarded. If clear spine responses were present, stimulation intensity was adjusted so that it triggered spine responses but not global calcium dendritic spikes (10 - 25%, up to 1.5 mW, measured after the objective). However, global calcium events could not always be avoided (Figure 4-17). Next, the first structural z-stack of a stretch along the apical dendrite was taken (t1) and the dendritic stretch was re-imaged six times every 40 minutes on the first experimental day (Figure 4-3). Experiments were performed under 4 conditions: in control 1 the slices received neither light stimulation nor F&R treatment during the LTP induction phase; in control 2 the slices were stimulated with light and perfused with a vehicle solution; in control 3 only F&R treatment was applied, and in optical LTP, light stimulation was combined with F&R treatment. In experiments in which optical LTP or control 2 treatment was used, between structural imaging stacks, light-evoked fEPSPs and spine calcium responses were measured roughly once every 2 minutes. After the second structural image either F&R or vehicle was perfused for 15 minutes while light stimulation was continued at baseline frequency (in plasticity treatment: LTP induction phase). To identify new spines during the experiment, raw image stacks after each structural time point were collapsed into a maximum intensity projection and registered for shifts relative to the first structural time point using Linear Stack Alignment with SIFT (ImageJ). At the end of experimental day 1 the slice was placed on a fresh membrane and left in normal culture medium in the incubator for the overnight time. On the next day, experimental day 2, the last (after overnight incubation) structural image was acquired on the same dendritic stretch. Finally, spine calcium imaging was performed systematically on all spines from the structural field of view at different z-planes to further evaluate the light-responsive fraction of preexisting and new spines. LED stimulation intensity on experimental day 2 was set higher than on experimental day 1 (up to 70 %, roughly 3 mW after the

objective). In this way potentially all preexisting spines that functionally connect to ChR2-expressing axons could be detect and this could be used as estimation for the innervation density of ChR2-positive axons. In experiments with control 1 and control 3 conditions, slices did not receive blue light stimulation before the last structural image was acquired on the first experimental day. Therefore, spine calcium signals were mainly recorded after the last structural imaging time point of the first experimental day and during the second experimental day.

3.2.8 Image analysis

Image analysis was performed using ImageJ and custom-programmed MATLAB software and functions.

Structural data

Spine dynamics (gain and loss) over time was analyzed in three dimensions using custom MATLAB software (spineAnalysis, ScanImage HHMI/Janelia Farm). In the analysis only spines were included that pointed laterally from the dendritic shaft for more than 5 pixels (0.37 µm) and had average pixel intensity higher than the sum of the mean background intensity and 3 fold its standard deviation. All visible spines along a dendritic stretch irrespective of their shape were annotated. The spines on a dendritic stretch were annotated independently for every imaging session (time point). For each two consecutive imaging sessions the annotated spines were compared to determine if they were preserved, lost or gained. For every experiment a matrix of numbers was extracted that summarized the spine dynamics. In this matrix, each spine received a unique identification number and a persistence value for every imaging session (time point) depicting whether the spine was present (persistence value = 1), lost (persistence value = 2) or gained (persistence value = 3). Persistence value of 4 indicated transient structures which appeared at one imaging session and disappeared at the next one. All further structural analysis was performed on the obtained from each experiment matrix of numbers (spine summary table).

Functional data

Light-triggered calcium responses of new and preexisting spines over time were analyzed using ImageJ and custom written functions in MATLAB.

Drawing region of interests (ROIs) for spines and dendrites

First, all calcium imaging trials performed in one experiment were loaded and opened with a custom-written MATLAB function (MRPcv). For every trial, the mean fluorescence signal from the baseline imaging frames was used to visualize a dendritic stretch with its spines. Around each spine and a dendrite stretch in its vicinity polygon regions of interest (ROIs) were drawn. Each spine and its corresponding dendritic ROI received a unique group number which was kept the same for the whole experiment. When a particular spine/dendrite pair was out of the field of view (FOV) or out of focus for the particular trial their group was kept empty. One group contained ROI from the background signal. In ImageJ the raw image (both maximum intensity projection and 3D image stack) of the first structural time point, taken at the beginning of the experiment was loaded. Using the multi-point tool in ImageJ, spines visible in the first structural imaging session were marked in parallel to drawing the spine and dendrite ROIs in MRPcv. In this way, new spines were identified because they were not detected in the structural image made in the beginning of the experiment but were present later on when the functional imaging trials were acquired. When a new spine was identified, its ROI was labeled as 'new spine'. To identify the time of spine formation the structural imaging session was identified when the spine was visible above background for the first time. In particular, the mean spine ROI fluorescence signal was higher than the sum of the mean background fluorescence signal and 3 fold its standard deviation. The 'birthday' of a new spine was then approximated by taking the acquisition time of the last structural time point before the spine became visible. So, for example, if a spine became visible in structural imaging session 2 (time point 2 or t2) then it formed between the first and the second structural imaging sessions and would receive a birthday value of 1. Its time of formation would be approximated with the time when the first structural imaging session was acquired. After ROIs were drawn around all spines and their dendrite in the FOV (Figure 3-3A), ROIs coordinates were saved as a MAT file. For the next calcium imaging trial the same ROIs coordinates were loaded and readjusted if the same or neighboring z-plane was imaged or drawn new if the imaged FOV or z-plane was changed.

$\Delta F/F_0$ calculation and spine calcium response

After spine/dendrite pairs from all calcium imaging trials acquired in one experiment were marked, calcium analysis was performed. For every trial, the image file, the MAT file containing

the saved ROIs and the Ephus file (termed XSG files) were loaded. A single XSG file contained information from all running during the experiment Ephus programs. This file was used to extract the number of frames acquired before and after light stimulation, the time when every trial was recorded, name of the experiment, the treatment protocol applied etc. The mean value of all pixels enclosed in each drawn ROI represents the GCaMP6s fluorescence intensity signal for the respective spine or dendrite for the time point at which the respective frame of the trial was acquired. Each trial contained around 200 - 300 frames. For calcium responses, the change of GCaMP6s fluorescence signal intensity after stimulation (ΔF) was calculated. Background fluorescence intensity signal was subtracted. The mean ROI fluorescence signal of all frames before stimulation (F_0) was subtracted from the ROI fluorescence signal in all frames (ΔF) and the result was normalized by dividing with F_0 and multiplying with 100. This resulted in $\Delta F/F_0$ and was used for subsequent analysis as the calcium response value. The peak of the calcium response was calculated as the maximum $\Delta F/F_0$ value after smoothing using a 7-point moving average. A calcium response after light stimulation was considered successful when the peak $\Delta F/F_0$ signal exceeded the sum of the mean baseline fluorescence signal (F_0) and 3 fold its standard deviation. A spine calcium response was considered successful, meaning a spine received presynaptic input from a ChR2-positive axon, when light stimulation triggered a successful calcium response in the spine but not its corresponding dendrite (Figure 3-3B, case 1). In cases, where both in the spine and in its dendrite the fluorescence signal increased above baseline (Figure 3-3B, case2), it was checked whether the fluorescence signal increased first in the spine and then in the dendrite. If the calcium response in the spine preceded that in the dendrite it was considered a successful spine calcium response to light stimulation. To test whether the increase of calcium signal took place first in the spine, the amplitude of the calcium responses in the spine and its dendrite were scaled to each other and each was fitted to an exponential curve. In this way, the time of calcium signal increase was calculated independently of the signal amplitude. If the acquisition frame at which the spine calcium signal reached 67% of its maximum preceded the frame at which the dendritic calcium signal reached 67% of its maximum, the spine was considered to be responsive (Figure 3-3B case 2.1). If the exponential curve was not a good fit due to noise, the frame after stimulation when the half maximum of the scaled signal was reached was compared between the spine and its dendrite (Figure 3-3B case 2.2). If the signal in the spine reached its half maximum earlier than the signal in the dendrite, the spine was considered responsive. For every trial, the raw calcium

response traces of the spines and dendrites were visually inspected to confirm the calculated results and only then saved. Finally, the spine calcium responses from all calcium imaging trials from one experiment were combined together in one final MAT file (ROI3). In the end, the information about new spines' 'birthday', the structural images acquisition times and the presence of new spines after overnight incubation was added. All further calcium imaging analysis was performed on the ROI3 MAT files.

Equalizing spine calcium imaging trials

In experiments without light stimulation during the LTP induction phase and the first 6 structural imaging time points on the first experimental day (control 1 and control 3), spine calcium responses after light stimulation were mainly recorded on the second experimental day. Therefore, the number of calcium imaging trials acquired from each spine under those conditions was on average smaller compared to the number of functional trials acquired in plasticity treatment and light-only control (control 2) experiments. To equalize the number of spines and trials per spine between no-light control experiments (control 1 and control 3) and plasticity treatment experiments, the following procedure was used (as schematically depicted in Figure 3-4). In brief, spine calcium imaging trials from all experiments from the same treatment were pooled together. Functional imaging trials recorded from spines that received plasticity treatment were shuffled and a subpopulation was selected at random so that it was

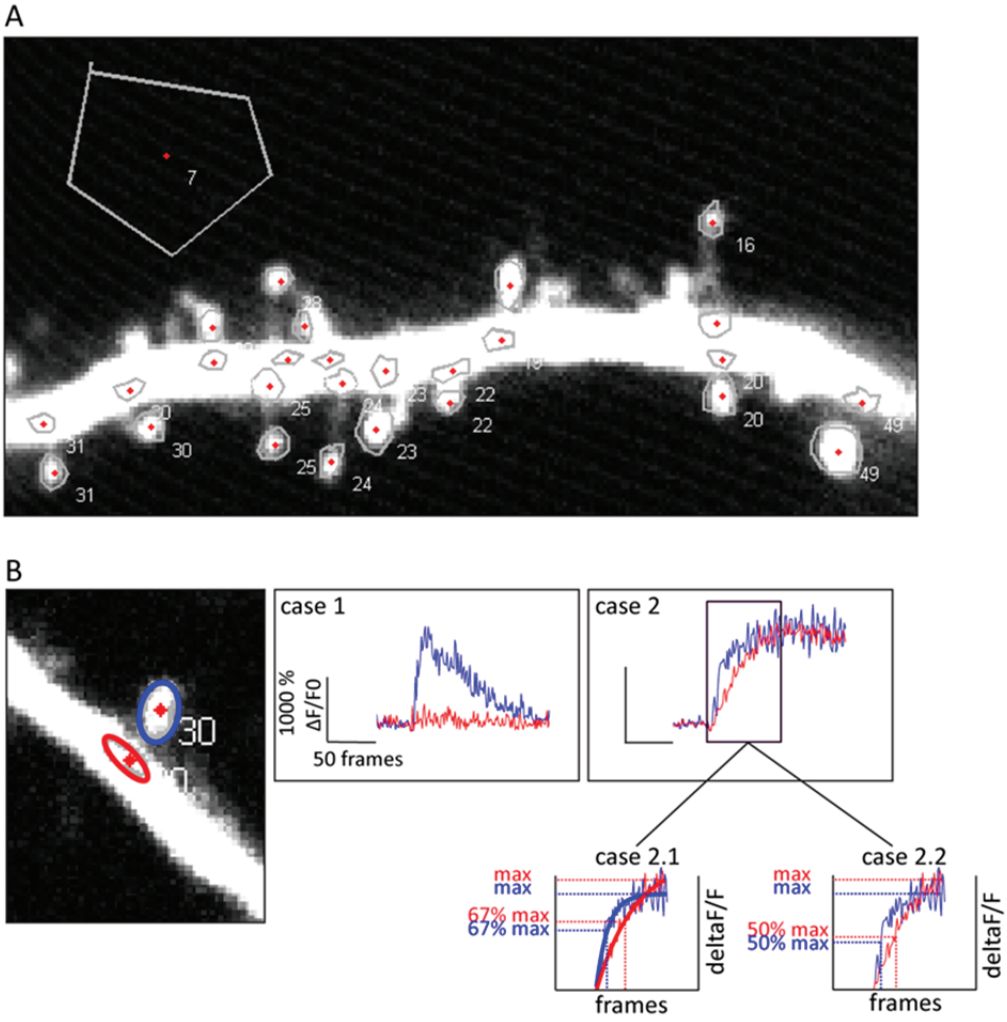

Figure 3-3: Criteria for a successful spine calcium response after light stimulation

A) A typical field of view from a single calcium imaging trial after ROIs were drawn around spines and their corresponding dendrites. One ROI was drawn to measure background fluorescence signal (group number 7). B) An image shows a typical spine ROI (blue) and its corresponding dendritic ROI (red). On the right side example $\Delta F/F_0$ traces depict cases when a spine was considered responsive after light stimulation i.e. received an input from a ChR2-expressing axon. In case 1, the spine showed calcium response after stimulation while its dendrite did not. In case 2, both in the spine and its dendrite an increase in the calcium signal after stimulation was detected. To test whether the spine calcium signal increased first, an exponential curve was fitted and the frame when the calcium signal reaches 67% of its maximum was extracted from the fit (case 2.1). Alternatively, the frame when the calcium signal reached half maximum was compared between the spines and its dendrite (case 2.2).

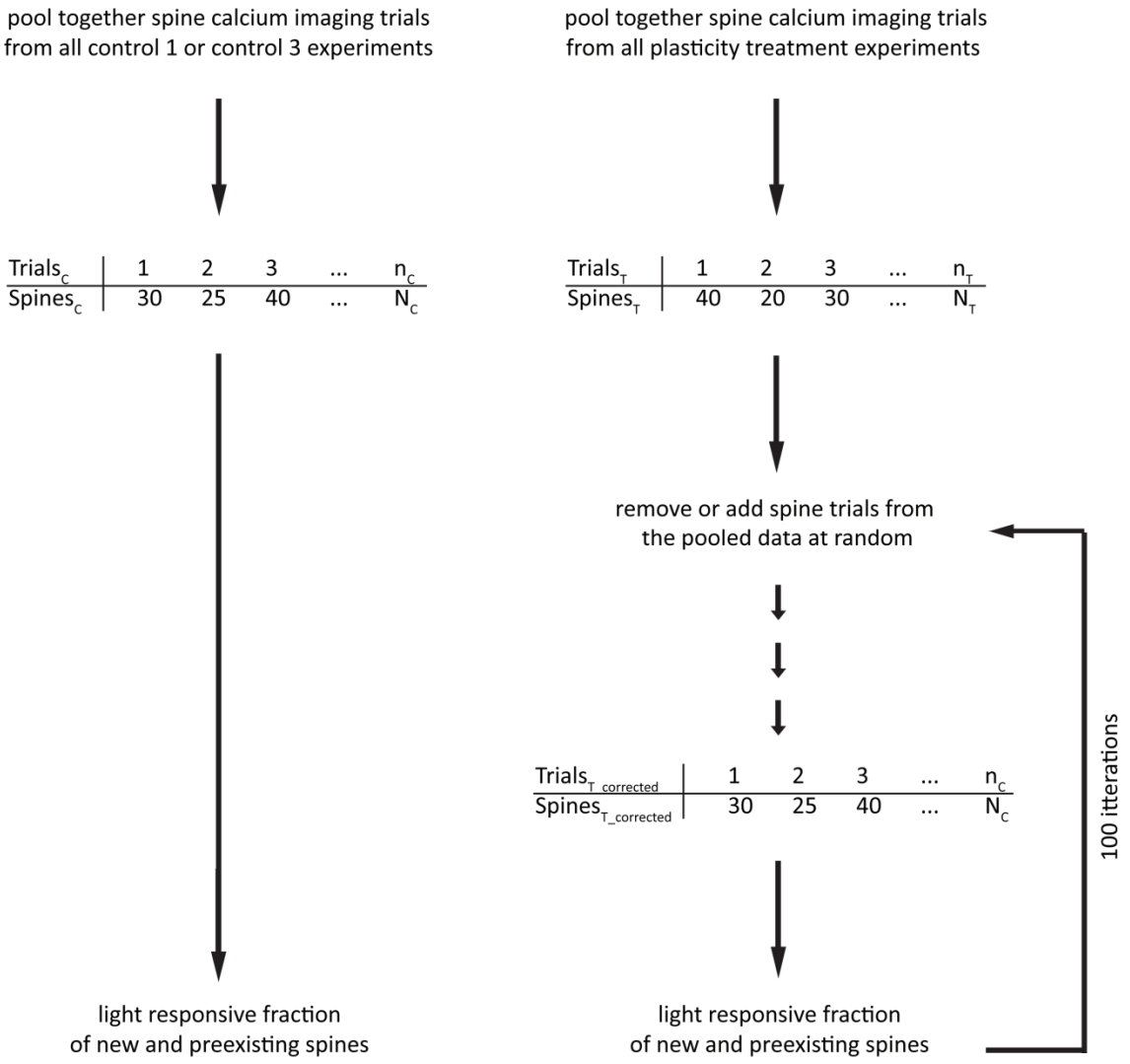

Figure 3-4: A schematic representation how spine functional trials were equalized between different treatment conditions

From all experiments from one treatment condition the total number of spines that received the same number of calcium imaging trials (ranging from one to the maximum number of calcium imaging trials acquired from the spines) was extracted. In the depicted example, from all control experiments there were 30 spines that received one calcium imaging trial, while in treatment experiments the number of spines that receive one calcium imaging trial was 40. Spine calcium imaging trials collected under plasticity treatment conditions were added or removed at random until the number of spines and trials per spine were equalized to those of the respective control. After the spine trials were equalized the light-responsive spine fraction was calculated. This was repeated 100 times.

equal to the number of spines and trials per spine acquired in the respective control experiments (control 1 or control 3). After equalizing the number of spines and trials per spine,

the light-responsive spine fraction (the number of light-responsive spines expressed as a fraction of all spines) was calculated. Similar approach was used to equalize the spines and trials per spine between new and preexisting spines within the same treatment group.

3.2.9 Statistics

The results are reported in mean ± standard error of mean (SEM) or mean ± standard deviation (STD) as indicated in individual figures. Statistical significance of the effect of optical LTP was measured with paired two-tailed t-test. Statistical significance of the effect of different treatments on structural spine dynamics was measured using Kruskal-Wallis test (nonparametric test for multiple unpaired groups) or Friedman test (nonparametric test for multiple paired groups) followed by Tukey-kramer or Bonferonni posthoc test to correct for multiple comparisons. Mann-Whitney U test was applied when only 2 groups were compared. Cumulative distributions were compared by using Kolmogorov-Smirnov test. Asterisks indicate significance values as follows: * $p<0.05$, ** $p<0.001$.

4. Results

4.1 Experimental approach

The goal of this project is to determine whether new spines that form after LTP make functional synapses with axons that were activated during the LTP induction. In order to address this question, is it essential to differentiate between active and inactive boutons and to be able to experimentally control the active population of axons during the LTP induction. To this end, a pharmacological and optogenetic approach called subcellular ChR2-assisted circuit mapping (sCRACM) [82] was used. By using sCRACM, activity can be triggered exclusively in ChR2–expressing axons and blocked elsewhere. In order to activate the axons of the presynaptic cells with light, AAV CAG ChR2HR mCherry virus was injected in the CA3 region of an organotypic hippocampal slice. Individual postsynaptic cells (CA1 pyramidal cells) were targeted via SCE and expressed mTurquiose2AGC6s (Figure 4-1).

To silence spontaneous activity in the slice, action potential generation was inhibited by blocking voltage-gated sodium channels with bath application of tetrodotoxin (TTX, 1 µM). Furthermore, to allow sufficient depolarization of ChR2-expressing boutons, a population of voltage-gated potassium channels responsible for the slow inactivating transient potassium currents (I_D currents) was blocked by bath application of 4-aminopyridine (4-AP, 100 µM). I could successfully reproduce the sCRACM approach and detect light-evoked excitatory postsynaptic currents (EPSPCs) as measured by voltage clamp recordings from CA1 cells (Figure 4-2).

To visualize synaptic contacts, I imaged spine calcium signals with the genetically encoded calcium indicator GCaMP6s [83] after optogenetic activation of ChR2-expressing axons. The detection of spine calcium influx through NMDARs was facilitated by a low external Mg^{2+} concentration (0.15 mM) and the presence of serine (10 µM) in the bath. A recording electrode placed in proximity to the imaged cell was used to measure light-triggered fEPSPs and to follow the induction and maintenance of LTP. Light-evoked calcium spine responses were measured as a proxy for functional synapses. Therefore, light-triggered calcium responses in newly formed spines indicated that they had built functional synapses with ChR2-expressing axons which were also activated during the LTP induction. Furthermore, the

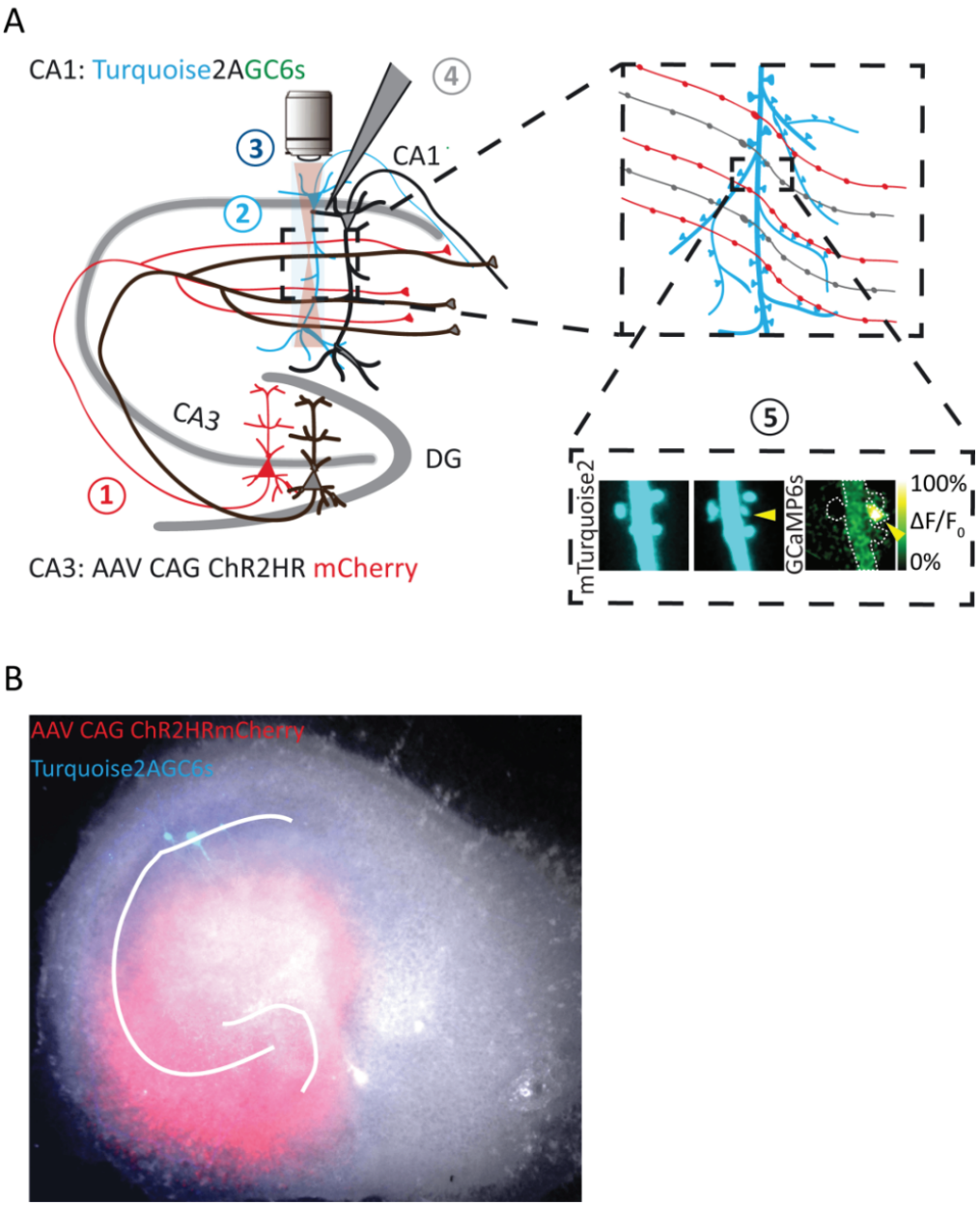

Figure 4-1: Experimental approach

A) CA3 cells expressing ChR2mCherry (1) are schematically depicted in red and individual CA1 cells expressing Turquoise2AGC6s (2) in blue. Local light stimulation through the objective as depicted in (3) is used to depolarize and trigger synaptic transmission exclusively from ChR2-positive axons under conditions of blocked endogenous activity in the slice. A recording electrode is used to measure light evoked fEPSPs (4). Structural and functional imaging is used to identify new spines and test whether they show light-triggered calcium responses i.e. contact ChR2-positive axons (5). B) Overview of an organotypic hippocampal slice expressing ChR2HRmCherry in CA3 region (red) and Turquoise2AGC6s in individual CA1 cells (blue).

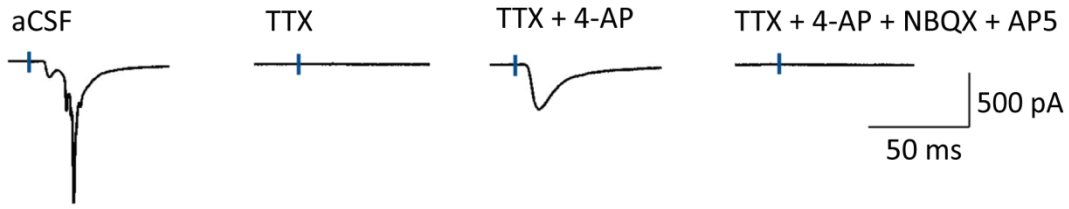

Figure 4-2: Light-evoked synaptic transmission between ChR2-expressing axons and CA1 apical dendrites
Whole-cell recording from CA1 pyramidal neuron after light stimulation (blue bar) of CA3 axons expressing ChR2HReYFP. In the presence of TTX alone light-evoked EPSCs could not be detected. After addition of 4-AP, depolarization in ChR2-expressing axons was prolonged and neurotransmitter release could be detected. Light-evoked currents were sensitive to glutamatergic neurotransmission block and were blocked after application of 2,3-dihydroxy-6-nitro-7-sulfamoyl-benzo[f]quinoxaline-2,3-dione (NBQX) and 2*R*-amino-5-phosphonovaleric acid (AP5).

fraction of preexisting spines that showed functional responses to light stimulation provided valuable information about the density of light-activated ChR2-positive axons along the imaged dendritic stretch.

4.2 Experimental timeline

Experiments were performed on slices after 16 - 23 days *in vitro* (DIV), 15 - 20 days post infection with AAV virus containing ChR2HRmcherry and 3 - 5 days post electroporation with Turquoise2AGC6s, a time window that provided optimal expression of all the constructs. To follow the formation of new spines and access their responsiveness to light stimulation the experimental timeline shown in Figure 4-3 was used (for more details refer to section: Experimental timeline in Material & Methods). Slices received either optical LTP treatment (plasticity treatment) or one of three control treatments. In plasticity treatment slices received light stimulation and 15 minutes perfusion of F&R (LTP induction phase). Slices that received control treatment 1 (control 1) were neither stimulated with light nor with F&R. In control treatment 2 (control 2), slices received light stimulation and 15 minutes perfusion of vehicle solution (DMSO 0.05%). In control treatment 3 (control 3) slices were not stimulated with light but received 15 minutes perfusion of F&R.

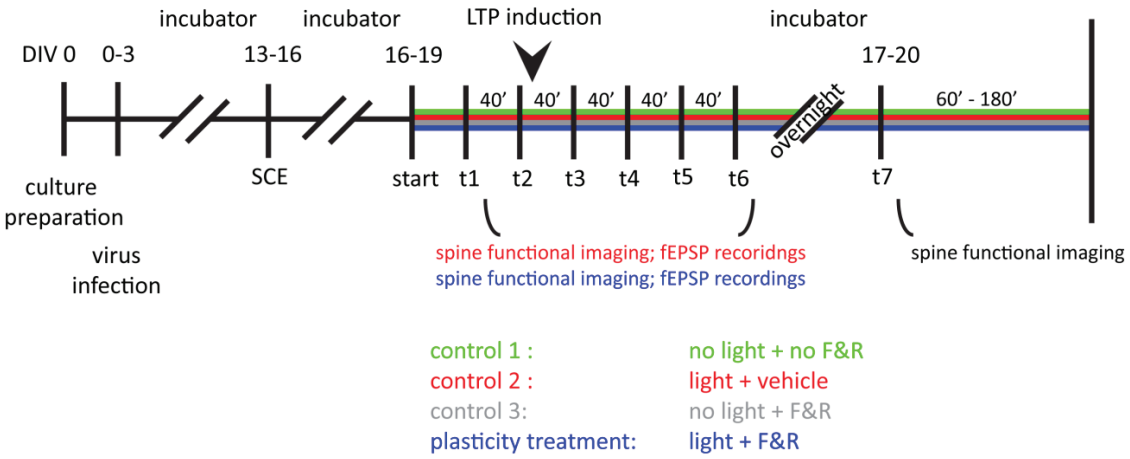

Figure 4-3: Experimental timeline
For experiments, slices were injected with ChR2mCherry virus after 0 - 3 days *in vitro* (DIV) and single cells electroporated with Turquoise2AGC6s after 13 - 16 DIV. Experiments were performed on slices after 16 - 19 DIV. In control 1 (green) and control 3 (gray) treatment, slices were not stimulated with light during the LTP induction phase and the first 6 structural imaging time points taken on the first experimental day. Structural changes were imaged at six time points spaced by 40 minutes (t1 to t6). In control 2 (red) and plasticity treatment (blue) slices received light stimulation to assess spine calcium responses and measure fEPSPs between structural imaging sessions on the first experimental day. Depending on the type of treatment slices received a perfusion of F&R (plasticity treatment) or vehicle (control 2) after the second structural imaging time point (black arrow). Slices were returned to the incubator and the last structural image was taken on the following day (t7). After t7, light-triggered spine calcium responses were measured in all experiments.

4.3 Developing a noninvasive optical LTP protocol under conditions of blocked AP generation

4.3.1 LTP induction by pairing depolarization and light stimulation

To control the population of active axons during LTP induction, I tested whether I can trigger LTP under sCRACM conditions. There are numerous LTP induction protocols in the literature that can roughly be divided into two groups: protocols using high frequency theta-burst stimulation (TBS, tetanus) and protocols using pairing of presynaptic and postsynaptic activity. Since the axons in my experiments were activated by ChR2 instead of by electrical stimulation, high frequency stimulation for the induction of LTP was not possible due to ChR2 kinetics that allows only up to 30 Hz stimulation frequencies [84] [85]. In pairing protocols, however, postsynaptic cells are depolarized and presynaptically stimulated with several hundred pulses in the range of 1 - 2 Hz [86] which is in the feasible range of ChR2 kinetics. In slices, expressing

ChR2 in the CA3 region, whole-cell voltage-clamp recordings from CA1 cells were performed. Light-evoked EPSCs were measured in the presence of TTX and 4-AP by giving a test light pulse roughly once every minute. After collecting a brief baseline (5 minutes), the cell was clamped at 0 mV and 200 light pulses at 2 Hz were given. Next, the cell was returned to its resting membrane potential and EPSCs were measured. In 3 out of the 4 pilot experiments this pairing protocol resulted in a significant potentiation (Figure 4-4, mean ± STD, 156 ± 15 % increase in norm. EPSCs 10 minutes after pairing compared to baseline, n = 3 cells with pairing protocol, 2-tailed paired t-test $p < 0.05$). In a control experiment, where light pulses were delivered without the depolarization of the cell, potentiation was not seen (Figure 4-4, 91% of baseline 10 minutes after light pulse stimulation, n = 1 cell with unpaired control protocol, red data points).

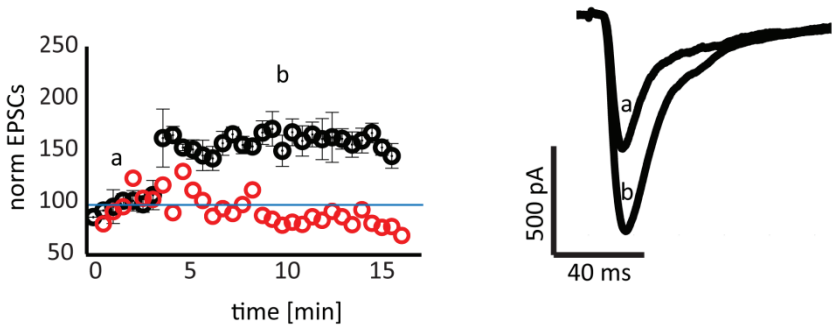

Figure 4-4: LTP induction by pairing depolarization with light stimulation
Normalized light-triggered EPSCs for LTP experiments (paired protocol, black, n = 3 cells) and a control experiment (unpaired control, red, n = 1 cell). Example traces depict light-triggered EPSCs before (a) and after pairing (b) in a LTP experiment.

These pilot experiments demonstrate that plasticity could be triggered in the absence of AP generation and when some of the voltage-gated potassium channels were blocked. However, a pairing LTP protocol requires patching and depolarizing the cell which makes it unsuitable for long-term structural and functional imaging of spines. A noninvasive approach to trigger LTP is essential for this project because it will allow assessment of the functionalization of spines hours and even days after LTP induction. Patching the imaged postsynaptic cell might compromise its health due to a run-down of essential intracellular components, and early cell death would prevent long-term imaging.

4.3.2 LTP induction by light stimulation combined with F&R treatment

To trigger LTP in a noninvasive manner I adapted a protocol described by Otmakhov et al. [81] and combined light stimulation with a 15 minute treatment with F&R. This LTP protocol was used for all experiments in which spine formation and functionality were investigated. A short treatment with F&R is known to lead to an increased intracellular concentration of cAMP and thus to facilitate processes that are essential for the induction of late LTP (L-LTP) [38, 87]. I measured the light-triggered fEPSPs to assess the induction of LTP. Low Mg^{2+} concentration and the presence of serine in the bath facilitated the opening of NMDARs which was not only essential for the detection of spine calcium influx but also for LTP induction under the conditions used for this study. By using this bath condition and 15 minutes perfusion of F&R, slices were brought in a highly plastic state where light test pulse stimulation, given once every 1-2 minutes, was sufficient to trigger LTP (Figure 4-5). Higher frequency stimulation under similar conditions has been shown to reduce the magnitude and duration of LTP [81]. Perfusion of F&R for 15 minutes, but not of vehicle solution, during ongoing low-frequency optical stimulation, resulted in a significant increase of the normalized fEPSPs slope compared to baseline (Figure 4-5, 161 ± 38 % increase of norm. fEPSPs 30 minutes after LTP induction compared to baseline, mean ± STD, n = 11 slices/experiments with light + F&R treatment, 2-tailed paired t-test $p < 0.01$; 77 ± 13 % decrease of norm. fEPSPs 30 minutes after vehicle perfusion compared to baseline, n = 7 slices/experiments with vehicle treatment, 2-tailed paired t-test, $p < 0.05$).

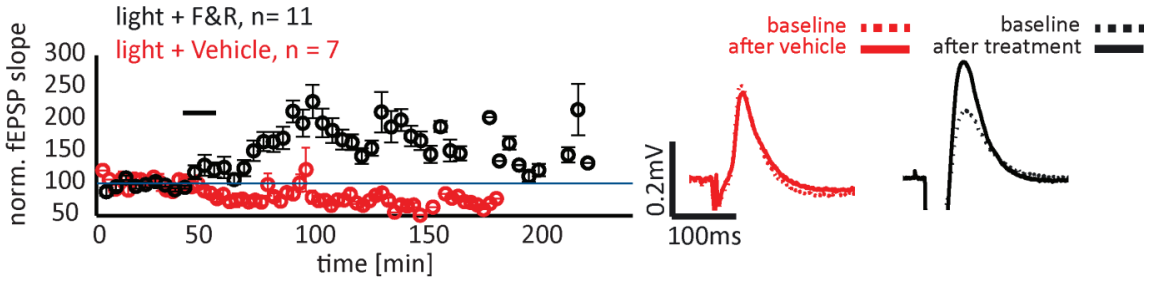

Figure 4-5: LTP induction by combining light stimulation and F&R treatment.
Normalized light-evoked fEPSPs slope in experiments where F&R was perfused for 15 minutes (black) and where vehicle was perfused (red). Example traces of fEPSPs during baseline (dashed line) and after F&R treatment (black solid line) or vehicle treatment (red solid line).

The data indicates that this optical LTP protocol provides a noninvasive and tightly controlled approach to trigger plasticity and can thus be used to assess the formation and functionality of new spines.

4.4 Imaging activity-driven structural spine plasticity after optical LTP

4.4.1 Optical LTP leads to an increased number of new persistent spines

To test whether the optical LTP protocol used for this study triggered structural spine plasticity, spine formation and elimination on the apical dendrites of postsynaptic CA1 cells was assessed. Spine structural dynamics (spine gain and loss) under optical LTP treatment was compared to spine dynamics under control conditions (Figure 4-6). Three control conditions were included in this study as described in the experimental timeline (Figure 4-3). The total dendritic length and spine number analyzed were 2091 µm and 1022 spines, respectively. A total of 27 experiments were quantified and the spines along one dendritic stretch per cell per experiment were analyzed.

Under conditions of optical LTP, the number of new persistent spines was significantly higher than in control conditions without light stimulation (Figure 4-6, fraction of new persistent spines, mean ± SEM, in conditions of optical LTP: $0.10 \pm 5.6 \times 10^{3}$, n = 9 cells/experiments; control 1: $0.03 \pm 3.1 \times 10^{3}$, n = 8 cells/experiments, in control 3: $0.03 \pm 3.9 \times 10^{3}$, n = 5 cells/experiments, Kruskal-Wallis test, $p<0.05$). The number of new persistent spines formed in optical LTP experiments and control 2 experiments (light stimulation + vehicle treatment) were not statistically different (Figure 4-6, fraction of new persistent spines, mean ± SEM, in conditions of control 2: $0.06 \pm 7.1 \times 10^{3}$, n = 5 cells/experiments). Under conditions of light-evoked activity (optical LTP and control 2) the number of lost spines were on average higher than the number of lost spines in control conditions without light stimulation (Figure 4-6, fraction of lost persistent spines, mean ± SEM, optical LTP: $0.05 \pm 6.8 \times 10^{3}$, n = 9 cells/experiments, control 2: $0.09 \pm 1.2 \times 10^{2}$, n = 5 cells/experiments compared to control 1: $0.02 \pm 2.3 \times 10^{3}$, n = 7 cells/experiments and control 3: $0.02 \pm 5.4 \times 10^{3}$, n = 5 cells/experiments, Kruskal-Wallis test, n.s). However, these trends were not statistically significant.

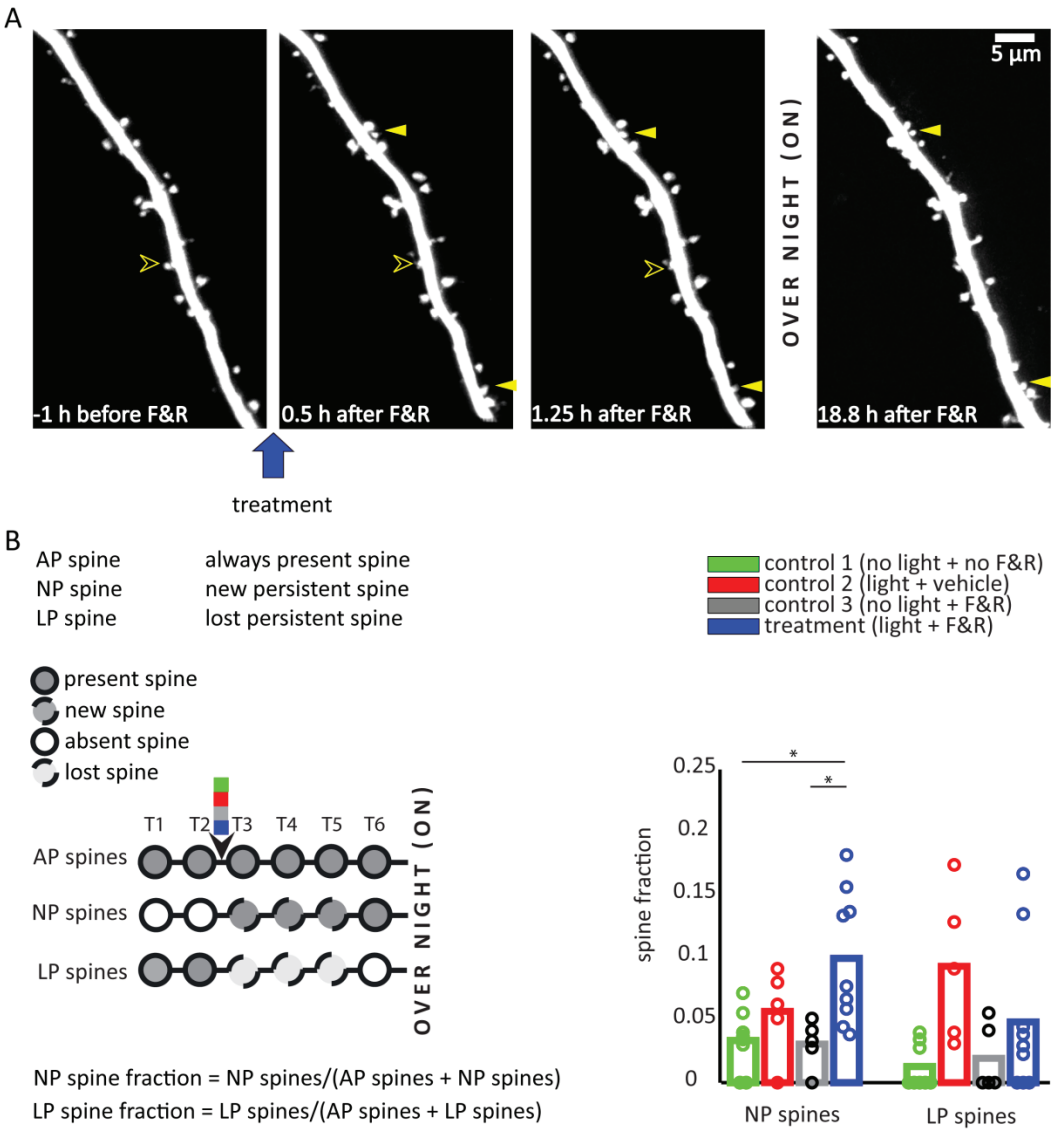

Figure 4-6: Spine structural plasticity after optical LTP induction

A) Maximum intensity projections of a labelled dendritic stretch of a CA1 cell at four different time points. Blue arrow indicates LTP induction. Filled arrow heads mark two new spines, while empty arrow heads mark a lost spine. The first three images were taken on the first experimental day, while the last one was acquired on the second experimental day. B) The definitions of always present (AP), new persistent (NP) and lost persistent (LP) spines are schematically depicted. AP spines are present throughout the experiment. NP spines are absent in the beginning of the experiment (white circles with solid line), appear at some point after treatment (gray circle with dotted line) and are present (gray circle with solid line) at least in the last structural time point of the first experimental day. LP spines are present at the beginning of the experiment, disappear after treatment (light gray circle with dotted line) and are absent at least in the last structural time point of the first experimental day. Bar plot summarizes the fraction of new (NP) and lost persistent (LP) spines for all conditions.

These results indicate that optical LTP induction triggers similar spine structural changes to those previously reported in studies where classical LTP induction protocols were used [68, 70, 71].

4.4.2 Optical LTP leads to a decreased spine survival fraction and increased spine turnover rate

To investigate the effect of optical LTP on spine structural stability and dynamics over time, spine survival fraction and spine turnover rate were assessed and compared between different treatment conditions (Figure 4-7).

The spine survival fraction is a measure of the stability of preexisting spines and reports for each time point the fraction of spines initially present that remain. The stability of preexisting spines was decreased significantly in conditions of light-evoked activity (Figure 4-7, spine survival fraction after 200 minutes, mean ± SEM, under plasticity treatment: 0.94 ± 6.0 x 10^3, n = 9 cells/experiments; under control 2 conditions: 0.91 ± 4.0 x 10^3, n = 5 cells/experiments, Friedman test, $p < 0.05$). In contrast, in control conditions without light stimulation there was no significant change in the spine survival fraction (Figure 4-7, spine survival fraction after 200 minutes, mean ± SEM, control 1: 0.97 ± 3.0 x 10^3 , n = 8 cells/experiments ; control 3: 0.97 ± 4.0 x 10^3, n = 5 cells/ experiments, Friedman test, n.s.).

The spine turnover rate is a measure of the number of spines gained and lost expressed as a fraction of the total number of spines present for every two adjacent imaging time points. Spine turnover rate was enhanced in optical LTP conditions compared to control conditions without light stimulation roughly by a factor of 2 (Figure 4-7, mean spine turnover rate, mean ± SEM, under plasticity treatment: 0.06 ± 3.2 x 10^3, n = 9 cells/experiments, under control 1 conditions: 0.03 ± 1.9 x 10^3, n = 8 cells/experiments, under control 3: 0.02 ± 0.7 x 10^3, n = 5 cells/experiments, Kruskal-Wallis test, $p < 0.05$). In comparison, there was no significant difference in the spine turnover rate between optical LTP experiments and control experiments where light stimulation was combined with vehicle treatment (Figure 4-7, mean turnover rate, mean ± SEM, under control 2: 0.05 ± 2.0 x 10^3, n = 5 cells/experiments, Kruskal-Wallis test, n.s).

Spine densities were similar between different time points and different treatment conditions (Figure 4-7, spine density, mean ± SEM, optical LTP: 0.43 ± 3.4 x 10^3 spines/µm n = 9 cells/experiments; control 1: 0.42 ± 1.1 x 10^3 spines/µm, n = 8 cells/experiments; control 2: 0.5

± 2.9 x 10^3 spines/µm, n = 5 cells/experiments and control 3: 0.47 ± 0.8 x 10^3 spines/µm, n = 5 cells/experiments, Friedman test, n.s.).

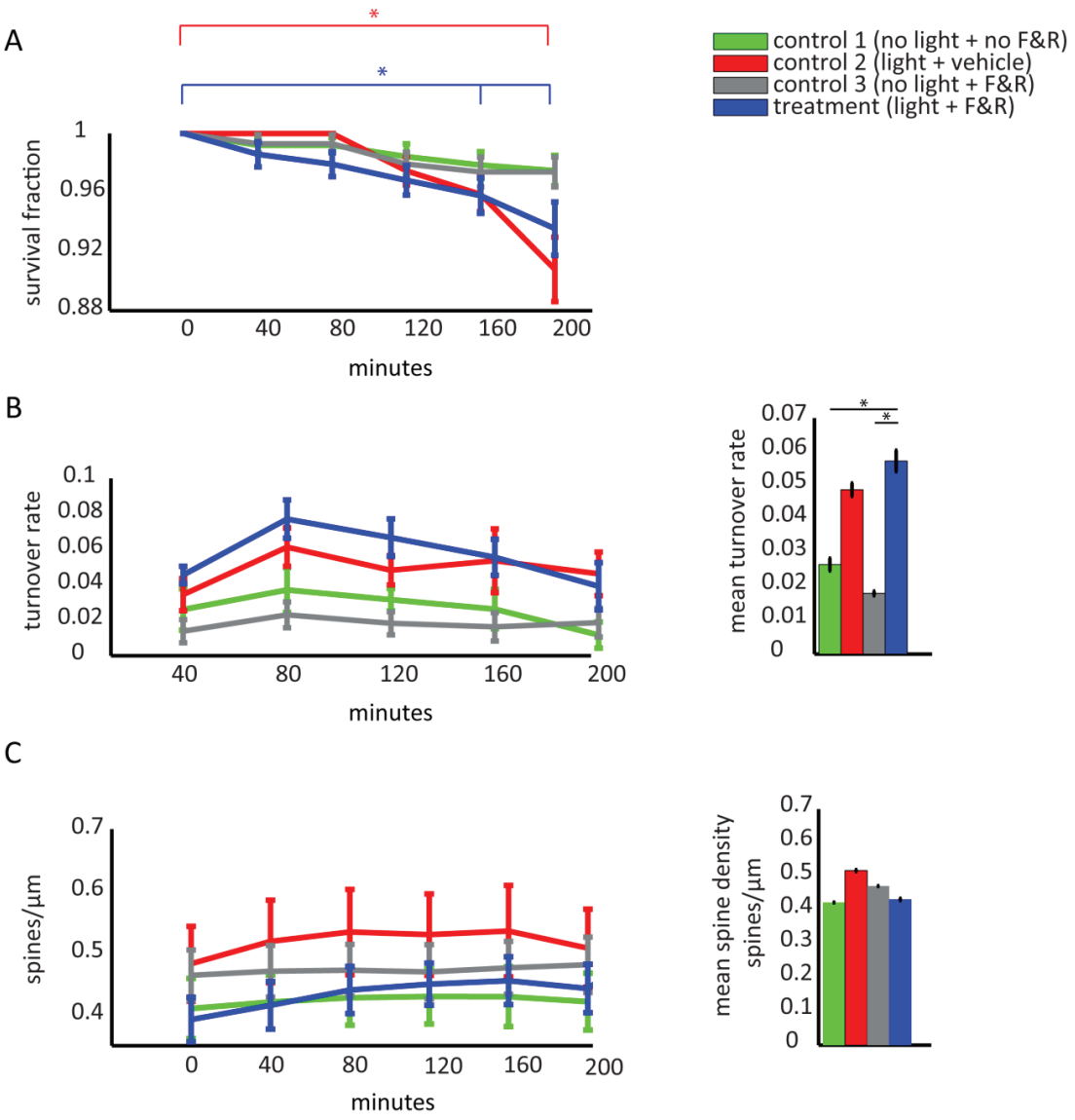

Figure 4-7: Spine stability and dynamics after optical LTP

A) Preexisting spine survival fraction (mean ± SEM) over the time course of the first experimental day in different treatment conditions. B) On the left: spine turnover rate (mean ± SEM) over the time course of the first experimental day in different treatment conditions. On the right: bar plot depicts the mean spine turnover rate over all time points of the first experimental day (mean ± SEM). C) On the left: spine density (mean ± SEM) over the time course of the first experimental day in different treatment conditions. On the right: bar plot depicts the mean spine density over all imaged time points of the first experimental day. 27 cells/experiments.

A destabilizing effect of LTP on preexisting spines and similar increases in spine turnover rate have already been reported in other studies [11] that used TBS to induce LTP, suggesting that the optical approach used here triggered structural changes that were comparable to those observed after conventional LTP paradigms with electrical stimulation.

4.4.3 Optical LTP leads to an increased overnight survival of new spines

To test whether new spines formed after optical LTP are stabilized, the fractions of new persistent spines that survived after overnight incubation were compared for the different treatment conditions. Spines that formed after plasticity induction had an increased overnight survival fraction compared to spines that formed in the absence of light stimulation and F&R treatment (Figure 4-8, fraction of new persistent spines that were present after overnight incubation, mean ± SEM, under plasticity treatment: 0.1 ± 6.3 x 10^{-3}, n = 8 cells/experiments compared to under control 1 conditions: 0.02 ± 4.5 x 10^{-3}; n = 7 cells/experiments, Kruskal-Wallis, $p < 0.05$). In comparison, although the fractions of new persistent spines that survived overnight under control 2 and control 3 conditions were on average smaller than the fraction under plasticity treatment, the difference was not statistically significant (Figure 4-8, under control 2 conditions: 0.04 ± 1.2 x 10^{-2}; n= 5 cells/experiments; under control 3 conditions: 0.02 ± 5.5 x 10^{-3}, n = 5 cells/experiments, Kruskal-Wallis, n.s.).

In summary, optical LTP triggers increased spine formation, destabilizes preexisting spines and stabilizes new spines.

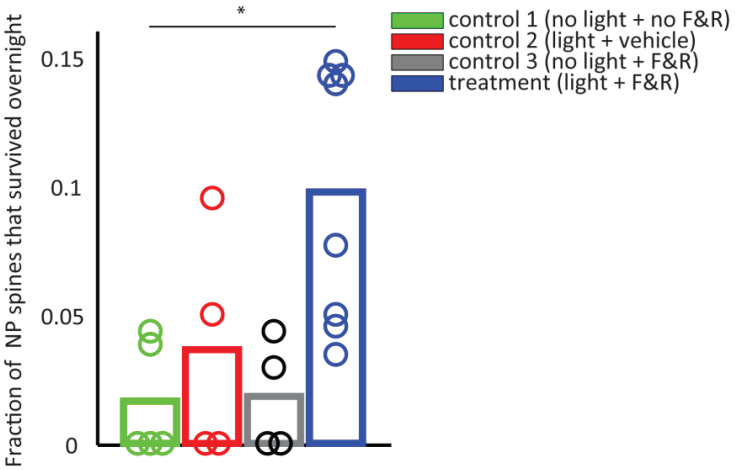

Figure 4-8: New persistent spines formed after optical LTP are more likely to survive overnight than new spines formed in the absence of light stimulation and F&R treatment.
The number of new spines that formed after treatment and survived until the second experimental day, expressed as a fraction of all spines present on the second experimental day is depicted. Each data point is the fraction of surviving new spines from single experiments. Bars depict the mean value from all experiments from the respective treatment group.

4.5 Spine calcium imaging after light stimulation

4.5.1 Calcium responses can be reliably detected in preexisting and new spines

In order to assess the presence of functional contacts between the spines on apical dendrites of CA1 cells and ChR2-expressing axons, spine calcium transients in response to light stimulation were imaged. To detect changes in calcium concentration, GCaMP6s [83] was expressed via SCE in individual CA1 cells for several days.

The noninvasive stimulation and imaging approach that I used in this study enabled me to perform a long-term calcium imaging in multiple spines. A total of 1037 preexisting spines were imaged. While some of the spines received as many as 96 calcium imaging trials some received only 1 trial. The reason all spines did not receive the same number of trials is twofold. On one hand, the structural imaging field of view (FOV) was bigger than the functional imaging FOV because of the different zoom factor used for imaging (Figure 4-9). Therefore, the complete dendritic stretch imaged for spine structural changes could not be scanned for spine

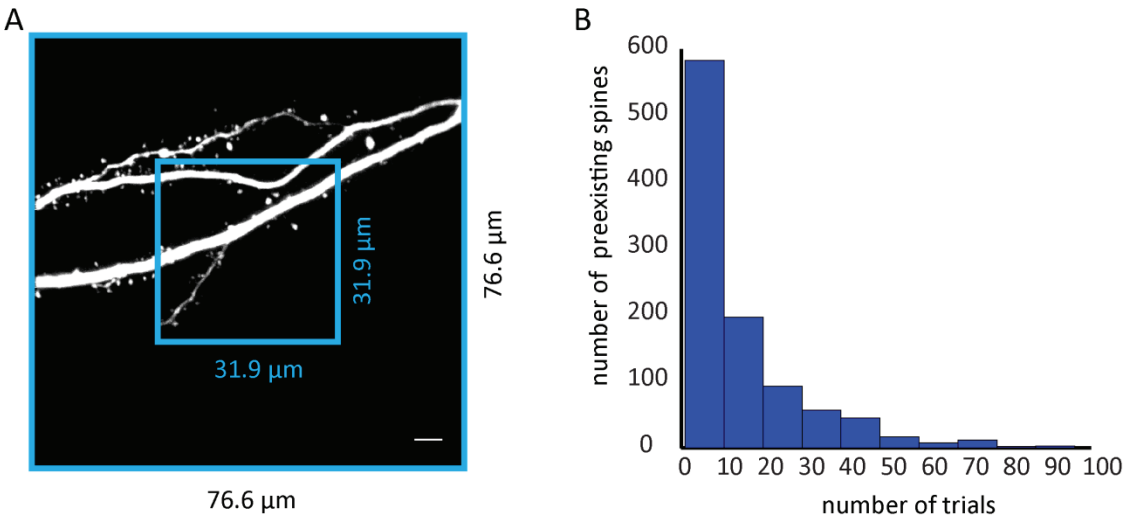

Figure 4-9: A typical imaging field of view and the number of calcium imaging trials recorded from preexisting spines

A) A maximum projection image from a CA1 cell apical dendrites in a typical field of view for structural imaging (big square) and a typical field of view for calcium imaging (small square). Scale bar, 5 µm. B) The histogram summarizes the number of calcium imaging trials performed on all imaged preexisting spines.

calcium responses to light at the same time. Secondly, because spines were found in different z-planes relative to each other and calcium imaging was performed on a single z-plane, only a subpopulation of spines that resided next to each other in the same z-plane could be imaged. Therefore, multiple functional imaging trials on multiple z-planes were performed to cover the whole structural field of view.

Some spines showed clear and reliable calcium responses after light stimulation which indicated that they possessed a functional connection with a ChR2-positive axon. Examples of spine calcium transients considered as successful responses after light stimulation are shown in Figure 4-10. A spine response to light was considered successful when, after light stimulation, there was increased calcium signal in the spine but not in the dendrite or when the increase of the signal was first in the spine and then in the dendrite (for more detail refer to section: $\Delta F/F_0$ calculation and spine calcium response in Material & Methods).

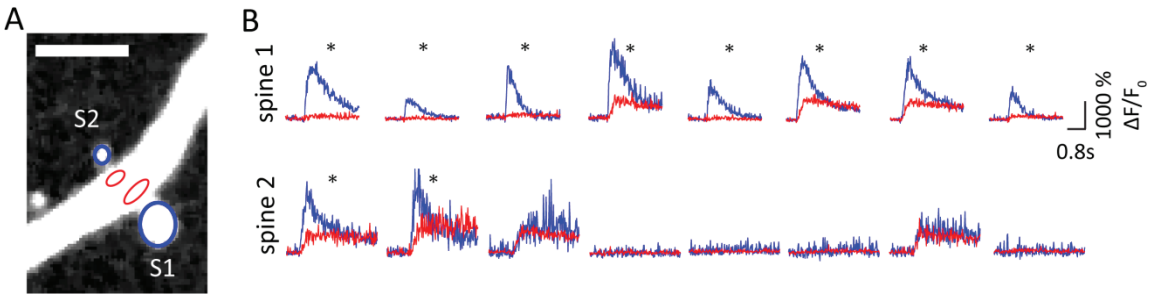

Figure 4-10: Light-triggered calcium transients in preexisting spines.
A) Summed GCaMP6s signal from 300 frames acquired from the same z-plane. Blue ellipses mark typical spine regions of interest (ROIs), while red ellipses mark their corresponding dendritic ROIs. Scale bar, 5 µm. B) Example of 8 individual calcium transient responses to light stimulation in two preexisting spines (blue) and their dendritic ROIs (red). Black asterisks indicate spine responses considered successful.

Some preexisting spines responded very reliably to light stimulation and had a high response success rate (successful calcium response trials as a fraction of all trials) throughout the experiment and on both experimental days. However, there were also spines with a very low success rate and many spines that never responded to light stimulation (response success rate 0) most likely due to the absence of functional synapses with ChR2-positive axons. Spine responses did not significantly change in amplitude over time as revealed by comparing the first and the last successful spine calcium responses (Figure 4-11B, mean $\Delta F/F_0$ peak response

amplitude, mean ± SEM, first response: 1554 ± 1.5 %, last response: 1627 ± 1.6 %, n = 175 preexisting responsive spines, Mann-Whitney test, n.s.).

Some preexisting spines showed light-triggered calcium responses only on the first experimental day (Figure 4-12). To quantify what fraction of preexisting spines was responsive on both experimental days I included experiments where at least 4 responsive spines were imaged on both days. In this way, I could exclude experiments where spines were mainly imaged on the second experimental day or where a non-overlapping population of spines was imaged on both experimental days. On average 54.6 ± 2.5 % of the preexisting spines showed responses on both days (n = 113 preexisting spines). In two of the ten included experiments the fractions of responsive preexisting spines were reduced overnight more than on average (Figure 4-12 red data points). One possible reason why some spines stopped responding to light stimulation over time could be that the spines had lost their functional contacts with ChR2-expressing boutons.

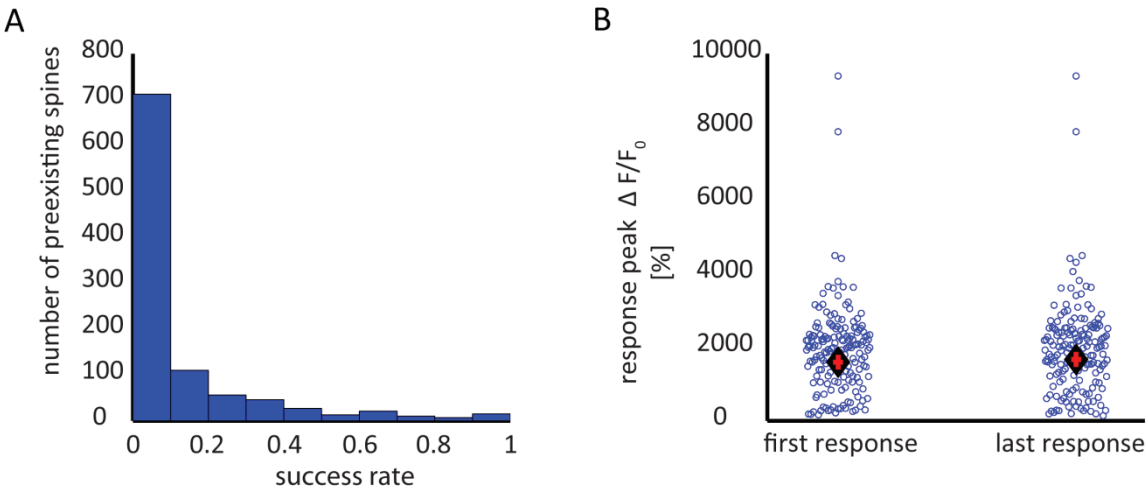

Figure 4-11: Light response success rate and stability of response amplitude in preexisting spines
A) Histogram depicts the light response success rate of all imaged preexisting spines, n = 1037 preexisting spines. B) Peak amplitude of the first and last successful calcium response after light stimulation in all responsive preexisting spines, n = 174 responsive preexisting spines. Blue data points depict responses in individual spines. Black diamonds and red error bars depict the mean amplitude and SEM of the successful responses, respectively.

Alternative explanation could be that the spines had changed their presynaptic partner to one that did not express ChR2. However, it cannot be excluded that the multiple light stimulations and spine calcium imaging trials might have caused damage to some of the connections.

Therefore, in spine calcium analysis where calcium imaging trials from both experimental days were considered, the two experiments with strongly reduced overnight responsive spine fractions were excluded (marked in red in Figure 4-12).

The above estimated overnight survival fraction could be underestimated because there were many spines that were tested only on the second experimental day and, therefore, it was not clear whether they were responsive previously. Furthermore, during the second experimental day it was possible to undertake a more systematic approach and to test as many spines as possible from the structural field of view and therefore many spines tested for light-triggered calcium responses on the second experimental day were not previously imaged.

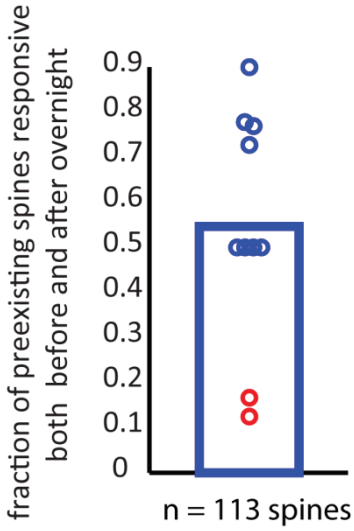

Figure 4-12: A fraction of preexisting spines shows responses to light on both experimental days
Individual data points depict for every experiment the fraction of preexisting spines that had been responsive to light on the first experimental day, were retested and still showed successful responses on the second experimental day. Bar indicates the mean value from all included experiments. n = 113 responsive preexisting spines included.

4.5.2 New spines can obtain input-specific functional synapses shortly after their formation

To test whether and when new spines, generated after optical LTP, form functional synapses with the active (ChR2-expressing) population of axons, their calcium transient responses to light stimulation were analyzed. New spines were identified during the experiment by using

registered maximum projections from consecutive structural time points. Furthermore, after the experiments, detailed posthoc analysis was used to confirm the identified new spines and screen for additional new spines that were not initially detected during the experiments. Unless otherwise stated, only new spines that formed on the first experimental day after the second structural imaging session (after treatment) were included. Furthermore, as for preexisting spines, a new spine was considered functional and light-responsive when it showed at least one successful calcium response triggered by light stimulation. Under conditions of optical LTP, a total of 33 new spines were identified. 20 of those spines showed at least one successful response to light stimulation indicating that they had formed a functional contact with one of the ChR2-expressing boutons. An example of two newly formed, functional spines is shown in Figure 4-13.

To estimate the time of spine formation I used the time when the last structural image was acquired before the spine was detectable above background. The age of a new spine at the time of its first successful response to light stimulation was approximated by the time elapsed between spine formation and the acquisition time of the calcium imaging trial in which the spine responded to the stimulation. Interestingly, the majority of new spines showed their first successful calcium response to optical stimulation already during the first experimental day i.e. less than 4 hours after their formation (Figure 4-13). The median and minimum age at which new spines were responsive to light stimulation was 1.3 hours and 8.5 minutes, respectively. However, it should be kept in mind that because not all new spines were tested for functionality immediately after their formation and in all trials, the time required for new spines to become functional might be shorter.

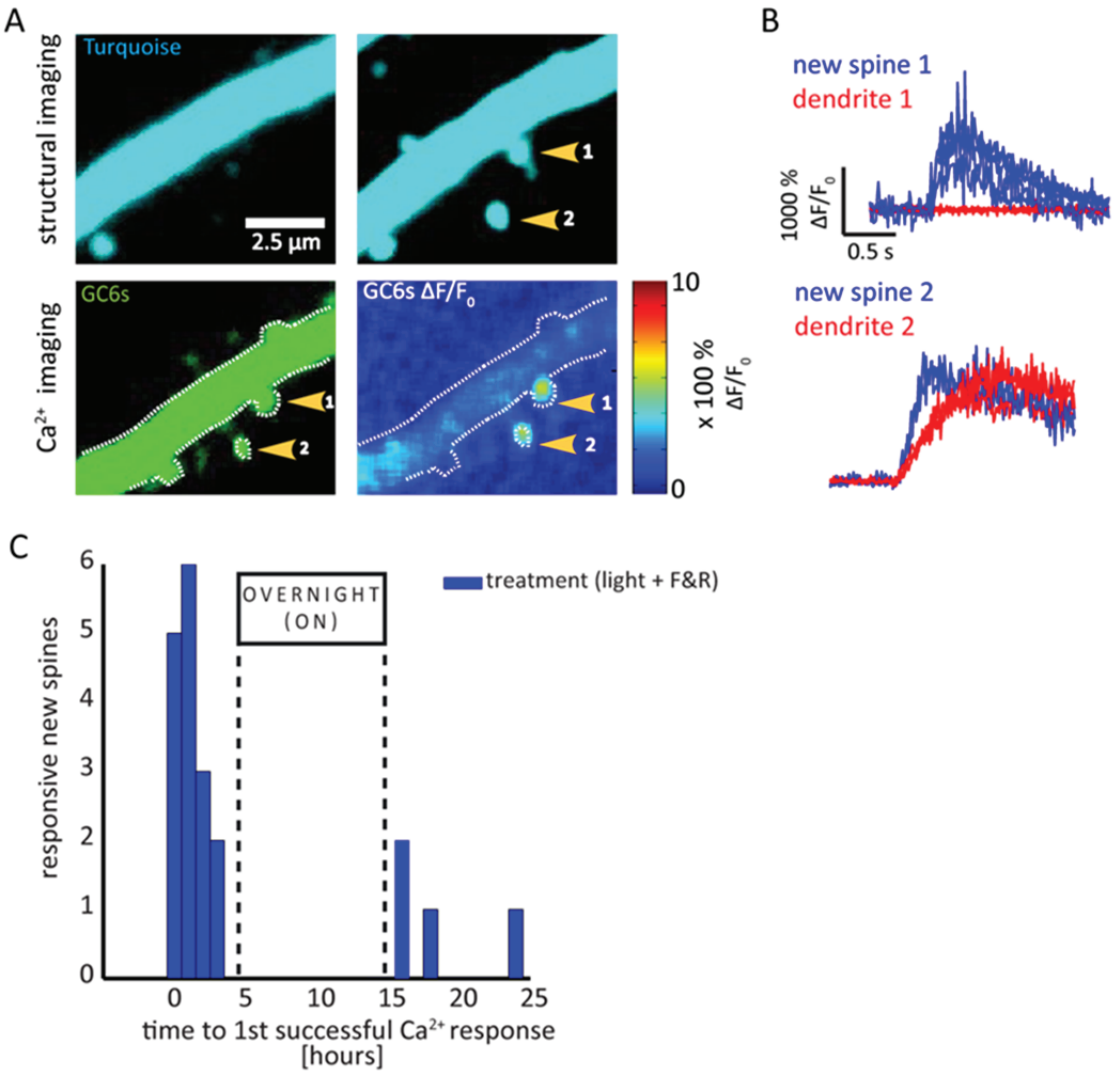

Figure 4-13: New spines can be responsive to light stimulation shortly after formation.
A) Image top panel: maximum intensity projection from a structural stack of a dendritic stretch showing the growth of two new spines (orange arrows) under conditions of optical LTP. Image bottom left panel: summed GCaMP6s signal from a single z-plane containing the two new spines, bottom right panel: GCaMP6s $\Delta F/F_0$ change in calcium fluorescence in percentage as a heat map showing a clear increase in calcium signal in both of the marked new spines after light stimulation. B) Several calcium response traces obtained from the two new spines (blue) and their corresponding dendrites (red). C) A histogram depicts in conditions of optical LTP treatment, the time elapsed between the formation of a new spine and its first successful calcium response to presynaptic optical stimulation.

4.5.3 New spines generated under light stimulation conditions form synapses with light-activated axons

To address the question of whether optical LTP increases the probability of new spines to form functional contacts with axons that are active during LTP (ChR2-positive), the light-responsive fractions of new spines in different treatment conditions were compared. The light-responsive spine fraction reports the number of responsive spines, i.e. spines that synapse with ChR2-positive boutons, expressed as a fraction of all spines. Analysis revealed that while the light-responsive fractions of preexisting spines were comparable across different treatment conditions, the light-responsive fractions of new spines were higher under plasticity treatment compared to control conditions (Figure 4-14). The fractions of preexisting spines in optical LTP experiments that showed responses to light stimulation were not significantly different from those in control treatment experiments (Figure 4-14, preexisting spines responsive fraction, mean ± SEM, optical LTP: 0.55 ± 0.02, n = 7 cells/experiments, control 1: 0.29 ± 0.03, n = 7 cells/experiments, control 2: 0.36 ± 0.04, n = 4 cells/experiments, control 3: 0.43 ± 0.05, n = 5 cells/experiments, Kruskal-Wallis, n.s.). This indicates that in all experiments the innervation density of ChR2-activated axons was comparable. However, the light-responsive fraction of new spines in plasticity treatment experiments was significantly higher than in no-light control 1 experiments (Figure 4-14, new spines responsive fraction, mean ± SEM, optical LTP: 0.64 ± 0.04, n = 7 cells/experiments, control 1: 0 ± 0, n = 7 cells/experiments, Kruskal-Wallis, $p < 0.05$). The light-responsive fractions of new spines formed under control 2 and control 3 conditions were on average smaller than those of spines formed under optical LTP treatment, but the difference was not statistically significant (Figure 4-14, new spines responsive fraction, mean ± SEM, optical LTP: 0.64 ± 0.04, n = 7 cells/experiments, control 2: 0.13 ± 0.04, n = 4 cells/experiments, control 3: 0.11 ± 0.04, n = 5 cells/experiments, Kruskal-Wallis, n.s). The light-responsive spine fractions are depicted as a function of the minimum number of functional imaging trials acquired from the spines (Figure 4-14B), showing that changing the number of trials per spine included does not change the results.

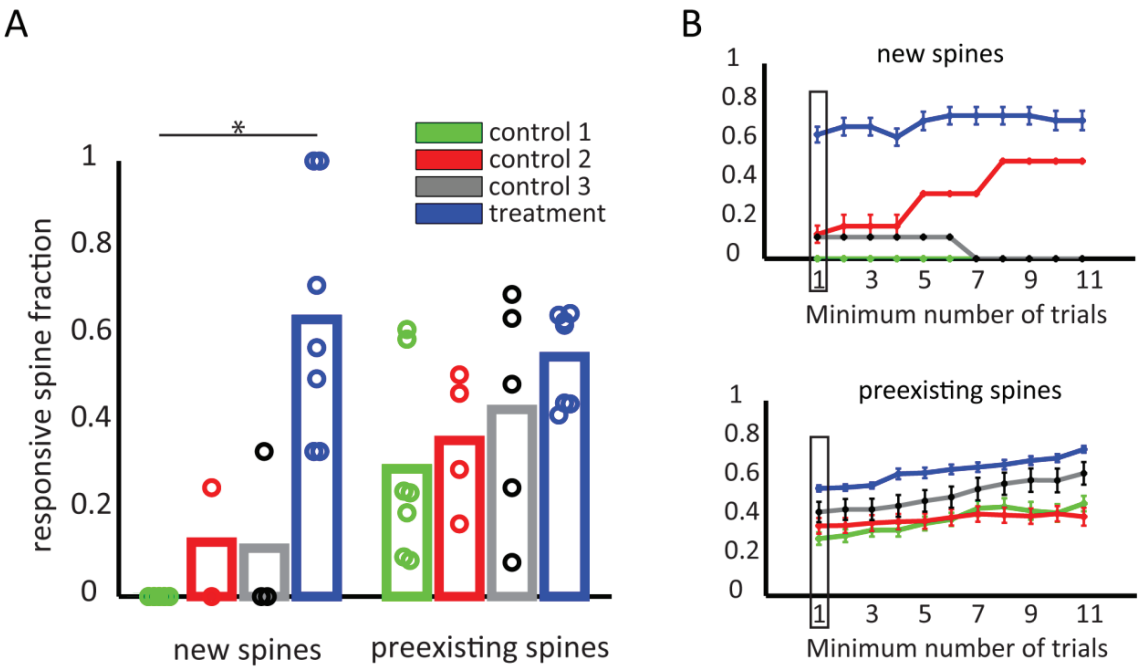

Figure 4-14: New spines in optical LTP experiments have the highest light-responsive fraction
A) Bar plot shows the mean light-responsive fraction of new and preexisting spines under different treatment conditions. Each data point depicts the responsive spine fraction from one experiment. A total of 50 new and 849 preexisting spines from all experimental treatments are included. B) Top panel: light-responsive fraction of new spines as a function of the minimum number of calcium imaging trials recorded from each spine. Rectangle indicates the data used in the bar plot for new spines in A). Bottom panel: light-responsive fraction of preexisting spines as a function of the minimum number of calcium imaging trials recorded from each spine. Rectangle indicates the data used in the bar plot for preexisting spines in A).

In experiments with control 1 or control 3 treatment, hardly any light stimulation was given until the last structural time point on the first experimental day was acquired. Therefore, under those conditions spines received fewer functional imaging trials compared to plasticity treatment conditions. To account for this difference, the light-responsive fraction of new and preexisting spines was recalculated after the number of spines and trials per spine between plasticity treatment experiments and those control experiments were equalized (for details refer to section: Equalizing spine calcium imaging trials in Material & Methods). Spines and their trials from all treatment experiments were shuffled and chosen at random until they were equal to the total number of spines and trials from all experiments of the respective control. This was repeated 100 times and the recalculated responsive fractions (mean ± STD) are shown in Figure 4-15. The responsive spine fraction for control 1 and control 3 is given as a

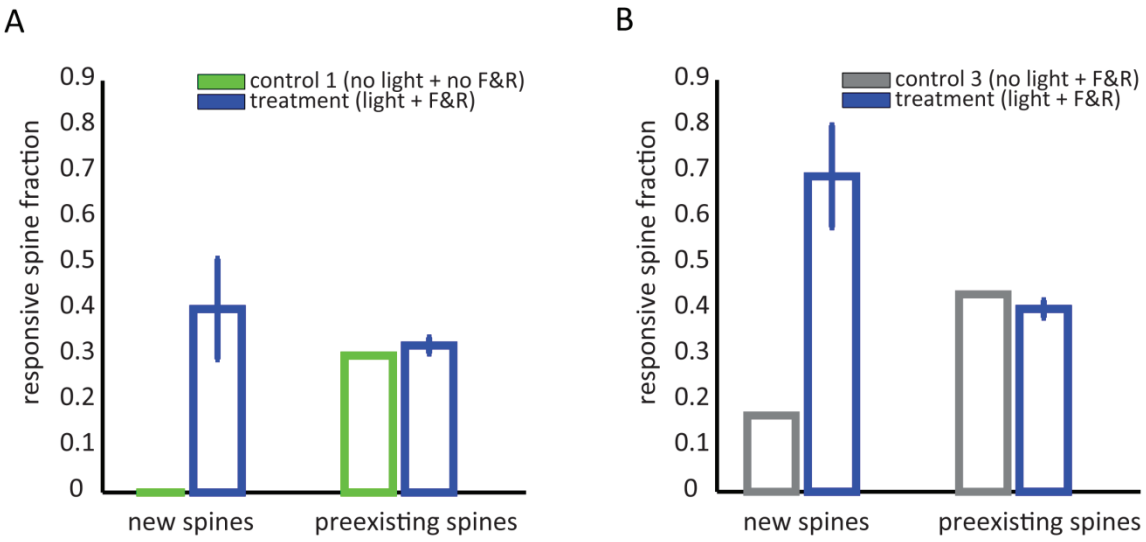

Figure 4-15: Light-responsive spine fractions after equalizing calcium imaging trials between treatment and no-light control conditions.
Light-responsive spine fraction calculated after the number of spines and trials per spines were equalized between: A) control 1 (in green, no light + no F&R) and plasticity treatment experiments (in blue, light + F&R, mean ± STD) and B) control 3 (in gray, no light + F&R) and plasticity treatment experiments (in blue, light + F&R, mean ± STD).

single value because it was calculated from all spines from all experiments of the respective control.

The results reproduce the previous finding (Figure 4-14), namely that the fractions of responsive preexisting spines were comparable in treatment and control conditions (control responsive spine fraction was in the range set by the 2.5th and the 97.5th percentile of the shuffled treatment responsive spine fractions). Furthermore, the fractions of responsive new spines were significantly higher in treatment than in control experiments (control responsive new spine fraction were below the range set by the 2.5th and the 97.5th percentile of the shuffled treatment responsive new spine fractions).

Yet, another interesting observation is that light stimulation alone contributed to increased spine dynamics as compared to no-light control conditions (see Figure 4-6). More new spines formed between the first two imaging sessions i.e. before the perfusion of F&R or vehicle in conditions with light stimulation (plasticity treatment and control 2) compared to conditions without light stimulation (control 1 and control 3). The number of new spines and new responsive spines was higher when spines formed after the first baseline imaging time point

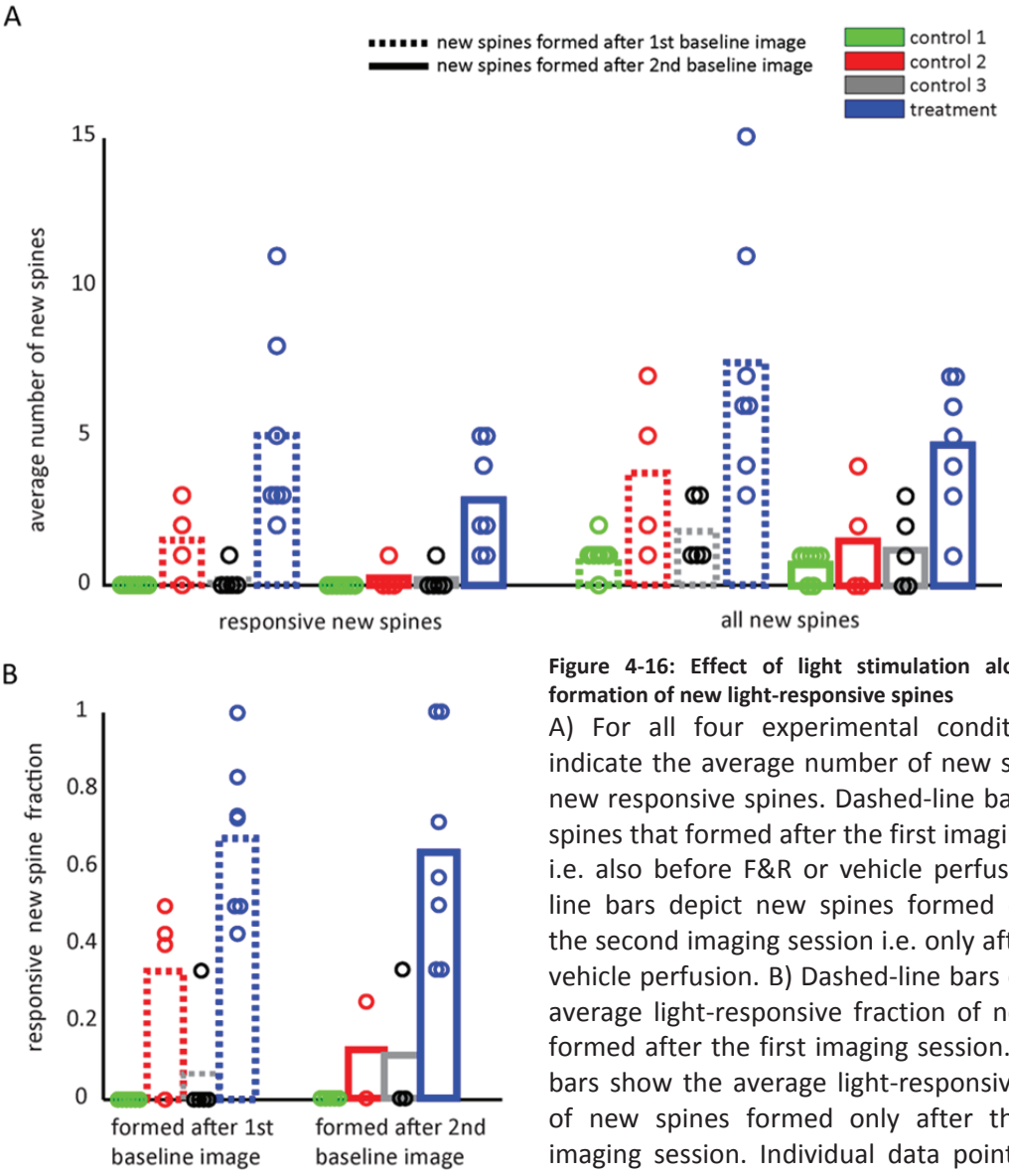

Figure 4-16: Effect of light stimulation alone on the formation of new light-responsive spines
A) For all four experimental conditions bars indicate the average number of new spines and new responsive spines. Dashed-line bars include spines that formed after the first imaging session i.e. also before F&R or vehicle perfusion, solid-line bars depict new spines formed only after the second imaging session i.e. only after F&R or vehicle perfusion. B) Dashed-line bars depict the average light-responsive fraction of new spines formed after the first imaging session. Solid-line bars show the average light-responsive fraction of new spines formed only after the second imaging session. Individual data points are the fractions from single experiments.

were considered compared to when spines generated after the second baseline imaging time point were included (Figure 4-16, in conditions of optical LTP, the average number of spines formed after the first and after the second imaging time point was 7.4 and 4.7, respectively; the average number of responsive spines formed after the first and after the second imaging time point was 5 and 2.9, respectively). Therefore, in optical LTP experiments 2.71 ± 0.36 (mean ± SEM) new spines were generated between the first two baseline imaging sessions, in control 2: 2.25 ± 0.24 (mean ± SEM) spines. In comparison, in conditions without light

stimulation, there were fewer spines formed between the first two imaging sessions: in control 1: 0.29 ± 0.07 (mean ± SEM) spines, in control 3: 0.55 ± 0.11 spines (mean ± SEM). The fraction of light-responsive new spines in all treatment conditions, however, was not affected (Figure 4-16B).

The effect of light stimulation alone on spine plasticity might be due to the fact that despite the localized optical stimulation (diameter of ~70 - 80 µm), the high number of ChR2-positive axons and the low Mg^{2+} concentration in the bath can result in the simultaneous activation of multiple spines and this can trigger the generation of dendritic calcium spikes. Indeed, such calcium events have been triggered by light stimulation quite often in these experiments. An example of a dendritic calcium spike is depicted in Figure 4-17.

Therefore, dendritic spikes evoked after light stimulation might have already induced some plastic spine changes that were further reinforced and enhanced by the F&R treatment.

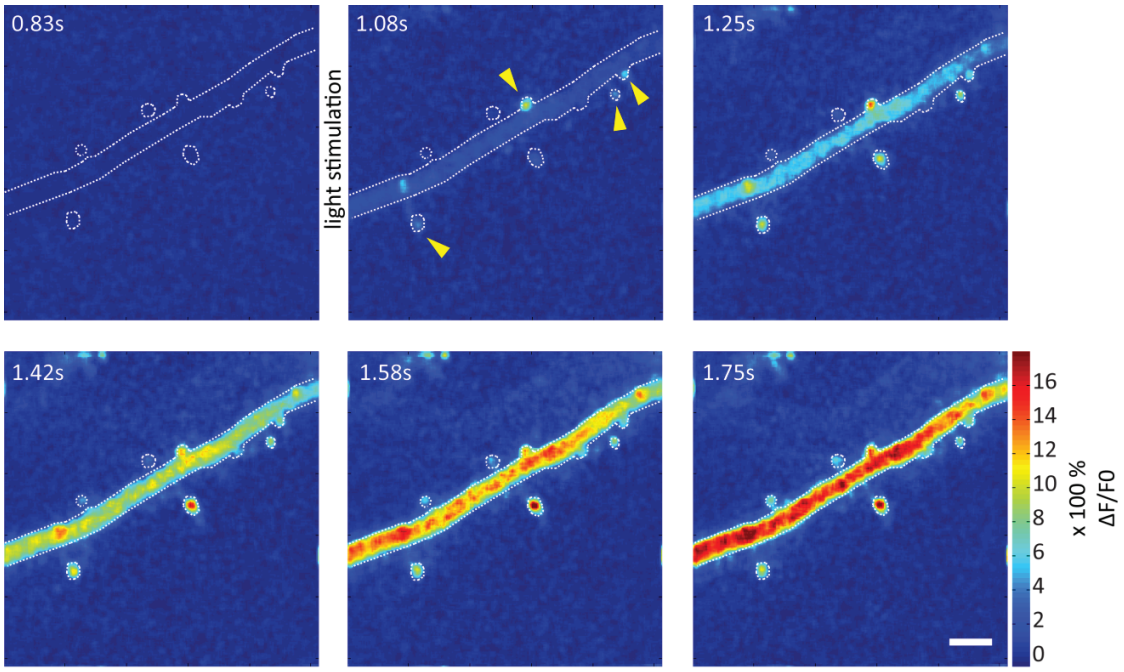

Figure 4-17: Light-evoked dendritic calcium spike

White dotted line outlines a dendritic stretch that received light stimulation 0.83 seconds after the start of the image acquisition. After stimulation calcium signals initially increased in several spines (indicated with yellow arrows) and subsequently in the whole imaged dendritic stretch. Images depict $\Delta F/F_0$ change in calcium fluorescence in percentage as a heat map (color scale, bottom right). Scale bar, 5 µm.

4.5.4 Comparing the response properties of new and preexisting spines in optical LTP conditions

To further characterize new spines formed after plasticity treatment, their response success rates, response amplitudes and the light-responsive fraction were compared to those of the preexisting spines in the same experiments. For the comparison light-triggered calcium responses from 33 new and 240 preexisting spines were included. Only new spines formed after the second baseline imaging time point were considered. Response success rate is defined by the number of successful calcium responses to light stimulation in a spine, expressed as a fraction of all calcium trials performed on the spine.

There was no significant difference between the light response success rates of new and preexisting spines (Figure 4-18A, two-sample Kolmogorov-Smirnov test was used to compare the cumulative distribution of the response success rate of new and preexisting spines.). For simplicity, the cumulative distribution of the response success rate of all spines from all plasticity treatment experiments is shown (Figure 4-18 A).

The peak amplitudes of successful calcium responses after optical stimulation in newly formed and preexisting spines were also similar (Figure 4-18B, mean $\Delta F/F_0$ response peak ± SEM, in new spines: 1670.6 ± 14.8 %, n = 33 new spines, in preexisting spines: 1572.5 ± 1.3 %, n = 240 preexisting spines, Mann-Whitney test, n.s.).

Furthermore, as already shown in Figure 4-14A, under optical LTP conditions, the light-responsive fractions of new and preexisting spines were also comparable (Figure 4-18, mean light-responsive spines ± SEM, new spines: 0.64 ± 0.04, n = 33 new spines; preexisting spines: 0.55 ± 0.02, n = 240 preexisting spines). To test whether the light-responsive spine fractions are affected by the fact that new spines were fewer than preexisting ones, the fractions were recalculated after the number of spines and trials per spine were equalized between new and preexisting spines (for details refer to section: Equalizing spine calcium imaging trials in Material & Methods). From all included treatment experiments preexisting spines and their trials were shuffled and chosen at random until they were equal to the number of new spines and their trials. This was repeated 100 times and the recalculated responsive fractions (mean ± STD) are displayed as a function of the minimum number of trials performed on the spines (Figure 4-18D). For example, a minimum number of one trial means that all spines that were included in the analysis received at least one calcium imaging trial (Figure 4-18C). A single value is depicted for the light-responsive fraction of new spines which is the fraction for all

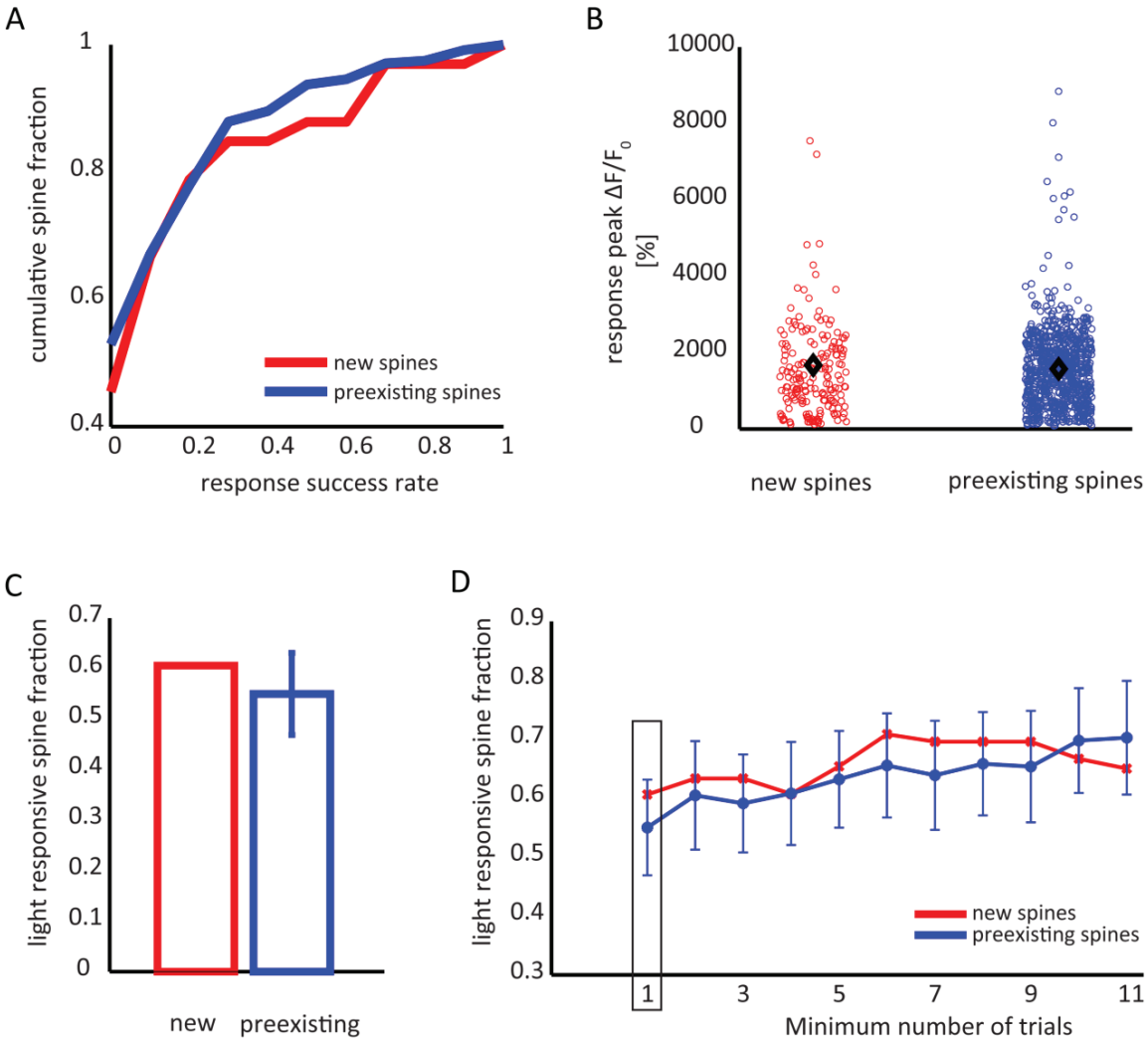

Figure 4-18: Response success rate, response amplitude and light-responsive spine fractions are comparable between new and preexisting spines in optical LTP treatment experiments

A) Cumulative distribution of the light response success rate of new (red) and preexisting spines (blue). B) Individual (red and blue dots) and mean (black diamonds) peak response amplitude of new and preexisting spines. C) Light-responsive spine fraction of new and preexisting spines after the number of preexisting spines and trials per spine has been equalized to the number of new spines and their trials. Bar plot includes data from spines with at least one calcium imaging trial. D) Light-responsive spine fraction of new and preexisting spines as a function of the minimum number of calcium imaging trials recorded from the spines. Rectangle indicates the data used for the bar plot in C).

new spines with a defined minimum number of trials from all included treatment experiments. The light-responsive fraction of new and preexisting spines is comparable (the responsive fraction of new spines was in the range set by the 2.5th and 97.5th percentile of the shuffled

responsive fractions of preexisting spines).With an increase of the minimum number of trials performed on the spines, the light-responsive fractions of preexisting spines increased slightly since the number of spines considered as unresponsive due to insufficient number of trials was reduced.

4.5.5 Overnight survival of new spines

TTX, 4-AP and serine were not washed out before the slices were moved to the incubator for overnight but they were diluted by the added fresh culture medium, so that spontaneous activity was likely to take place in the hippocampal slice during the overnight incubation (not tested). An interesting question to address is whether the network shows a preference to keep the new spines formed after optical LTP overnight even though spontaneous activity is restored and might 'overwrite' the information introduced by the LTP. To address this question, the overnight survival of new light-responsive spines was compared to the survival of new unresponsive spines.

Overnight survival fraction is the number of new responsive or new unresponsive spines that survived overnight (are present on the second experimental day) as a fraction of all new responsive or all new unresponsive spines, respectively. New light-responsive spines formed after optical LTP showed a higher tendency (however, not significantly) to survive overnight compared to new light-unresponsive spines (Figure 4-19, overnight survival fraction, mean ± SEM, new responsive spines: 0.81 ± 0.03, new unresponsive spines: 0.58 ± 0.04, n = 7 cells/experiments, Mann-Whitney test, n.s.).

For this quantification I included only new spines that formed after the second baseline imaging time point (i.e. after LTP induction in treatment conditions) on the first experimental day. A new spine was considered responsive if it showed at least one successful calcium response to light stimulation at any point during the experiment (i.e. either on experimental day 1 and/or day 2). Therefore, a new spine would also be considered responsive if it showed a successful calcium response to optical stimulation only on the second experimental day. In this way, spines that needed more than several hours to form a functional synapse were also included. However, an alternative interpretation could be that some newly formed spines had not been at first functionally connected to ChR2-expressing axons but became so overnight. The later scenario is rather unlikely since the survival fraction of new responsive spines did not change much when functional imaging trials only from the first experimental day were

considered (survival fraction when only functional trials recorded on the first experimental day were included, mean ± SEM: 0.82 ± 0.03, compared to when trials recorded from both days were included: 0.81 ± 0.03). Interestingly, the survival fraction of unresponsive spines was slightly increased when calcium imaging trials collected only before overnight incubation were considered (0.65 ± 0.04 as compared to 0.58 ± 0.04). One possible reason could be that some of the new spines that were considered unresponsive to light stimulation based on functional imaging trials recorded on the first experimental day were indeed connected to ChR2-positive axons and stabilized.

In summary, new spines generated after optical LTP induction that functionally connect to active axons appear to be more protected from elimination than new spines that failed to form functional synapse with those axons.

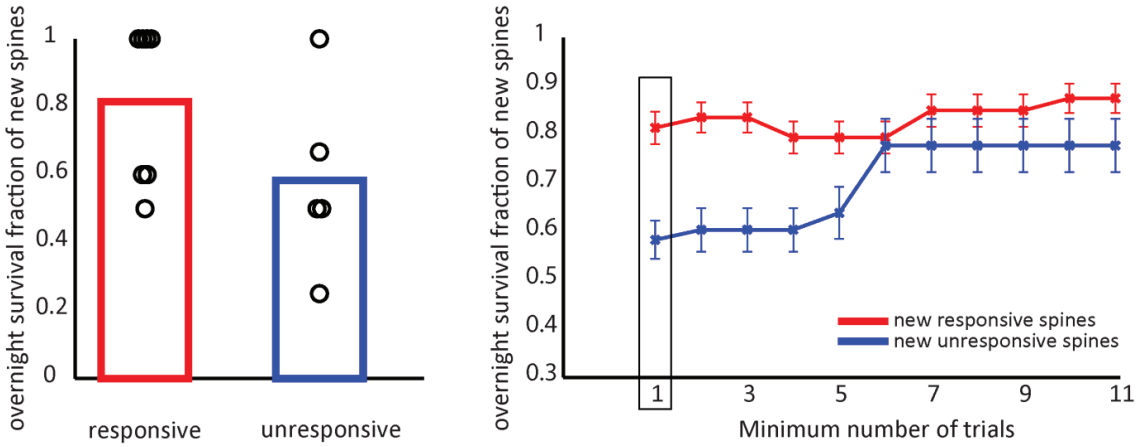

Figure 4-19: Overnight survival of responsive and unresponsive new spines
Left panel: Individual data points depict overnight spine survival fraction from single experiments. Bars depict the mean survival fraction for new light-responsive spines (red) and new light-unresponsive spines (blue). Right panel: Overnight survival fraction (mean ± STD) of new spines expressed as a function of the minimum number of calcium imaging trials recorded from the spines. Rectangle indicates the data used for the bar plot on the left side.

5. Discussion

Today, a widely accepted concept is that learning and memory can occur due to restructuring of the existing neuronal network, i.e. changing the connectivity between neurons. Moreover, LTP is assumed to represent the learning and memory process at a fundamental, cellular and molecular level. Therefore, LTP is a well-established and broadly used model for investigating the structural and functional changes that accompany synaptic plasticity. Hebb and Konorski were among the first to propose that synapses linking two cells were strengthened when the cells were active at the same time, known as the Hebbian plasticity rule: 'Cells that fire together, wire together'. Despite the fact that the true nature of the structural correlates of memories still remain elusive, there are multiple studies, *in vitro* and *in vivo*, showing that the formation of new spines is an inseparable part of synaptic plasticity and learning. However, a direct experimental proof of the Hebbian rule at the level of newly formed synapses is still missing.

Therefore, in my PhD project I set out to investigate in more detail the functional role of new spines induced by LTP. In particular, I tested whether new spines formed after LTP followed the Hebbian plasticity rule and, hence, were functionally connected to presynaptic partners that had been activated during LTP induction. To achieve this, I combined pharmacology and optogenetics to strictly control the locus of synaptic transmission in a hippocampal organotypic slice. Based on this approach, I developed an optical LTP induction paradigm. Finally, using two-photon time-lapse structural and calcium imaging, I monitored the effects of optical LTP on spine dynamics and assessed the functionality of new and preexisting spines.

First, I demonstrated that LTP can be induced under conditions of suppressed AP generation and adapted a noninvasive optical LTP induction protocol. Second, I showed that optical LTP induction resulted in spine structural changes similar to those reported after classical LTP induction approaches. In particular, optical LTP increased spine formation, decreased the stability of preexisting spines and increased the stability of new spines. Third, I found that new spines after optical LTP can rapidly form (within hours) functional synapses with active (ChR2-expressing) axons. Importantly, I demonstrated that optical LTP not only increased the rate of spine formation but also increased the chance of new spines to form stable functional

synapses with ChR2-positive axons i.e. the population of axons that was activated during the LTP induction.

5.1 A noncanonical approach to trigger LTP

Testing whether new spines that were formed after LTP induction contact the axons that were active during LTP requires a strict control over the locus of neuronal activity. Therefore, I adapted the sCRACM approach which Pentreanu et al. developed to map monosynaptic functional connections between ChR2-expressing presynaptic neurons and their postsynaptic partners [82]. In the current work, LTP was induced under sCRACM conditions by combining light stimulation with F&R treatment. LTP induction and maintenance were followed by measuring fEPSPs. This approach allowed control over the region of neuronal activity and plasticity induction in a noninvasive manner which enabled me to investigate long-term functional and structural changes of dendritic spines.

It could be argued that the plasticity paradigm used here to test the Hebbian rule is quite different from the classical LTP induction paradigms described in spike-timing-dependent plasticity (STDP). In canonical STDP, a strict temporal relationship between pre- and postsynaptic spiking is required, i.e. when presynaptic action potentials precede the postsynaptic ones by ~20 ms, LTP takes place and when the order is reversed LTD is triggered [88, 89]. There is strong evidence suggesting that the postsynaptic spiking during STDP provides the essential depolarization for releasing the Mg^{2+} block from NMDARs which in turn facilitates the calcium influx [90-92]. However, in this study, Mg^{2+} block was decreased by keeping the Mg^{2+} concentration in the bath reduced throughout the experiment which facilitated the opening of NMDARs during the LTP induction. In this work I showed that LTP can be triggered in the absence of AP generation. Indeed, there is accumulating evidence indicating that AP firing is not required for the induction of LTP but rather the cooperative synaptic inputs that drive regenerative calcium dendritic spikes are essential [93, 94]. Furthermore, it appears more physiologically relevant that dendritic spikes and not artificially triggered APs contribute to the postsynaptic depolarization and calcium influx. Moreover, while backpropagation of APs is quite efficient in the proximal parts of the dendritic tree, this declines significantly with the increased distance from the soma. Therefore, plasticity rules

might vary with distance from the soma. This might explain why there are many types of STDP and LTP-induction protocols.

It has recently been shown that optogenetics can also be used to trigger synaptic plasticity. In one report, LTP was induced by pairing a brief postsynaptic depolarization with light-evoked EPSCs [95]. Yet, another study triggered LTP by pairing APs in the presynaptic cells (CA3 neuron) with ChR2-mediated depolarization of postsynaptic cell (CA1 neuron) [96]. Both of these protocols are unfortunately not suitable for this project. The first one requires whole-cell configuration of the postsynaptic cell for depolarization which makes it unsuitable for long-term spine imaging. The second approach lacks optogenetic control over the presynaptic population. Therefore, in this work for LTP induction a protocol from Otmakhov et al. [81] was modified and the light stimulation of the presynaptic neuronal population was combined with a 15 minute chemical treatment with F&R in the bath. LTP triggered by the combination of F&R treatment with presynaptic activation has been shown to be NMDAR-dependent, to require presynaptic activation i.e. to be input-specific and to occlude subsequent LTP triggered by TBS, indicating that it shares common mechanisms with the latter [81, 97]. A brief application of F&R is known to increase the intracellular concentration of cAMP and trigger signaling cascades and biochemical machinery in the cells that are required for LTP induction [38, 98]. This treatment relies on the activation of PKA which is known to play an important role not only in L-LTP induction [87, 99, 100], but also in learning and memory [57, 101, 102].

5.2 Optical LTP leads to spine structural plasticity

Because the plasticity paradigm used in this study has not been described previously, it was essential to validate that it triggers spine structural changes similar to those triggered by classical LTP induction. I showed that optical LTP led to an increased number of gained spines, increased spine turnover rate, destabilization of preexisting spines and stabilization of new spines. Indeed, similar changes after LTP induction have already been reported. Engert et al. [68] and Maletic-Savatic et al. [70] were the first to show a correlation between LTP induction and new spine formation. Another report from the same year using EM and the accumulation of calcium precipitation to label active spines reported an increase in the number of perforated synapses and multi-spine boutons after LTP [69]. After these pioneering reports, there have been a number of publications showing similar results. Nägerl et al. [103] described

that TBS led to the generation of new spines, while low-frequency stimulation resulted in spine retraction. Yet, another report [71] followed structural changes for 3 days and confirmed that TBS led to a roughly 2-3 fold increase of spine formation and turnover. These numbers are, in fact, compatible with the results I report here. Very few studies describe the effect on spine structural plasticity after LTP induction by F&R treatment. One report showed that a single application of forskolin resulted in LTP but not in synaptogenesis and only after repeated application of forskolin and with a delay of 1 week synaptogenesis could take place [104, 105]. In the current work, however, formation of functional synapses occurred rapidly (within hours) and after a single application of F&R combined with light-driven presynaptic activation. This discrepancy might be due to the fact that the plasticity treatment protocols used in the cited papers and in this study were different. While the forskolin treatment in the cited reports took place in the incubator in normal culture medium, in this study more plastic conditions could be achieved by reducing Mg^{2+} concentration in the bath combined with optically generated synaptic input during the pharmacological treatment. Moreover, in this work the stimulation of cAMP synthesis by forskolin was complemented with rolipram treatment, a phosphodiesterase inhibitor which prevents the degradation of cAMP. In summary, the optical LTP plasticity paradigm used in this study triggers spine structural changes comparable to those reported to take place after LTP and therefore offers a suitable approach to study synaptic plasticity.

New spine generation has not only been reported to accompany LTP induction but also to take place during learning and memory. In a pioneering work the structural spine plasticity during whisker trimming was chronically followed *in vivo* and revealed the formation and stabilization of new spine synapses and the destabilization of previously persistent spines [106]. New spines triggered by changes in sensory experience, such as closure of one eye (monocular deprivation), were stabilized and survived even after eye reopening, i.e. restoration of normal sensory input, and might be responsible for the rapid functional change that happens after repeated monocular deprivation [72]. In another work, spine changes in the motor cortex were investigated upon learning of a motor task. Here, the rapidly formed new spines were stabilized by subsequent training sessions and the number of new spines were correlated with the proficiency of the task performance [73].

With the current study I aim to understand the role of new spines in LTP. However, this, in turn, might also shed some light into their function in learning and memory given that at a

fundamental level LTP and memory share many of their underlying mechanisms. The fact that LTP generates new spines that potentially carry synapses makes it tempting to think that these new spines are the structural correlate of the potentiated synaptic transmission. However, this cannot be the only mechanism because LTP induction results in an instantaneous potentiation while spine outgrowth takes at least several minutes [68]. It is already quite well-accepted that initially, after triggering of LTP, strengthening occurs at preexisting synapses by modification of the postsynaptic receptor composition and synaptic release properties [31, 107, 108]. Later, the appearance of new spines makes them potential candidates to support the late phase of LTP and provide the long-lasting restructuring of the network. However, to confirm this, it needs to be shown that new spines form functional synapses with presynaptic partners that are coactive during the LTP induction.

5.3 Preexisting and new spines show light-evoked calcium transients

In the current work I showed that under sCRACM conditions [82] the expression of calcium indicator GCaMP6s in the postsynaptic cell allowed the detection of light-evoked calcium transients in spines. In this way, functional synapses can be visualized noninvasively and their formation can be assessed. Schaffer collaterals were stimulated locally with blue light (diameter of 70 µm) at their contact sites with the apical dendrite of CA1 cells. Since Na^+-dependent AP generation was blocked under sCRACM conditions this depolarization could not travel back along the axon to the CA3 cell bodies and trigger recurrent activity but rather remained contained at the boutons. There, it served to open VGCCs through which calcium can enter the boutons and trigger synaptic release from the synaptic vesicles [109-111]. The released neurotransmitter together with the reduced Mg^{2+} concentration facilitated the opening of AMPARs and NMDARs on the postsynaptic side of the synapse where the influx of calcium thought NMDARs was detected by the change in GCaMP6s fluorescence signal. It has been shown in previous studies that the detection of calcium increase in spines after presynaptic stimulation is a reliable method to identify functional synapses [112]. Calcium imaging of genetically encoded calcium indicators (GECI) under sCRACM conditions can be used to reliably localize in a noninvasive and optogenetically controlled manner functional synaptic contacts and can provide a valuable tool to map monosynaptic connectivity between neuronal populations at the single synapse level.

While detection of a light-driven calcium response in the spine indicates that it possesses a functional synapse with a ChR2-expressing axon, the lack of such a response can have multiple interpretations. The following interpretations should be considered: 1. a spine can have a functional contact with a ChR2-positive axon but light stimulation does not provide the necessary depolarization for synaptic transmission to take place, 2. the spine lacks a synapse altogether, 3. the spine has a synapse with uninfected axon i.e. axon that lacks ChR2. To simplify the interpretation, it is assumed in this work that a successful spine-localized calcium response to light indicates a functional contact with a ChR2-positive axon and a lack of such response means that a functional contact is missing. To remove this ambiguity each of the light-unresponsive spines should have been assessed for functionality by other means such as calcium responsiveness to local electrical stimulation, visualization at EM level or labelling for typical postsynaptic makers (e.g PSD 95). However, establishing these methods for further analysis was not within the scope of my PhD thesis and future experiments will be required to address this.

With the approach I used in this study, silent synapses could not be differentiated from the rest of the synapses because of the reduced Mg^{2+} block at the NMDARs and were most likely activated as well. Silent synapses exhibit NMDARs-mediated currents but lack AMPARs currents and they have been detected in high numbers in the developing hippocampus but are also present at adult stages [113, 114]. Therefore, it is not possible to exclude the possibility that some of the newly formed functional synapses are silent.

I demonstrated that in many trials light stimulation resulted in a global calcium event that invaded the complete dendrite in the imaged field of view. Despite the presence of global dendritic spikes I showed that synaptic inputs could still be detected because the calcium signal increased faster in the spines receiving direct presynaptic input when compared to their neighboring dendrites.

Interestingly, I observed that the average calcium peak amplitude in spines (1578.2 ± 1.52%) was higher than that recently reported in an *in vivo* study where spine calcium signals triggered by motor activity were reported to be on average around 500% [115]. This difference in the calcium response amplitude could be due to the fact that in the current study the extracellular Mg^{2+} concentration was reduced and this could have resulted in larger NMDARs currents than under physiological conditions.

Furthermore, I report here that the average spine peak response amplitude did not change over time, however, some spines that showed light responses when tested on the first experimental day did not respond to optical stimulation on the second experimental day. This could be due either to lost synapses or a synaptic change of the presynaptic partner - from a ChR2-expressing bouton to a ChR2-lacking one. However, with the current experimental approach is not possible to differentiate between those two possibilities.

5.3.1 New spines can rapidly form functional synapses

The majority (16 out of 20) of new spines formed after optical LTP treatment showed successful calcium responses to light stimulation on the first experimental day. This indicates that new spines can form functional synapses with ChR2-expressing axons on average just several hours after they have become structurally detectable. The time required for synapse formation is still unresolved in the literature. Therefore, this finding is in agreement with only some studies.

Zito et al. used glutamate uncaging to test whether spontaneously formed new spines have postsynaptic components of a functional synapse. They reported that new spines possessed AMPAR and NMDAR currents that were indistinguishable from those of preexisting spines only 35 minutes after their formation [116]. In another study [117], it has been shown that new spine formation can be induced in cortical slices from early postnatal animals by applying a glutamate uncaging protocol or TBS. There, it was reported that in 5 out of 7 new spines calcium transients after glutamate uncaging could be detected within 30 minutes after their formation, indicating they possess the characteristics of a functional synapse.

However, there are multiple studies that have suggested that despite the fast spine formation, synaptogenesis requires a longer time. A study [118] that used TBS to trigger new spine formation showed by means of EM that spines only a few hours old and in physical contact with boutons lacked typical staining of mature synapses in their synaptic cleft and therefore were not considered to possess functional synapses. They concluded that a synapse requires more than 19 hours after spine formation to form.

Interestingly, studies that rely on spine calcium imaging to identify functional synapses (as the one described here) detect faster synaptogenesis compared to studies relying on EM. Therefore, the different results might be due to the difference in the detection method. One possible explanation could be that with EM the threshold for synapse detection is higher than

with calcium imaging. However, to be able to compare the results relying on these two detection approaches, a detailed and systematic study is needed where all spines displaying calcium responses to presynaptic activation are reevaluated with EM.

Although it cannot be completely ruled out that the new spine synapses I detected in this study were present on the dendrite as shaft synapses before the spine growth, this scenario is rather unlikely since previous work has showed that the spine outgrowth precedes accumulation of postsynaptic markers [119, 120]. Mechanistically and experimentally, rapid synapse assembly is possible and has been demonstrated. By means of immunostaining and live-cell imaging it was shown that all necessary protein components for a glutamatergic synapse assembly can be detected several hours after axodendritic contact and that the accumulation of presynaptic components preceded postsynaptic ones [120-122]. Thus, since the cell machinery is capable of gathering and assembling all building blocks of a synapse within several hours, it is feasible that functional synapses can appear in a rapid manner. Of course, this does not necessarily mean that all synapses form with the same speed. However, a perpetual change in the environment requires mechanisms that provide the nervous system with an ability to change rapidly and adapt.

5.3.2 New spines generated under light stimulation conditions form synapses with light-activated axons

Here I demonstrated that under optical LTP treatment the fraction of new spines that showed successful calcium responses to light stimulation i.e. had successfully formed functional synapses with ChR2-positive axons, was the highest (in optical LTP: 0.64, control 1: 0, control 2: 0.13, control 3: 0.11). The number of ChR2-positive axons in treatment and control experiments was similar because slices received comparable amounts of virus injection independent of which treatment would be applied to them at later stages of the experiment. Moreover, the light-responsive fraction of preexisting spines was also comparable between different experimental conditions (optical LTP: 0.55; control 1: 0.29; control 2: 0.36; control 3: 0.43) indicating again that the innervation density of ChR2-activated axons was similar. The light-responsive fraction of preexisting spines can be used as a rough estimate for the innervation density of ChR2-activated axons. This estimate does not give information about the absolute number of ChR2-expressing axons, but provides the only possible (given the experimental data) approach to approximate the ratio between light-stimulated and light-

unstimulated axons. This ratio is essential for determining the preference of a new spine to synapse with a ChR2-activated axon. However, because in optical LTP experiments the light-responsive fraction of preexisting spines (0.55 ± 0.02) is not significantly lower than the light-responsive fraction of the new spines (0.64 ± 0.04) I cannot exclude, at this point, that new spines form without a clear preference for active versus inactive presynaptic partners.

Another tested approach to estimate the fraction of ChR2-positive axons was to use maximum likelihood estimation for the probability that a certain number of spines are connected to a ChR2-expressing axon (personal communication with Prof. Leibold). In this analysis, the spine response success rate after optical stimulation was used to calculate the most likely subpopulation of spines connected to ChR2-positive axons that would produce the observed success rate. Although such estimation was adequate for the preexisting spines, it was, however, not suitable for the new spines because of their low numbers.

Why new spines formed under optical LTP conditions are more likely to functionally contact the active, ChR2-expressing axons, compared to spines formed under control conditions? One possible explanation is that glutamate spillover in the immediate proximity of light-stimulated boutons might serve as an initiating cue for the growth of new spines. Indeed, it has been shown that glutamate uncaging close to a dendrite can trigger spine outgrowth in slices from early postnatal animals [117]. Yet, another study reported that exogenous application of glutamate and spontaneous glutamate release can trigger the formation of spine head protrusions, structures consisting of a filopodia-like process and a terminal swelling that originated from a spine [123]. The reduced synaptic transmission in control experiments where no light stimulation was given before the last structural imaging time point on the first experimental day, can explain the reduced number of new spines that functionally contact ChR2-positive boutons. Moreover, light stimulation alone can result in massive synaptic transmission and trigger dendritic spikes. This can explain why there were on average more new spine synapses connected to ChR2-expressing axons in light-only control (control 2) compared to the no-light control conditions (control 1 and control 3). Calcium spikes are regenerative calcium events that can span large portions of the dendritic tree. Multiple studies, both *in vivo* and *in vitro*, have indicated the importance of dendritic calcium spikes in plasticity induction and in behavior [86, 93, 124, 125]. A possible confirmation of the above proposed idea that new spines grow in the direction of a glutamate source would be to show that new spines preferentially form in the proximity of a light-responsive preexisting spine.

However, this spatial information can easily be missed considering that the dendrites of only one of the numerous CA1 cells were labelled.

However, I did not detect successful calcium responses in all of the newly formed spines after optical LTP, i.e. not all of them managed to functionally contact ChR2-positive axons. Indeed, the light-responsive fraction of new spines (~ 63 %) is not significantly different from the light-responsive fraction of preexisting spines (~ 55 %). Unfortunately, the lack of information about whether new spines that are unresponsive to light possess a synapse and with which type of presynaptic partner (with or without ChR2), makes the interpretations speculative. Nevertheless, one can imagine at least three possible scenarios. Firstly, it is possible that new spines, despite being unresponsive to light, contact ChR2-positive axons but need more time to develop their synapses. Indeed, 4 out of the 20 new spines formed under optical LTP treatment conditions showed light-triggered calcium response only on the second experimental day (after overnight incubation). However, many spines stop responding to light stimulation on the second experimental day due to unknown reasons and, thus, some of the new spines might lose their light-responsiveness before it could be detected. Secondly, it could be that all new unresponsive spines completely lack synapses. To confirm this, future experiments are required to test whether light-unresponsive spines possess a putative functional synapse by means of EM, local electrical stimulation or glutamate uncaging. Alternatively, a less technically demanding approach would be to label postsynaptic markers in light-responsive and unresponsive spines and compare their expression levels. If either of the first two scenarios is taking place, this indicates that new functional spine synapses preferentially form towards the active axons. However, there is also a third possible scenario. It could be that new light-unresponsive spines possess a functional synapse with an axon that lacks ChR2. Many new unresponsive spines were also present after overnight incubation (~ 58 %), indicating they had enough time to mature and obtain a functional synapse. If new spines do not display a preference for active versus inactive axons this indicates that optical LTP enhanced in the postsynaptic cell a global unspecific synapse formation process that occurred independently of the nature of the presynaptic partner i.e. towards both active and inactive axons. Such a result would deviate from one of the currently proposed ideas in the field, namely that new spines triggered by LTP or learning target preferentially active presynaptic partners immediately after their formation and thus contribute to storing new information. There are multiple studies following the pioneering work of Per Andersen [21], showing that

LTP is input-specific, meaning it can only be induced between connections that experience the LTP triggering stimulation and not between connections that received a control stimulation and are farther than 70 µm away from the potentiated connections [22]. However, since it is currently not clear whether the input-specific potentiation is carried by the enhancement of the preexisting connections alone or also by the newly formed spines it cannot be concluded that functional spine synapses also form in an input-specific manner. Could in fact such a global new synapse functionalization be taking place after LTP and only later network activity determines which of the synapses are needed and preserved or dispensable and removed? At this point the most straightforward way to tackle this would be to use the approach here and to obtain a more precise estimation about the fraction of ChR2-expressing axons or to analyze in further detail the light-unresponsive spines.

5.3.3 Comparing the response properties of new and preexisting spines in optical LTP conditions

In the present work I find that new and preexisting spines in optical LTP experiments show comparable response success rate, response amplitude and light-responsive fractions. However, at least two studies reported that the amplitude of calcium transients in new spines was smaller than in preexisting spines [116, 117]. One possible reason for the difference in the results is that in one of these studies only spontaneously formed new spines were investigated and calcium responses were triggered by uncaging and not by presynaptic stimulation as in this work. In the second study, new spines formed on still developing neurons were tested.

5.3.4 Overnight survival of new spines

Finally, I demonstrated that in conditions of optical LTP new spines that formed functional synapses with one of the active, ChR2-expressing axons were more protected from elimination than new spines that did not respond to light stimulation and most likely lacked a functional synapse with a ChR2-positive axon. On average 81% of all new light-responsive spines were still present on the second experimental day as compared to 58% of all new light-unresponsive spines. This finding makes it tempting to speculate that new spines synapsing with ChR2-positive axons and presumably carrying information brought into the neuronal network by the optical LTP stimulus are preferentially preserved. Indeed, it has been shown that applying LTP inducing stimuli on spontaneously formed new spines increased their stability and prolonged

their survival compared to the stability and survival of newly formed unstimulated spines [62]. This stabilization might be facilitated by the activity-driven translocation of CaMKII to the dendritic spines [126, 127]. At the spine, CaMKII might contribute to spine stabilization by regulating PSD composition [128], receptor trafficking [129], actin polymerization [130]. Furthermore, LTP stimulus triggers the translocation of polyribosomes into preexisting spines [131] and it could achieve the stabilization of new spines via similar mechanisms.

In summary, the enhanced probability of new spines to form functional synapse with an active presynaptic partner after optical LTP combined with their protection from elimination might, indeed, represent the Hebbian plasticity rule at newly formed spines Figure 5-1.

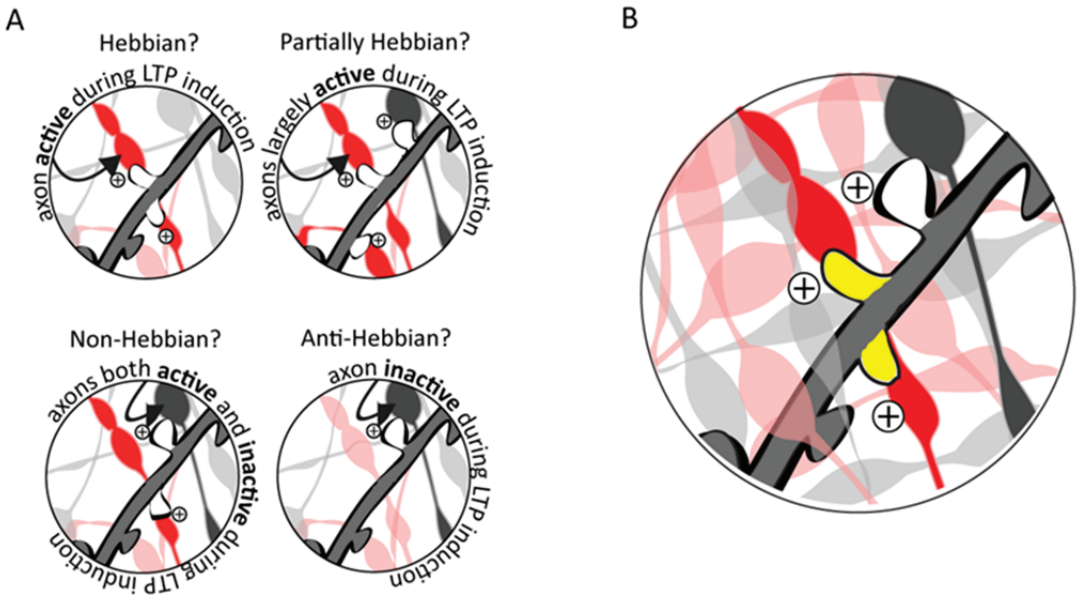

Figure 5-1: A schematic representation of the central question of this study and the results of the experimental data

A) The goal of the project was to test whether new spines generated after LTP form synapses in a Hebbian manner i.e. with co-active axons or not. B) Data indicates that some of the new spines form functional synapses in a Hebbian manner i.e. with active, ChR2-expressing axons and respond to light (yellow spines). However, there were also new spines that were not responsive to light stimulation (white spine). These findings speak against Hebbian and anti-Hebbian manner of new spine formation. Because it is unclear whether new light-unresponsive spines possess a synapse, currently it is not possible to differentiate between the two remaining scenarios – partially Hebbian and non-Hebbian manner of spine formation.

6. Conclusion & Outlook

An expanding body of literature has suggested that structural and functional synaptic changes are tightly interleaved and provide the basis of activity-dependent modification of neuronal networks. In my thesis, I used an optical LTP induction protocol, light stimulation and spine calcium imaging of GECI to study the formation of functional synapses after plasticity induction. I demonstrated that the optical LTP protocol led to structural spine changes that were comparable to the changes already reported to take place after classical LTP protocols. Furthermore, the results from this work support a view of a rapid functionalization of spines after plasticity induction and indicate that LTP not only triggers the generation of new spines but also increases the probability of those new spines to build a functional synapse with the axons that were active during LTP induction. This finding makes it tempting to speculate that the newly formed synapses are the structural correlate that incorporates the information introduced by LTP in the network.

The current work, however, leaves some open questions behind. It will be important to determine whether spines formed after LTP that did not show calcium responses to light stimulation possess putative functional synapses. Furthermore, it is essential to test the findings described here *in vivo* and investigate whether they still hold true. Learning–driven optogenetic targeting (e.g under *cFos* promoter) of a presynaptic cell population combined with calcium imaging of newly formed spines on the postsynaptic cell might provide the answer to this question. Finally, to ultimately resolve the role of new spines in learning and memory, a complementary study is required to address the question whether the selective destruction of new spines formed after learning results in loss of the memory of the learnt task.

Bibliography

1. Diels, H., *Alcmaeon, no 13 aët. V 17, 3 (d. 427), In: Die fragmente der vorsokratiker, Weidmannsche Buchhandlung*. 1906, Berlin.
2. Foster, M. and C.S. Sherrington, *A Textbook of Physiology* 7th ed. 1897, London: Macmillan.
3. Hebb, D.O., *The organization of Behavior: A Neurophysiological Theory*. 1949, New York: John Wiley and Sons.
4. Konorski, J., *Conditioned Reflexes and Neuron Organization*, 1948, Cambridge University Press: Cambridge.
5. Bliss, T.V. and T. Lømo, *Long-lasting potentiation of synaptic transmission in the dentate area of the anaesthetized rabbit following stimulation of the perforant path.* J Physiol, 1973. **232**(2): p. 331-56.
6. Andersen, P., et al., *The Hippocampus Book*. 2007, Oxford: Oxford University Press.
7. Altman, J. and S.A. Bayer, *Prolonged sojourn of developing pyramidal cells in the intermediate zone of the hippocampus and their settling in the stratum pyramidale.* J Comp Neurol, 1990. **301**(3): p. 343-64.
8. Arnold, S.E. and J.Q. Trojanowski, *Human fetal hippocampal development: I. Cytoarchitecture, myeloarchitecture, and neuronal morphologic features.* J Comp Neurol, 1996. **367**(2): p. 274-92.
9. Eriksson, P.S., et al., *Neurogenesis in the adult human hippocampus.* Nat Med, 1998. **4**(11): p. 1313-7.
10. Mohedano-Moriano, A., et al., *Convergence of unimodal and polymodal sensory input to the entorhinal cortex in the fascicularis monkey.* Neuroscience, 2008. **151**(1): p. 255-71.
11. Rajmohan, V. and E. Mohandas, *The limbic system.* Indian J Psychiatry, 2007. **49**(2): p. 132-9.
12. Mark, L.P., et al., *Limbic connections.* AJNR Am J Neuroradiol, 1995. **16**(6): p. 1303-6.
13. Scoville, W.B. and B. Milner, *Loss of recent memory after bilateral hippocampal lesions.* J Neurol Neurosurg Psychiatry, 1957. **20**(1): p. 11-21.
14. O'Keefe, J. and J. Dostrovsky, *The hippocampus as a spatial map. Preliminary evidence from unit activity in the freely-moving rat.* Brain Res, 1971. **34**(1): p. 171-5.
15. Vanderwolf, C.H., *Hippocampal electrical activity and voluntary movement in the rat.* Electroencephalogr Clin Neurophysiol, 1969. **26**(4): p. 407-18.
16. Arnolds, D.E., et al., *The spectral properties of hippocampal EEG related to behaviour in man.* Electroencephalogr Clin Neurophysiol, 1980. **50**(3-4): p. 324-8.
17. Gray, C.M., et al., *Oscillatory responses in cat visual cortex exhibit inter-columnar synchronization which reflects global stimulus properties.* Nature, 1989. **338**(6213): p. 334-7.
18. Schwartzkroin, P.A., *Characteristics of CA1 neurons recorded intracellularly in the hippocampal in vitro slice preparation.* Brain Res, 1975. **85**(3): p. 423-36.
19. Stoppini, L., P.A. Buchs, and D. Muller, *A simple method for organotypic cultures of nervous tissue.* J Neurosci Methods, 1991. **37**(2): p. 173-82.
20. Gahwiler, B.H., *Organotypic monolayer cultures of nervous tissue.* J Neurosci Methods, 1981. **4**(4): p. 329-42.

21. Andersen, P., et al., *Specific long-lasting potentiation of synaptic transmission in hippocampal slices.* Nature, 1977. **266**(5604): p. 736-7.
22. Engert, F. and T. Bonhoeffer, *Synapse specificity of long-term potentiation breaks down at short distances.* Nature, 1997. **388**(6639): p. 279-84.
23. McNaughton, B.L., R.M. Douglas, and G.V. Goddard, *Synaptic enhancement in fascia dentata: cooperativity among coactive afferents.* Brain Res, 1978. **157**(2): p. 277-93.
24. Bliss, T.V. and G.L. Collingridge, *A synaptic model of memory: long-term potentiation in the hippocampus.* Nature, 1993. **361**(6407): p. 31-9.
25. Levy, W.B. and O. Steward, *Synapses as associative memory elements in the hippocampal formation.* Brain Res, 1979. **175**(2): p. 233-45.
26. Sastry, B.R., J.W. Goh, and A. Auyeung, *Associative induction of posttetanic and long-term potentiation in CA1 neurons of rat hippocampus.* Science, 1986. **232**(4753): p. 988-90.
27. Malinow, R. and J.P. Miller, *Postsynaptic hyperpolarization during conditioning reversibly blocks induction of long-term potentiation.* Nature, 1986. **320**(6062): p. 529-30.
28. Nicoll, R.A. and R.C. Malenka, *Contrasting properties of two forms of long-term potentiation in the hippocampus.* Nature, 1995. **377**(6545): p. 115-8.
29. Salin, P.A., R.C. Malenka, and R.A. Nicoll, *Cyclic AMP mediates a presynaptic form of LTP at cerebellar parallel fiber synapses.* Neuron, 1996. **16**(4): p. 797-803.
30. Castro-Alamancos, M.A. and M.E. Calcagnotto, *Presynaptic long-term potentiation in corticothalamic synapses.* J Neurosci, 1999. **19**(20): p. 9090-7.
31. Malenka, R.C. and R.A. Nicoll, *Long-term potentiation--a decade of progress?* Science, 1999. **285**(5435): p. 1870-4.
32. Collingridge, G.L., S.J. Kehl, and H. McLennan, *Excitatory amino acids in synaptic transmission in the Schaffer collateral-commissural pathway of the rat hippocampus.* J Physiol, 1983. **334**: p. 33-46.
33. Anwyl, R., *Metabotropic glutamate receptor-dependent long-term potentiation.* Neuropharmacology, 2009. **56**(4): p. 735-40.
34. Wu, J., et al., *Involvement of group I mGluRs in LTP induced by strong high frequency stimulation in the dentate gyrus in vitro.* Neurosci Lett, 2008. **436**(2): p. 235-8.
35. Lledo, P.M., et al., *Calcium/calmodulin-dependent kinase II and long-term potentiation enhance synaptic transmission by the same mechanism.* Proc Natl Acad Sci U S A, 1995. **92**(24): p. 11175-9.
36. Lisman, J., et al., *Learning mechanisms: the case for CaM-KII.* Science, 1997. **276**(5321): p. 2001-2.
37. Giese, K.P., et al., *Autophosphorylation at Thr286 of the alpha calcium-calmodulin kinase II in LTP and learning.* Science, 1998. **279**(5352): p. 870-3.
38. Seamon, K.B. and J.W. Daly, *Forskolin: a unique diterpene activator of cyclic AMP-generating systems.* J Cyclic Nucleotide Res, 1981. **7**(4): p. 201-24.
39. Schuman, E.M. and D.V. Madison, *A requirement for the intercellular messenger nitric oxide in long-term potentiation.* Science, 1991. **254**(5037): p. 1503-6.
40. O'Dell, T.J., et al., *Tests of the roles of two diffusible substances in long-term potentiation: evidence for nitric oxide as a possible early retrograde messenger.* Proc Natl Acad Sci U S A, 1991. **88**(24): p. 11285-9.

41. Derkach, V., A. Barria, and T.R. Soderling, *Ca2+/calmodulin-kinase II enhances channel conductance of alpha-amino-3-hydroxy-5-methyl-4-isoxazolepropionate type glutamate receptors.* Proc Natl Acad Sci U S A, 1999. **96**(6): p. 3269-74.
42. Hayashi, Y., et al., *Driving AMPA receptors into synapses by LTP and CaMKII: requirement for GluR1 and PDZ domain interaction.* Science, 2000. **287**(5461): p. 2262-7.
43. Shi, S.H., et al., *Rapid spine delivery and redistribution of AMPA receptors after synaptic NMDA receptor activation.* Science, 1999. **284**(5421): p. 1811-6.
44. Bayazitov, I.T., et al., *Slow presynaptic and fast postsynaptic components of compound long-term potentiation.* J Neurosci, 2007. **27**(43): p. 11510-21.
45. Lynch, M.A., *Long-term potentiation and memory.* Physiol Rev, 2004. **84**(1): p. 87-136.
46. Vickers, C.A., K.S. Dickson, and D.J. Wyllie, *Induction and maintenance of late-phase long-term potentiation in isolated dendrites of rat hippocampal CA1 pyramidal neurones.* J Physiol, 2005. **568**(Pt 3): p. 803-13.
47. Steward, O., *Alterations in polyribosomes associated with dendritic spines during the reinnervation of the dentate gyrus of the adult rat.* J Neurosci, 1983. **3**(1): p. 177-88.
48. Fonseca, R., et al., *A balance of protein synthesis and proteasome-dependent degradation determines the maintenance of LTP.* Neuron, 2006. **52**(2): p. 239-45.
49. Kuhl, D. and P. Skehel, *Dendritic localization of mRNAs.* Curr Opin Neurobiol, 1998. **8**(5): p. 600-6.
50. Frey, U. and R.G. Morris, *Synaptic tagging and long-term potentiation.* Nature, 1997. **385**(6616): p. 533-6.
51. Whitlock, J.R., et al., *Learning induces long-term potentiation in the hippocampus.* Science, 2006. **313**(5790): p. 1093-7.
52. Gambino, F., et al., *Sensory-evoked LTP driven by dendritic plateau potentials in vivo.* Nature, 2014. **515**(7525): p. 116-9.
53. Morris, R.G., et al., *Selective impairment of learning and blockade of long-term potentiation by an N-methyl-D-aspartate receptor antagonist, AP5.* Nature, 1986. **319**(6056): p. 774-6.
54. Takahashi, T., K. Svoboda, and R. Malinow, *Experience strengthening transmission by driving AMPA receptors into synapses.* Science, 2003. **299**(5612): p. 1585-8.
55. Rumpel, S., et al., *Postsynaptic receptor trafficking underlying a form of associative learning.* Science, 2005. **308**(5718): p. 83-8.
56. Miller, S., et al., *Disruption of dendritic translation of CaMKIIalpha impairs stabilization of synaptic plasticity and memory consolidation.* Neuron, 2002. **36**(3): p. 507-19.
57. Wu, Z.L., et al., *Altered behavior and long-term potentiation in type I adenylyl cyclase mutant mice.* Proc Natl Acad Sci U S A, 1995. **92**(1): p. 220-4.
58. Abel, T. and P.V. Nguyen, *Regulation of hippocampus-dependent memory by cyclic AMP-dependent protein kinase.* Prog Brain Res, 2008. **169**: p. 97-115.
59. Yuste, R. and T. Bonhoeffer, *Morphological changes in dendritic spines associated with long-term synaptic plasticity.* Annu Rev Neurosci, 2001. **24**: p. 1071-89.
60. Matsuzaki, M., et al., *Structural basis of long-term potentiation in single dendritic spines.* Nature, 2004. **429**(6993): p. 761-6.
61. Malinow, R. and R.C. Malenka, *AMPA receptor trafficking and synaptic plasticity.* Annu Rev Neurosci, 2002. **25**: p. 103-26.
62. Hill, T.C. and K. Zito, *LTP-induced long-term stabilization of individual nascent dendritic spines.* J Neurosci, 2013. **33**(2): p. 678-86.

63. Lisman, J., R. Yasuda, and S. Raghavachari, *Mechanisms of CaMKII action in long-term potentiation.* Nat Rev Neurosci, 2012. **13**(3): p. 169-82.
64. Sacktor, T.C., *How does PKMzeta maintain long-term memory?* Nat Rev Neurosci, 2011. **12**(1): p. 9-15.
65. Bednarek, E. and P. Caroni, *beta-Adducin is required for stable assembly of new synapses and improved memory upon environmental enrichment.* Neuron, 2011. **69**(6): p. 1132-46.
66. Cingolani, L.A. and Y. Goda, *Actin in action: the interplay between the actin cytoskeleton and synaptic efficacy.* Nat Rev Neurosci, 2008. **9**(5): p. 344-56.
67. Holtmaat, A. and K. Svoboda, *Experience-dependent structural synaptic plasticity in the mammalian brain.* Nat Rev Neurosci, 2009. **10**(9): p. 647-58.
68. Engert, F. and T. Bonhoeffer, *Dendritic spine changes associated with hippocampal long-term synaptic plasticity.* Nature, 1999. **399**(6731): p. 66-70.
69. Toni, N., et al., *LTP promotes formation of multiple spine synapses between a single axon terminal and a dendrite.* Nature, 1999. **402**(6760): p. 421-5.
70. Maletic-Savatic, M., R. Malinow, and K. Svoboda, *Rapid dendritic morphogenesis in CA1 hippocampal dendrites induced by synaptic activity.* Science, 1999. **283**(5409): p. 1923-7.
71. De Roo, M., P. Klauser, and D. Muller, *LTP promotes a selective long-term stabilization and clustering of dendritic spines.* PLoS Biol, 2008. **6**(9): p. e219.
72. Hofer, S.B., et al., *Experience leaves a lasting structural trace in cortical circuits.* Nature, 2009. **457**(7227): p. 313-7.
73. Xu, T., et al., *Rapid formation and selective stabilization of synapses for enduring motor memories.* Nature, 2009. **462**(7275): p. 915-9.
74. Yang, G., F. Pan, and W.B. Gan, *Stably maintained dendritic spines are associated with lifelong memories.* Nature, 2009. **462**(7275): p. 920-4.
75. Caroni, P., F. Donato, and D. Muller, *Structural plasticity upon learning: regulation and functions.* Nat Rev Neurosci, 2012. **13**(7): p. 478-90.
76. Lai, C.S., T.F. Franke, and W.B. Gan, *Opposite effects of fear conditioning and extinction on dendritic spine remodelling.* Nature, 2012. **483**(7387): p. 87-91.
77. Fu, M., et al., *Repetitive motor learning induces coordinated formation of clustered dendritic spines in vivo.* Nature, 2012. **483**(7387): p. 92-5.
78. Chklovskii, D.B., B.W. Mel, and K. Svoboda, *Cortical rewiring and information storage.* Nature, 2004. **431**(7010): p. 782-8.
79. Stepanyants, A., P.R. Hof, and D.B. Chklovskii, *Geometry and structural plasticity of synaptic connectivity.* Neuron, 2002. **34**(2): p. 275-88.
80. Judkewitz, B., et al., *Targeted single-cell electroporation of mammalian neurons in vivo.* Nat Protoc, 2009. **4**(6): p. 862-9.
81. Otmakhov, N., et al., *Forskolin-induced LTP in the CA1 hippocampal region is NMDA receptor dependent.* J Neurophysiol, 2004. **91**(5): p. 1955-62.
82. Petreanu, L., et al., *The subcellular organization of neocortical excitatory connections.* Nature, 2009. **457**(7233): p. 1142-5.
83. Chen, T.W., et al., *Ultrasensitive fluorescent proteins for imaging neuronal activity.* Nature, 2013. **499**(7458): p. 295-300.
84. Berndt, A., et al., *High-efficiency channelrhodopsins for fast neuronal stimulation at low light levels.* Proc Natl Acad Sci U S A, 2011. **108**(18): p. 7595-600.

85. Lin, J.Y., *A user's guide to channelrhodopsin variants: features, limitations and future developments.* Exp Physiol, 2011. **96**(1): p. 19-25.
86. Chen, H.X., N. Otmakhov, and J. Lisman, *Requirements for LTP induction by pairing in hippocampal CA1 pyramidal cells.* J Neurophysiol, 1999. **82**(2): p. 526-32.
87. Huang, Y.Y. and E.R. Kandel, *Recruitment of long-lasting and protein kinase A-dependent long-term potentiation in the CA1 region of hippocampus requires repeated tetanization.* Learn Mem, 1994. **1**(1): p. 74-82.
88. Markram, H., et al., *Regulation of synaptic efficacy by coincidence of postsynaptic APs and EPSPs.* Science, 1997. **275**(5297): p. 213-5.
89. Bi, G.Q. and M.M. Poo, *Synaptic modifications in cultured hippocampal neurons: dependence on spike timing, synaptic strength, and postsynaptic cell type.* J Neurosci, 1998. **18**(24): p. 10464-72.
90. Magee, J.C. and D. Johnston, *A synaptically controlled, associative signal for Hebbian plasticity in hippocampal neurons.* Science, 1997. **275**(5297): p. 209-13.
91. Koester, H.J. and B. Sakmann, *Calcium dynamics in single spines during coincident pre- and postsynaptic activity depend on relative timing of back-propagating action potentials and subthreshold excitatory postsynaptic potentials.* Proc Natl Acad Sci U S A, 1998. **95**(16): p. 9596-601.
92. Nishiyama, M., et al., *Calcium stores regulate the polarity and input specificity of synaptic modification.* Nature, 2000. **408**(6812): p. 584-8.
93. Golding, N.L., N.P. Staff, and N. Spruston, *Dendritic spikes as a mechanism for cooperative long-term potentiation.* Nature, 2002. **418**(6895): p. 326-31.
94. Remy, S. and N. Spruston, *Dendritic spikes induce single-burst long-term potentiation.* Proc Natl Acad Sci U S A, 2007. **104**(43): p. 17192-7.
95. Zhang, Y.P. and T.G. Oertner, *Optical induction of synaptic plasticity using a light-sensitive channel.* Nat Methods, 2007. **4**(2): p. 139-41.
96. Zhang, Y.P., N. Holbro, and T.G. Oertner, *Optical induction of plasticity at single synapses reveals input-specific accumulation of alphaCaMKII.* Proc Natl Acad Sci U S A, 2008. **105**(33): p. 12039-44.
97. Makhinson, M., et al., *Adenylyl cyclase activation modulates activity-dependent changes in synaptic strength and Ca2+/calmodulin-dependent kinase II autophosphorylation.* J Neurosci, 1999. **19**(7): p. 2500-10.
98. Greengard, P., et al., *Enhancement of the glutamate response by cAMP-dependent protein kinase in hippocampal neurons.* Science, 1991. **253**(5024): p. 1135-8.
99. Chavez-Noriega, L.E. and C.F. Stevens, *Modulation of synaptic efficacy in field CA1 of the rat hippocampus by forskolin.* Brain Res, 1992. **574**(1-2): p. 85-92.
100. Pockett, S., J.R. Slack, and S. Peacock, *Cyclic AMP and long-term potentiation in the CA1 region of rat hippocampus.* Neuroscience, 1993. **52**(2): p. 229-36.
101. Vazquez, S.I., A. Vazquez, and S. Pena de Ortiz, *Different hippocampal activity profiles for PKA and PKC in spatial discrimination learning.* Behav Neurosci, 2000. **114**(6): p. 1109-18.
102. Mizuno, M., et al., *CREB phosphorylation as a molecular marker of memory processing in the hippocampus for spatial learning.* Behav Brain Res, 2002. **133**(2): p. 135-41.
103. Nägerl, U.V., et al., *Bidirectional activity-dependent morphological plasticity in hippocampal neurons.* Neuron, 2004. **44**(5): p. 759-67.

104. Tominaga-Yoshino, K., et al., *Repetitive activation of protein kinase A induces slow and persistent potentiation associated with synaptogenesis in cultured hippocampus.* Neurosci Res, 2002. **44**(4): p. 357-67.
105. Oe, Y., et al., *Dendritic spine dynamics in synaptogenesis after repeated LTP inductions: dependence on pre-existing spine density.* Sci Rep, 2013. **3**: p. 1957.
106. Knott, G.W., et al., *Spine growth precedes synapse formation in the adult neocortex in vivo.* Nat Neurosci, 2006. **9**(9): p. 1117-24.
107. Malinow, R. and R.W. Tsien, *Presynaptic enhancement shown by whole-cell recordings of long-term potentiation in hippocampal slices.* Nature, 1990. **346**(6280): p. 177-80.
108. Stevens, C.F. and Y. Wang, *Changes in reliability of synaptic function as a mechanism for plasticity.* Nature, 1994. **371**(6499): p. 704-7.
109. Smith, S.J. and G.J. Augustine, *Calcium ions, active zones and synaptic transmitter release.* Trends Neurosci, 1988. **11**(10): p. 458-64.
110. Koester, H.J. and B. Sakmann, *Calcium dynamics associated with action potentials in single nerve terminals of pyramidal cells in layer 2/3 of the young rat neocortex.* J Physiol, 2000. **529 Pt 3**: p. 625-46.
111. Schneggenburger, R. and E. Neher, *Presynaptic calcium and control of vesicle fusion.* Curr Opin Neurobiol, 2005. **15**(3): p. 266-74.
112. Yuste, R. and W. Denk, *Dendritic spines as basic functional units of neuronal integration.* Nature, 1995. **375**(6533): p. 682-4.
113. Isaac, J.T., R.A. Nicoll, and R.C. Malenka, *Evidence for silent synapses: implications for the expression of LTP.* Neuron, 1995. **15**(2): p. 427-34.
114. Durand, G.M., Y. Kovalchuk, and A. Konnerth, *Long-term potentiation and functional synapse induction in developing hippocampus.* Nature, 1996. **381**(6577): p. 71-5.
115. Cichon, J. and W.B. Gan, *Branch-specific dendritic Ca(2+) spikes cause persistent synaptic plasticity.* Nature, 2015. **520**(7546): p. 180-5.
116. Zito, K., et al., *Rapid functional maturation of nascent dendritic spines.* Neuron, 2009. **61**(2): p. 247-58.
117. Kwon, H.B. and B.L. Sabatini, *Glutamate induces de novo growth of functional spines in developing cortex.* Nature, 2011. **474**(7349): p. 100-4.
118. Nägerl, U.V., et al., *Protracted synaptogenesis after activity-dependent spinogenesis in hippocampal neurons.* J Neurosci, 2007. **27**(30): p. 8149-56.
119. De Roo, M., et al., *Activity-dependent PSD formation and stabilization of newly formed spines in hippocampal slice cultures.* Cereb Cortex, 2008. **18**(1): p. 151-61.
120. Okabe, S., A. Miwa, and H. Okado, *Spine formation and correlated assembly of presynaptic and postsynaptic molecules.* J Neurosci, 2001. **21**(16): p. 6105-14.
121. Friedman, H.V., et al., *Assembly of new individual excitatory synapses: time course and temporal order of synaptic molecule recruitment.* Neuron, 2000. **27**(1): p. 57-69.
122. Washbourne, P., J.E. Bennett, and A.K. McAllister, *Rapid recruitment of NMDA receptor transport packets to nascent synapses.* Nat Neurosci, 2002. **5**(8): p. 751-9.
123. Richards, D.A., et al., *Glutamate induces the rapid formation of spine head protrusions in hippocampal slice cultures.* Proc Natl Acad Sci U S A, 2005. **102**(17): p. 6166-71.
124. Palmer, L.M., et al., *NMDA spikes enhance action potential generation during sensory input.* Nat Neurosci, 2014. **17**(3): p. 383-90.
125. Sheffield, M.E. and D.A. Dombeck, *Calcium transient prevalence across the dendritic arbour predicts place field properties.* Nature, 2015. **517**(7533): p. 200-4.

126. Otmakhov, N., et al., *Persistent accumulation of calcium/calmodulin-dependent protein kinase II in dendritic spines after induction of NMDA receptor-dependent chemical long-term potentiation.* J Neurosci, 2004. **24**(42): p. 9324-31.
127. Shen, K. and T. Meyer, *Dynamic control of CaMKII translocation and localization in hippocampal neurons by NMDA receptor stimulation.* Science, 1999. **284**(5411): p. 162-6.
128. Steiner, P., et al., *Destabilization of the postsynaptic density by PSD-95 serine 73 phosphorylation inhibits spine growth and synaptic plasticity.* Neuron, 2008. **60**(5): p. 788-802.
129. Chung, H.J., et al., *Regulation of the NMDA receptor complex and trafficking by activity-dependent phosphorylation of the NR2B subunit PDZ ligand.* J Neurosci, 2004. **24**(45): p. 10248-59.
130. Okamoto, K., et al., *The role of CaMKII as an F-actin-bundling protein crucial for maintenance of dendritic spine structure.* Proc Natl Acad Sci U S A, 2007. **104**(15): p. 6418-23.
131. Ostroff, L.E., et al., *Polyribosomes redistribute from dendritic shafts into spines with enlarged synapses during LTP in developing rat hippocampal slices.* Neuron, 2002. **35**(3): p. 535-45.

Curriculum Vitae

Personal Information

Name	Cvetalina Nikolaeva Coneva
Date of Birth	26.03.1985
Place of Birth	Razgrad, Bulgaria

Education

Since 08/2010	**Doctoral studies** International Max-Planck Research School for Molecular and Cellular Life Sciences (IMPRS-LS) Ludwig–Maximilians-University, München, Germany
09/2008 – 04/2010	**MSc Cellular and Molecular Neuroscience** Graduate Training Center for Neuroscience, Eberhard Karl University of Tübingen, Tübingen, Germany Grade 1.5
09/2004 – 04/2008	**BSc Biotechnology** Mannheim University of Applied Sciences, Mannheim, Germany Grade 1.7

Research Work Experience

Since 08/2010	**PhD Thesis** Project: Activity-Driven Formation and Stabilization of Functional Spine Synapses Department: Synapse – Circuits - Plasticity Max-Planck Institute of Neurobiology, Martinsried, Germany
11/2009 - 03/2010	**Master Thesis** Project: The Role of SRF Mediated Transcription in Neuronal Mitochondrial Function Department of Molecular Biology, Neuronal Gene Expression

	Interfaculty Institute for Cell biology, Tübingen, Germany
02/2009 – 04/2009	**Internship**
	Project: Following Plaque Formation *in vivo* Using Two-Photon Microscopy in APPPS1/Iba1-eGFP Transgenic Mouse Model of Alzheimer's Disease
	Department of Cellular Neurology
	Hertie Institute for Clinical Brain Research, Tübingen, German
10/2007 – 09/2008	**Bachelor thesis and Internship**
	Project: Investigating Golgi to Endoplasmic Reticulum Recycling of Golgi Enzymes
	Research Unit of Cell Biology and Biophysics
	European Molecular Biology Laboratory (EMBL), Heidelberg, Germany
09/2006 – 02/2007	**Internship**
	Project: Mutagenesis Analysis of Non-Structural Hepatitis C Protein 4B
	Department of Molecular Virology
	University of Heidelberg, Heidelberg, Germany
04/2005 – 06/2006	**Lab Assistant**
	Institute of Inorganic Chemistry
	Mannheim University of Applied Sciences, Mannheim, Germany

Publication and Conference Contributions

Research article	**Schuberth CE[1], Tängemo C[2], Coneva C[2], Tischer C[3], Pepperkok R[4]**: Self-organization of core Golgi material is independent of COPII-mediated endoplasmic reticulum export. *J Cell Sci. 2015*
Poster	**Cvetalina N. Coneva, Tobias Bonhoeffer, Tobias Rose:** Activity-dependence and target specificity of synapse formation during long-term potentiation; *11th Göttingen Meeting of the German Neuroscience Society, March 18-21, 2015, Göttingen, Germany*

Awards and Scholarship

10/2008 – 10/2009	**Scholarship** for Master studies at Graduate Training Center for Neuroscience, Eberhard Karl University of Tübingen

2007 – 2008	**University fee waiver** due to high academic performance in the Bachelor's foundation course at Mannheim University of Applied Science
2001	**Team first place** on a national mathematics competition Lovech, Bulgaria

Skills

Language	**Bulgarian** (mother language); **English** (fluent); **German** (very good)
Computer	**MATLAB**, **Vector NTI (**Sequence Analysis Software), **ImageJ**, **Imaris**, **Huygens Deconvolution software**, **Amira (**Image Processing Program)

Community Work

09/2008 – 04/2010	**Library Work** at Graduate Training Center for Neuroscience, University Tübingen, Germany
2002 - 2004	**Voluntary library work** at foundation "Cyril and Methodius", Sofia, Bulgaria
2001 - 2004	**Voluntary work** at the Bulgarian Red Cross Organization, Sofia, Bulgaria

Acknowledgments

I thank Tobias Rose for his supervision, for his help with the 'moody' A-scope from Thorlabs which at the beginning of my PhD was a beta-version under development[2], and for sharing with me the mTurquoise2AGCaMP6s construct which I used in this work.

I am very thankful to Tobias Bonhoeffer for entrusting me with this project, making me part of his team and patiently encouraging me even when nothing seemed to work.

I would like to thank my PhD thesis committee – Tobias Bonhoeffer, Christian Leibold, Rainer Uhl, Wolfgang Enard, Heinrich Jung and Elisabeth Weiss for taking the time to read and evaluate my PhD thesis.

Many thanks I express to Frank Voss, Claudia Huber and Max Sperling for their technical support and to Helena Tultschin for helping me with the spine annotations.

Huge thanks goes to Volker Staiger who helped me with the organotypic slice preparation, who was an irreplaceable help for all those mundane but essential everyday practical problems and who also took the time to read and correct my thesis.

I am extremely thankful to Fiona Müllner who was the person always ready to offer a piece of advice in all experimental, theoretical and life-in-general obstacles. She also shared with me her MATLAB exponential fitting function exp_Yoffset which I used in my spine calcium analysis.

I would like to thank Pieter Goltstein for sharing his MATLAB function MRPcv which I used for my spine calcium analysis.

Onur Gökce helped me during my baby steps in learning MATLAB and tried to alleviate my pessimism in the most frustrating stages of my PhD.

[2] By the time I finished with my PhD the beta-version A-scope had turned into an antique and had been completely replaced by the upgraded rotating, translating B-Scope which beautifully illustrated how the time flow for a PhD student can sometimes slightly resemble that close to a Black Hole.

Marcus Knopp was very helpful when it came to fiddling with the setup. I thank him also for the countless fruitful and entertaining scientific and non-scientific discussions.

I am grateful to Lior Cohen for having the courage and patience to read through the very first draft of my PhD thesis and giving me invaluable input.

I thank Nadine Becker who despite the fact I do not know personally wrote her thesis in a way that I really enjoyed reading and I learnt a great deal from for writing my own thesis.

Rosa Garcia Verdugo, my office mate, I thank for our refreshing conversations and the great time we had together. I hope this goes beyond the PhD time.

Big thanks to Alison Barker and Michael Myoga for providing some native speaker survival kit for my thesis.

I thank all other members of the Bonhoeffer lab – for the nice discussions, lunch breaks, coffee breaks, barbeques and parties. I wish I did not miss quite some of those because of work but those I took part in I really enjoyed because of your company.

Finally, I thank the dearest to me, my family, who made me who I am and selflessly gave me the freedom to pursue my goals even though it meant to be far away – my mother, Zoya, my grandmother, Stanka, my brother, Stanislav and his wife, Neva and the cutest niece and nephew in the world, Zara and Stoil. Last but not least, I thank Benjamin for the relentless and unconditional support and his unsurpassable expertise in understanding me and fixing my sometimes unbearable moods, without you I feel incomplete and lost.

Appendix A

Sequence of plasmid DNA

pAAV- hSyn1-mTurquoise2-RSG-P2A-GC6s

AGCGCCCAATACGCAAACCGCCTCTCCCCGCGCGTTGGCCGATTCATTAATGCAGCTGGCACGACAGGT
TTCCCGACTGGAAAGCGGGCAGTGAGCGCAACGCAATTAATGTGAGTTAGCTCACTCATTAGGCACCC
CAGGCTTTACACTTTATGCTTCCGGCTCGTATGTTGTGTGGAATTGTGAGCGGATAACAATTTCACACA
GGAAACAGCTATGACCATGATTACGCCAGATTTAATTAAGGCCTTAATTAGGCTGCGCGCTCGCTCGCT
CACTGAGGCCGCCCGGGCAAAGCCCGGGCGTCGGGCGACCTTTGGTCGCCCGGCCTCAGTGAGCGAG
CGAGCGCGCAGAGAGGGAGTGGCCAACTCCATCACTAGGGGTTCCTTGTAGTTAATGATTAACCCGCC
ATGCTACTTATCTACGTAGCCATGCTCTAGGAAGATCTCTGCAGAGGGCCCTGCGTATGAGTGCAAGTG
GGTTTTAGGACCAGGATGAGGCGGGGTGGGGGTGCCTACCTGACGACCGACCCCGACCCACTGGACA
AGCACCCAACCCCCATTCCCCAAATTGCGCATCCCCTATCAGAGAGGGGGAGGGGAAACAGGATGCGG
CGAGGCGCGTGCGCACTGCCAGCTTCAGCACCGCGGACAGTGCCTTCGCCCCCGCCTGGCGGCGCGCG
CCACCGCCGCCTCAGCACTGAAGGCGCGCTGACGTCACTCGCCGGTCCCCCGCAAACTCCCCTTCCCGG
CCACCTTGGTCGCGTCCGCGCCGCCGCCGGCCCAGCCGGACCGCACCACGCGAGGCGCGAGATAGGG
GGGCACGGGCGCGACCATCTGCGCTGCGGCGCCGGCGACTCAGCGCTGCCTCAGTCTGCGGTGGGCA
GCGGAGGAGTCGTGTCGTGCCTGAGAGCGCAGTCGAATTCAAGCTGCTAGCAAGGATCCACCCGCCAC
CATGGTGAGCAAGGGCGAGGAGCTGTTCACCGGGGTGGTGCCCATCCTGGTCGAGCTGGACGGCGAC
GTAAACGGCCACAAGTTCAGCGTGTCCGGCGAGGGCGAGGGCGATGCCACCTACGGCAAGCTGACCC
TGAAGTTCATCTGCACCACCGGCAAGCTGCCCGTGCCCTGGCCCACCCTCGTGACCACCCTGTCCTGGG
GCGTGCAGTGCTTCGCCCGCTACCCCGACCACATGAAGCAGCACGACTTCTTCAAGTCCGCCATGCCCG
AAGGCTACGTCCAGGAGCGCACCATCTTCTTCAAGGACGACGGCAACTACAAGACCCGCGCCGAGGTG
AAGTTCGAGGGCGACACCCTGGTGAACCGCATCGAGCTGAAGGGCATCGACTTCAAGGAGGACGGCA
ACATCCTGGGGCACAAGCTGGAGTACAACTACTTTAGCGACAACGTCTATATCACCGCCGACAAGCAG
AAGAACGGCATCAAGGCCAACTTCAAGATCCGCCACAACATCGAGGACGGCGGCGTGCAGCTCGCCG
ACCACTACCAGCAGAACACCCCCATCGGCGACGGCCCCGTGCTGCTGCCCGACAACCACTACCTGAGCA
CCCAGTCCAAGCTGAGCAAAGACCCCAACGAGAAGCGCGATCACATGGTCCTGCTGGAGTTCGTGACC
GCCGCCGGGATCACTCTCGGCATGGACGAGCTGTACAAGTCCGGACTCAGATCCGGAGCCACGAACTT
CTCTCTGTTAAAGCAAGCAGGAGACGTGGAAGAAAACCCCGGTCCTGGTTCTCATCATCATCATCATCA

TGGTATGGCTAGCATGACTGGTGGACAGCAAATGGGTCGGGATCTGTACGACGATGACGATAAGGAT
CTCGCCACCATGGTCGACTCATCACGTCGTAAGTGGAATAAGACAGGTCACGCAGTCAGAGCTATAGG
TCGGCTGAGCTCACTCGAGAACGTCTATATCAAGGCCGACAAGCAGAAGAACGGCATCAAGGCGAACT
TCCACATCCGCCACAACATCGAGGACGGCGGCGTGCAGCTCGCCTACCACTACCAGCAGAACACCCCC
ATCGGCGACGGCCCCGTGCTGCTGCCCGACAACCACTACCTGAGCGTGCAGTCCAAACTTTCGAAAGA
CCCCAACGAGAAGCGCGATCACATGGTCCTGCTGGAGTTCGTGACCGCCGCCGGGATCACTCTCGGCA
TGGACGAGCTGTACAAGGGCGGTACCGGAGGGAGCATGGTGAGCAAGGGCGAGGAGCTGTTCACCG
GGGTGGTGCCCATCCTGGTCGAGCTGGACGGCGACGTAAACGGCCACAAGTTCAGCGTGTCCGGCGA
GGGTGAGGGCGATGCCACCTACGGCAAGCTGACCCTGAAGTTCATCTGCACCACCGGCAAGCTGCCCG
TGCCCTGGCCCACCCTCGTGACCACCCTGACCTACGGCGTGCAGTGCTTCAGCCGCTACCCCGACCACA
TGAAGCAGCACGACTTCTTCAAGTCCGCCATGCCCGAAGGCTACATCCAGGAGCGCACCATCTTCTTCA
AGGACGACGGCAACTACAAGACCCGCGCCGAGGTGAAGTTCGAGGGCGACACCCTGGTGAACCGCAT
CGAGCTGAAGGGCATCGACTTCAAGGAGGACGGCAACATCCTGGGGCACAAGCTGGAGTACAACCTG
CCGGACCAACTGACTGAAGAGCAGATCGCAGAATTTAAAGAGGCTTTCTCCCTATTTGACAAGGACGG
GGATGGGACAATAACAACCAAGGAGCTGGGGACGGTGATGCGGTCTCTGGGGCAGAACCCCACAGAA
GCAGAGCTGCAGGACATGATCAATGAAGTAGATGCCGACGGTGACGGCACAATCGACTTCCCTGAGTT
CCTGACAATGATGGCAAGAAAAATGAAATACAGGGACACGGAAGAAGAAATTAGAGAAGCGTTCGGT
GTGTTTGATAAGGATGGCAATGGCTACATCAGTGCAGCAGAGCTTCGCCACGTGATGACAAACCTTGG
AGAGAAGTTAACAGATGAAGAGGTTGATGAAATGATCAGGGAAGCAGACATCGATGGGGATGGTCA
GGTAAACTACGAAGAGTTTGTACAAATGATGACAGCGAAGCTAGTGCGGCCGCTTATGAAAGCTATCG
ATAATCAACCTCTGGATTACAAAATTTGTGAAAGATTGACTGGTATTCTTAACTATGTTGCTCCTTTTACG
CTATGTGGATACGCTGCTTTAATGCCTTTGTATCATGCTATTGCTTCCCGTATGGCTTTCATTTTCTCCTCC
TTGTATAAATCCTGGTTGCTGTCTCTTTATGAGGAGTTGTGGCCCGTTGTCAGGCAACGTGGCGTGGTG
TGCACTGTGTTTGCTGACGCAACCCCCACTGGTTGGGGCATTGCCACCACCTGTCAGCTCCTTTCCGGG
ACTTTCGCTTTCCCCCTCCCTATTGCCACGGCGGAACTCATCGCCGCCTGCCTTGCCCGCTGCTGGACAG
GGGCTCGGCTGTTGGGCACTGACAATTCCGTGGTGTTGTCGGGGAAATCATCGTCCTTTCCTTGGCTGC
TCGCCTGTGTTGCCACCTGGATTCTGCGCGGGACGTCCTTCTGCTACGTCCCTTCGGCCCTCAATCCAGC
GGACCTTCCTTCCCGCGGCCTGCTGCCGGCTCTGCGGCCTCTTCCGCGTCTTCGCCTTCGCCCTCAGACG
AGTCGGATCTCCCTTTGGGCCGCCTCCCCGCATCGATACCGTCGACCTCGACCCGGGCGGCCGCTTCGA
GCAGACATGATAAGATACATTGATGAGTTTGGACAAACCACAACTAGAATGCAGTGAAAAAAATGCTT
TATTTGTGAAATTTGTGATGCTATTGCTTTATTTGTAACCATTATAAGCTGCAATAAACAAGTTAACAAC
AACAATTGCATTCATTTTATGTTTCAGGTTCAGGGGGAGATGTGGGAGGTTTTTTAAAGCAAGTAAAAC

CTCTACAAATGTGGTAAAATCGATAAGGATCTTCCTAGAGCATGGCTACGTAGATAAGTAGCATGGCG
GGTTAATCATTAACTACAAGGAACCCCTAGTGATGGAGTTGGCCACTCCCTCTCTGCGCGCTCGCTCGC
TCACTGAGGCCGGGCGACCAAAGGTCGCCCGACGCCCGGGCTTTGCCCGGGCGGCCTCAGTGAGCGA
GCGAGCGCGCAGCCTTAATTAACCTAATTCACTGGCCGTCGTTTTACAACGTCGTGACTGGGAAAACCC
TGGCGTTACCCAACTTAATCGCCTTGCAGCACATCCCCCTTTCGCCAGCTGGCGTAATAGCGAAGAGGC
CCGCACCGATCGCCCTTCCCAACAGTTGCGCAGCCTGAATGGCGAATGGGACGCGCCCTGTAGCGGCG
CATTAAGCGCGGCGGGTGTGGTGGTTACGCGCAGCGTGACCGCTACACTTGCCAGCGCCCTAGCGCCC
GCTCCTTTCGCTTTCTTCCCTTCCTTTCTCGCCACGTTCGCCGGCTTTCCCCGTCAAGCTCTAAATCGGGG
GCTCCCTTTAGGGTTCCGATTTAGTGCTTTACGGCACCTCGACCCCAAAAAACTTGATTAGGGTGATGG
TTCACGTAGTGGGCCATCGCCCTGATAGACGGTTTTTCGCCCTTTGACGTTGGAGTCCACGTTCTTTAAT
AGTGGACTCTTGTTCCAAACTGGAACAACACTCAACCCTATCTCGGTCTATTCTTTTGATTTATAAGGGA
TTTTGCCGATTTCGGCCTATTGGTTAAAAAATGAGCTGATTTAACAAAAATTTAACGCGAATTTTAACAA
AATATTAACGCTTACAATTTAGGTGGCACTTTTCGGGGAAATGTGCGCGGAACCCCTATTTGTTTATTTT
TCTAAATACATTCAAATATGTATCCGCTCATGAGACAATAACCCTGATAAATGCTTCAATAATATTGAAA
AAGGAAGAGTATGAGTATTCAACATTTCCGTGTCGCCCTTATTCCCTTTTTTGCGGCATTTTGCCTTCCTG
TTTTTGCTCACCCAGAAACGCTGGTGAAAGTAAAAGATGCTGAAGATCAGTTGGGTGCACGAGTGGGT
TACATCGAACTGGATCTCAACAGCGGTAAGATCCTTGAGAGTTTTCGCCCCGAAGAACGTTTTCCAATG
ATGAGCACTTTTAAAGTTCTGCTATGTGGCGCGGTATTATCCCGTATTGACGCCGGGCAAGAGCAACTC
GGTCGCCGCATACACTATTCTCAGAATGACTTGGTTGAGTACTCACCAGTCACAGAAAAGCATCTTACG
GATGGCATGACAGTAAGAGAATTATGCAGTGCTGCCATAACCATGAGTGATAACACTGCGGCCAACTT
ACTTCTGACAACGATCGGAGGACCGAAGGAGCTAACCGCTTTTTTGCACAACATGGGGGATCATGTAA
CTCGCCTTGATCGTTGGGAACCGGAGCTGAATGAAGCCATACCAAACGACGAGCGTGACACCACGATG
CCTGTAGCAATGGCAACAACGTTGCGCAAACTATTAACTGGCGAACTACTTACTCTAGCTTCCCGGCAA
CAATTAATAGACTGGATGGAGGCGGATAAAGTTGCAGGACCACTTCTGCGCTCGGCCCTTCCGGCTGG
CTGGTTTATTGCTGATAAATCTGGAGCCGGTGAGCGTGGGTCTCGCGGTATCATTGCAGCACTGGGGC
CAGATGGTAAGCCCTCCCGTATCGTAGTTATCTACACGACGGGGAGTCAGGCAACTATGGATGAACGA
AATAGACAGATCGCTGAGATAGGTGCCTCACTGATTAAGCATTGGTAACTGTCAGACCAAGTTTACTCA
TATATACTTTAGATTGATTTAAAACTTCATTTTTAATTTAAAAGGATCTAGGTGAAGATCCTTTTTGATAA
TCTCATGACCAAAATCCCTTAACGTGAGTTTTCGTTCCACTGAGCGTCAGACCCCGTAGAAAAGATCAA
AGGATCTTCTTGAGATCCTTTTTTTCTGCGCGTAATCTGCTGCTTGCAAACAAAAAAACCACCGCTACCA
GCGGTGGTTTGTTTGCCGGATCAAGAGCTACCAACTCTTTTTCCGAAGGTAACTGGCTTCAGCAGAGCG
CAGATACCAAATACTGTTCTTCTAGTGTAGCCGTAGTTAGGCCACCACTTCAAGAACTCTGTAGCACCGC

CTACATACCTCGCTCTGCTAATCCTGTTACCAGTGGCTGCTGCCAGTGGCGATAAGTCGTGTCTTACCGG
GTTGGACTCAAGACGATAGTTACCGGATAAGGCGCAGCGGTCGGGCTGAACGGGGGGTTCGTGCACA
CAGCCCAGCTTGGAGCGAACGACCTACACCGAACTGAGATACCTACAGCGTGAGCTATGAGAAAGCGC
CACGCTTCCCGAAGGGAGAAAGGCGGACAGGTATCCGGTAAGCGGCAGGGTCGGAACAGGAGAGCG
CACGAGGGAGCTTCCAGGGGGAAACGCCTGGTATCTTTATAGTCCTGTCGGGTTTCGCCACCTCTGACT
TGAGCGTCGATTTTTGTGATGCTCGTCAGGGGGGCGGAGCCTATGGAAAAACGCCAGCAACGCGGCCT
TTTTACGGTTCCTGGCCTTTTGCTGGCCTTTTGCTCACATGTTCTTTCCTGCGTTATCCCCTGATTCTGTGG
ATAACCGTATTACCGCCTTTGAGTGAGCTGATACCGCTCGCCGCAGCCGAACGACCGAGCGCAGCGAG
TCAGTGAGCGAGGAAGCGGAAG

Appendix B

An overview of all spine responses

An overview of spine Ca^{2+} signals after light stimulation for all experiments of the same experimental treatment is schematically depicted below. The experimental treatments are labeled with a vertical line color-coded as follows: control 1 (no light stimulation + no F&R treatment) - green vertical line indicates the time point when under the other experimental conditions perfusion of vehicle or F&R takes place; control 2 (light stimulation + vehicle) - red vertical line indicates the time point of vehicle perfusion; control 3 (no light stimulation + F&R treatment) – black vertical line indicates the time point of F&R perfusion; treatment (light stimulation + F&R treatment) - blue vertical line indicates the time point of F&R perfusion.

Every horizontal line contains color-coded pixel information about the presence and the responsiveness of one spine over time. Preexisting spines are shown in the upper part of the panel (above the horizontal line colored depending on the experimental treatment), while new spines are shown in the lower part of the panel (below the horizontal line). For both preexisting and new spines, spines that did not show Ca^{2+} responses after optical stimulation (marked on the left side by a white rectangle) are displayed above the spines that were responsive to light stimulation (marked on the left side by patterned rectangle). For every line (spine) light-gray colored pixels indicate the calcium imaging trials without any information about the respective spine. Red pixels indicate the time of the trials when the spine showed successful Ca^{2+} responses to light stimulation. Orange pixels show trials when the spine was tested but failed to display light-triggered Ca^{2+} responses. Dark-gray color marks the time when the spine is absent (either still not formed or eliminated). Dark-shaded rectangle indicates the time when slices were left overnight in the incubator and were not imaged.

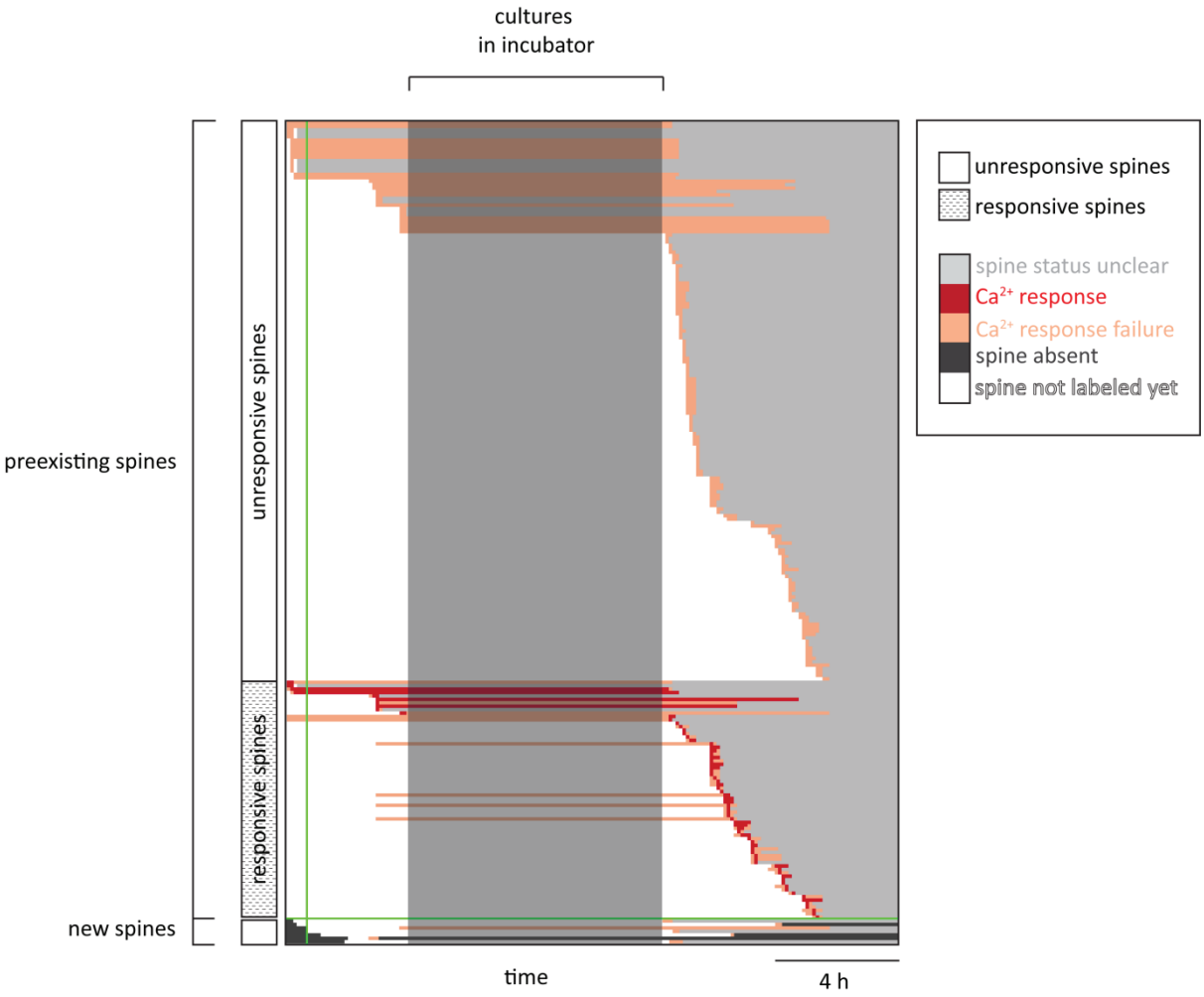

control 1; n = 241 spines, 7 slices

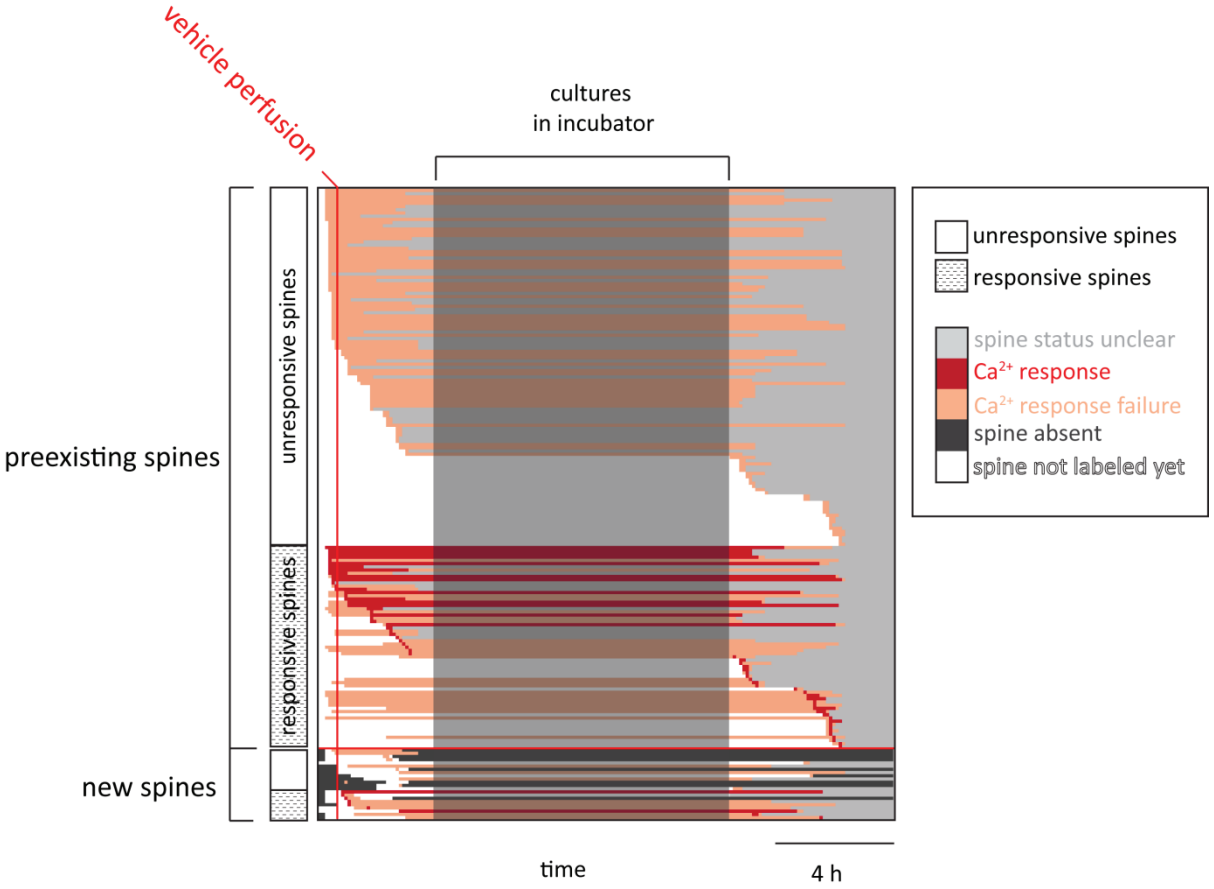

control 2; n = 196 spines, 5 slices

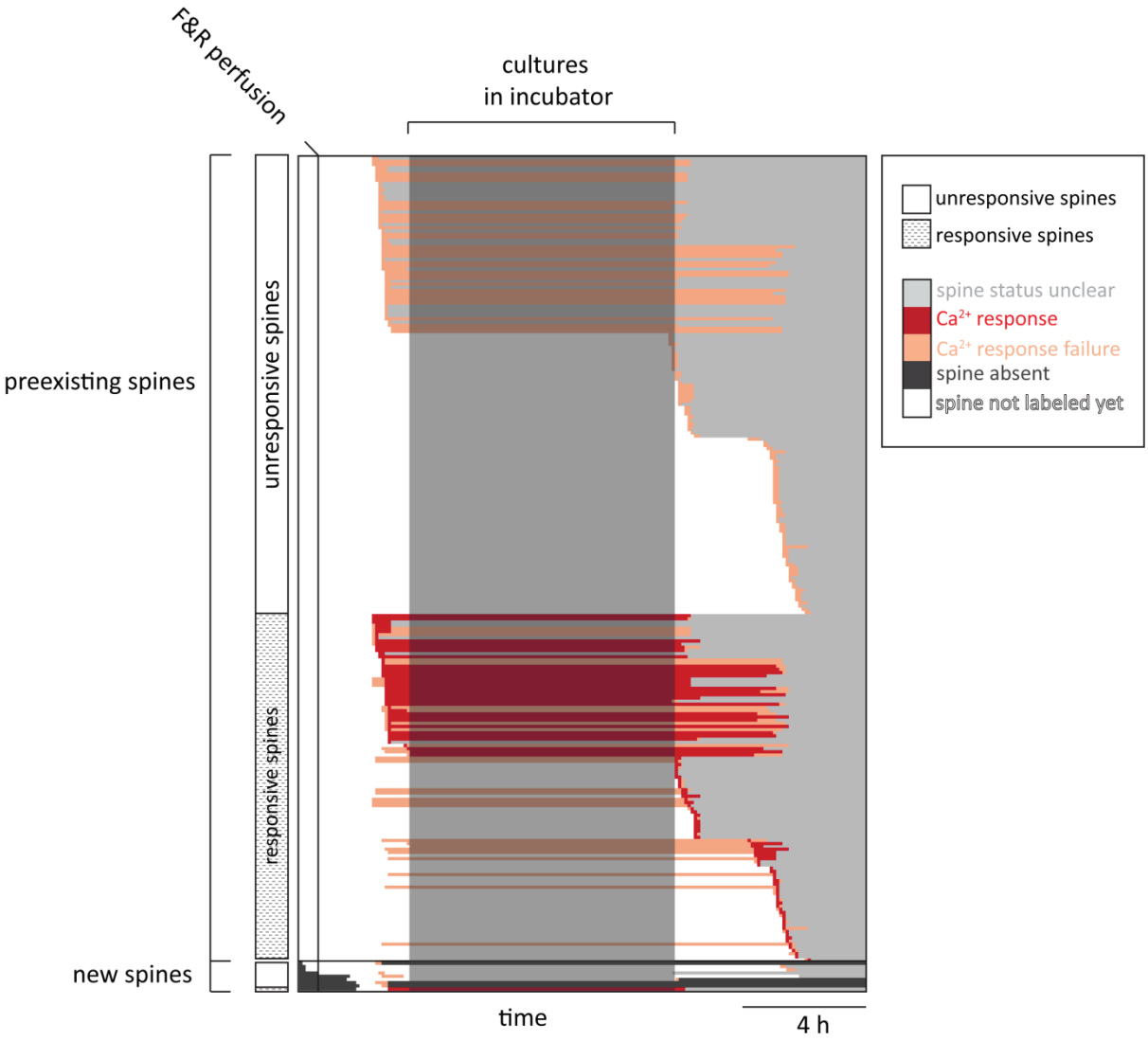

control 3; n = 264 spines, 5 slices

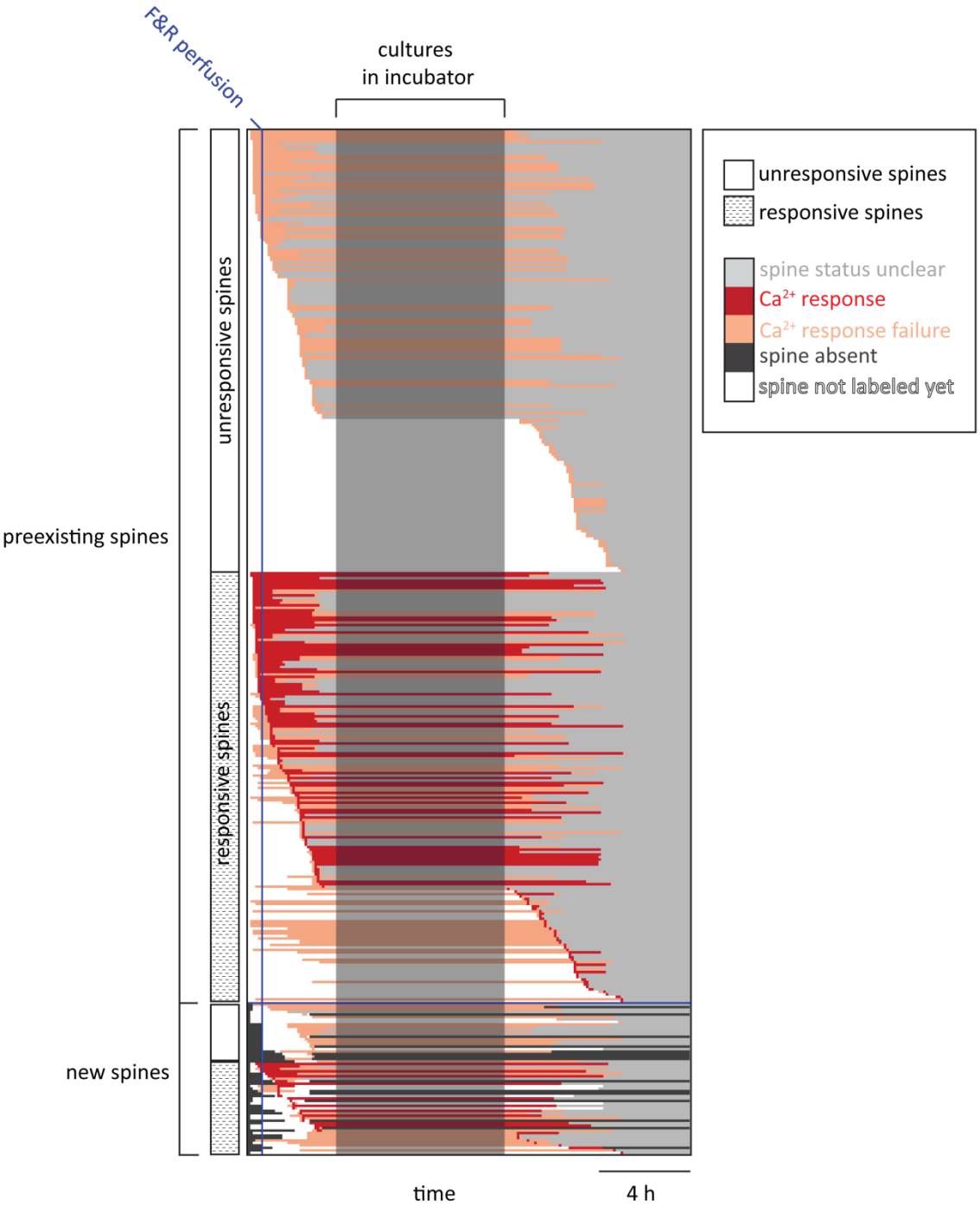

treatment; n = 414 spines, 9 slices